UNIVERSIDAD NACIONAL AUTÓNOMA DE MEXICO

POSGRADO EN CIENCIAS FÍSICAS
INSTITUTO DE FÍSICA
FÍSICA DE ALTAS ENERGÍAS, FÍSICA NUCLEAR, GRAVITACIÓN Y FÍSICA
MATEMÁTICA

NEUTRINO MASSES: RADIATIVE MODELS AND PHENOMENOLOGY

TESIS
QUE PARA OPTAR POR EL GRADO DE:
MAESTRO EN CIENCIAS (FÍSICA)

PRESENTA:
ROLANDO MARTÍNEZ RAMÍREZ

TUTOR PRINCIPAL
DR. EDUARDO PEINADO RODRÍGUEZ
INSTITUTO DE FÍSICA UNAM

MIEMBROS DEL COMITÉ TUTOR
DRA. AURORE MARIE PASCALE NICOLE COURTOY
INSTITUTO DE FÍSICA UNAM
DR. ÁNGEL SÁNCHEZ CECILIO
FACULTAD DE CIENCIAS UNAM

CIUDAD UNIVERSITARIA, CDMX, ABRIL 2024

**PROTESTA UNIVERSITARIA DE INTEGRIDAD Y
HONESTIDAD ACADÉMICA Y PROFESIONAL**
(Graduación con trabajo escrito)

De conformidad con lo dispuesto en los artículos 87, fracción V, del Estatuto General, 68, primer párrafo, del Reglamento General de Estudios Universitarios y 26, fracción I, y 35 del Reglamento General de Exámenes, me comprometo en todo tiempo a honrar a la Institución y a cumplir con los principios establecidos en el Código de Ética de la Universidad Nacional Autónoma de México, especialmente con los de integridad y honestidad académica.

De acuerdo con lo anterior, manifiesto que el trabajo escrito titulado:

Neutrino masses: radiative models and phenomenology

que presenté para obtener el grado de -----Maestria--- ▼ es original, de mi autoría y lo realicé con el rigor metodológico exigido por mi programa de posgrado, citando las fuentes de ideas, textos, imágenes, gráficos u otro tipo de obras empleadas para su desarrollo.

En consecuencia, acepto que la falta de cumplimiento de las disposiciones reglamentarias y normativas de la Universidad, en particular las ya referidas en el Código de Ética, llevará a la nulidad de los actos de carácter académico administrativo del proceso de graduación.

Atentamente

Rolando Martínez Ramírez
522013638

Rolando Mtz. R.

(Nombre, firma y Número de cuenta de la persona alumna)

A mi madre, padre y hermano.

Agradecimientos

Más Agradecimientos

- A mi familia, por su apoyo desmedido y siempre incondicional. A mis padres, por otorgarme estos apellidos que llevaré con cariño a todas partes. A mi hermano, por siempre estar ahí cuando lo he necesitado. Es un honor para mí que ustedes sean mi familia.

- A mi asesor, Eduardo, por las enseñanzas, las lecciones y los jalones de orejas. Por la preocupación constante, la entrega, el tiempo, los consejos de asesor y los consejos de amigo. Haberlo elegido como asesor es una de las mejores decisiones que he tomado.

- A los miembros de mi comité tutor, Aurora y Ángel, por su seguimiento constante y por encaminarme a lo largo de la maestría. También agradezco a Eric, por abrirme las puertas de su laboratorio y por su apoyo en mi formación.

- A los miembros de mi jurado de tesis: Myriam, Genaro, Manfred y Carlos, por sus valiosos comentarios y observaciones en la finalización de la presente tesis.

- A Jens y su equipo de trabajo, por su amable guía durante mi estancia en Mainz, y por proveerme de nuevas perspectivas dentro de la física de partículas.

- Al tridente de posdocs: León, Rodolfo y Patrick, por su disponibilidad para atender cualquier consulta por más simple que fuera. Cada uno con su propia personalidad, los considero grandes personas y grandes científicos.

- A mis colegas del Gallinero, por las discusiones y el acompañamiento. Haber compartido mi maestría con ustedes hizo que el Instituto se sintiera como mi hogar. Siempre les desearé el mejor de los futuros.

- Al IF-UNAM y su cálida hospitalidad a lo largo de estos dos años. Al décimo piso y su personal con toda la disposición de apoyar. El café aligeró los días más pesados.

- A la División de Partículas y Campos de la Sociedad Mexicana de Física (SMF), de nueva cuenta al IF-UNAM, y al comité organizador por sus esfuerzos en llevar a cabo el concurso Estancias de Verano Teóricas en el Extranjero.

- Al PRISMA+ Cluster of Excellence y al Nuclear Physics Institute de la Johannes Gutenberg University Mainz por su hospitalidad y por las facilidades brindadas durante mi estancia.

- A todas las amistades que de alguna manera me han compartido su pedazo de la CDMX. Me he sentido en casa gracias a ustedes.

Resumen

El Modelo Estándar de partículas describe las interacciones entre fermiones a nivel fundamental. Múltiples experimentos lo han puesto a prueba con éxito, haciendo predicciones para un gran número de propiedades. Sin embargo, la existencia de materia oscura, masas de neutrinos y asimetría de materia-antimateria en el universo, junto con la falta de una teoría verificada para dichos fenómenos, indica que el Modelo Estándar está incompleto. Esto motiva la búsqueda de nueva física, o física más allá del Modelo Estándar.

En este trabajo, nos enfocamos en el problema de las masas de neutrinos. Además de ser elusivas debido a su nula carga eléctrica, originalmente estas partículas eran consideradas sin masa en el Modelo Estándar. Con la observación de oscilaciones de neutrinos, se confirmó que éstos en realidad deberían ser masivos. Experimentos recientes de desintegración β han puesto una escala a la masa de neutrinos de 1 eV, menor a las partículas cargadas más ligeras del Modelo Estándar por más de seis órdenes de magnitud. Algunas preguntas que surgen son, ¿Por qué es esta masa tan pequeña? ¿Cómo adquieren masa los neutrinos? Por otra parte, los neutrinos son los únicos fermiones que podrían no ser de tipo Dirac, sino, de tipo Majorana. Esto añade otra incógnita al rompecabezas, siendo que cada posibilidad deriva en una fenomenología distinta, y experimentos actuales no han podido discernir entre ambas.

En la presente tesis, se abordan estas interrogantes desde dos perspectivas distintas. En el primer enfoque, se consideran neutrinos de Majorana y se proponen dos nuevos modelos radiativos de generación de masas. Estos consisten en una realización ultravioleta del operador efectivo de Weinberg. Dicha realización se logra extendiendo el Modelo Estándar con simetrías adicionales e incluyendo nuevos campos que a su vez podrían ser candidatos de materia oscura. En el primer modelo, se extiende el Modelo Estándar con una simetría Z_4, rompiéndose espontáneamente a una simetría Z_2. El campo más ligero con carga no trivial bajo Z_2 es protegido por conservación de carga, convirtiéndose en un candidato de materia oscura. En este modelo, las masas de neutrinos se generan a un lazo. En el segundo modelo, se extiende el Modelo Estándar con una simetría continua $U(1)_{B-L}$, rota espontáneamente a una simetría discreta Z_3, permitiendo también la estabilidad de materia oscura y generando masas de neutrinos a dos lazos. La fenomenología de ambos modelos es estudiada, incluyendo análisis de procesos de violación de sabor y canales de aniquilación de materia oscura como contribución a la densidad de reliquia.

El segundo enfoque consiste en un estudio fenomenológico considerando masas de Dirac y utilizando ceros de textura. Las texturas se construyen haciendo cero ciertas entradas de la matriz de masas de los neutrinos, derivando correlaciones entre los parámetros de oscilación. Así, dada cierta textura, es posible verificar si ésta está en concordancia con datos experimentales recientes o si está descartada por los mismos. En el presente trabajo se estudia cuáles de estas texturas están permitidas y se discuten las correlaciones que surgen a partir de ellas.

El trabajo realizado en esta tesis está basado en los siguientes proyectos de investigación:

- *Two-zero textures for Dirac neutrinos*
  Yessica Lenis[*], R. Martinez-Ramirez, Eduardo Peinado[†], William A. Ponce[*]
  arXiv:2311.06431. Enviado para publicación.

- *Two-loop neutrino masses in a broken $U(1)_{B-L}$ symmetry*
  Leon M.G. de la Vega[†‡], R. Martinez-Ramirez, Eduardo Peinado
  Trabajo en progreso

- *Cannibal dark matter from a Z_4 symmetry*
  Leon M.G. de la Vega, Patrick J. Fitzpatrick[§], R. Martinez-Ramirez, Eduardo Peinado
  Trabajo en progreso

Otro proyecto no incluido en la tesis:

- *Natural radioactivity concentration measurements in shrimp and sea bass samples from the Mexican Pacific Ocean and the Gulf of Mexico*
  R. Martinez-Ramirez, Ó. Valdés-Martínez[†], E. Vázquez-Jáuregui[†]
  Revista Mexicana de Física, **69** 061202 1-4

---

[*]Instituto de Física, Universidad de Antioquia
[†]Instituto de Física, UNAM
[‡]National Center for Theoretical Sciences, National Taiwan University
[§]Racah Institute of Physics, Hebrew University of Jerusalem

Contents

List of Figures

List of Tables

Rolando Martínez Ramírez
IF-UNAM
Neutrino Masses: Radiative Models and Phenomenology

1 Introduction

The Standard Model (SM) of particle physics [1–8] is the theory that describes the interactions between elementary particles. As one of the most validated theories in science of all time, numerous experiments have successfully tested the SM, providing precise predictions for a wide range of particle properties [9]. Despite this success, several open questions persist. These include the evidence of the existence of dark matter [10–13] where direct detection experiments have shown only negative results [14–17], baryon asymmetry in the universe [18–22], and neutrino masses. Each of these questions, lacking a probed theory behind them, suggests that the Standard Model is incomplete. This motivates the exploration of new physics, often referred as Beyond the Standard Model (BSM) physics.

Without any direct evidence for their mass at that time, the SM was originally built considering massless neutrinos. With the later observation of neutrino oscillations [23–34] it was confirmed that at least two of the three active neutrinos should carry a non-zero mass. Considering that oscillation phenomena are only sensitive to the squared mass differences between the three oscillating neutrinos, these experiments are unable to give an absolute mass scale.

In this respect, an upper limit for the sum of the three light neutrino masses can be obtained from cosmology. Assuming the ΛCDM cosmological model, the PLANCK collaboration in 2018 [12] obtained

$$\sum_i m_{\nu_i} \leq 0.12 \text{ eV}. \tag{1.1}$$

A model-independent way to obtain an upper limit for the absolute mass scale is from the kinematics of β decays. The Karlsruhe Tritium Neutrino (KATRIN) experiment [35, 36] measures the energy spectrum of a single β decay of molecular tritium:

$$\text{T}_2 \to {}^3\text{He} + \text{T}^+ + \text{e}^- + \bar{\nu}_\text{e}, \tag{1.2}$$

from which, the presence of neutrino masses results in a decrease in the maximum observed energy of the electron decay and a small distortion in the spectral shape near the kinematic endpoint of the β-spectrum. From this, a mass limit for neutrinos is obtained, with the last result yielding [36]

$$m_\nu \leq 0.8 \text{ eV}. \tag{1.3}$$

If we compare this result with the mass of the lightest charged fermion in the SM, the electron, given by

$$m_e \approx 0.511 \text{ MeV}, \tag{1.4}$$

we observe that m_e is at least 10^6 times greater than m_ν, establishing neutrinos as the lightest massive particles in the SM.

On the other hand, another open question is whether neutrinos are Dirac particles, like the charged fermions, or Majorana particles, implying they are their own antiparticle. Neither neutrino oscillations nor β-decay experiments are sensitive to this difference. If neutrinos are Majorana particles, there is a possibility to measure the neutrinoless double beta decay process [37], which, at present, remains the only method to differentiate the nature of neutrinos. This process has never been observed despite experimental efforts [38–41], and the question remains unanswered.

These unknowns motivate the exploration of BSM physics, in which the SM can be treated as an effective theory describing particle interactions only within a specific energy range Λ. In this context, the SM can be extended to consider new physics, offering an explanation for the smallness of neutrino masses while introducing additional degrees of freedom in sectors or energy scales not yet explored by experiments. These additions to the SM may also address the problem of the nature of dark matter.

The first evidence for dark matter came from observation of galaxy rotations [11]. Nowadays, observations developed by PLANCK of gravitational effects, structure formation and the Cosmic Microwave Background (CMB) are in agreement with the existence of dark matter in the universe, providing a value for its relic density [12]:

$$\Omega_c h^2 = 0.120 \pm 0.0012 \text{ at } 68\% \text{ C.L.} \tag{1.5}$$

A theoretical connection between neutrino masses and dark matter emerges when the SM is extended to consider BSM physics, with the extra degrees of freedom participating in the mass mechanism acting also as stable dark matter candidates, protected by an additional symmetry. Naturally, those new additions are constrained to reproduce phenomenology allowed by particle and cosmological observations.

A different method to study neutrino phenomenology involves model-independent assumptions subjected to experimental data. One example is the texture zeros approach, where specific entries of the neutrino mass matrix are set to zero, leading to correlations among oscillation parameters. While these textures should arise from a BSM theory, an analysis is possible without delving into these considerations, scrutinizing which of the textures is in good agreement with current observations.

Therefore, SM extensions are proposed, studied and tested against experimental constraints in order to provide a possible explanation to BSM puzzles, while model-independent and phenomenological approaches rely on assumptions related to data from observations. In this thesis, we explore both approaches, proposing new mass models for Majorana neutrinos, and using two-zero textures for Dirac neutrinos.

The thesis is organized as follows. In Section 2, we provide a brief overview of the general structure of the SM and the electroweak sector. Section 3 contains a short review of neutrino physics, considering massive neutrinos and their implications. Section 4 explores popular models for neutrino mass generation, both at tree-level and radiative. In Sections 5 and 6, we introduce two new radiative models based on a Z_4 symmetry and a gauge $U(1)_{B-L}$ symmetry, respectively. The first model generates Majorana neutrino masses at the one-loop level, while the second generates them at the two-loop level. These models contain dark matter candidates. In Section 7, we use the two-zero textures approach to study the phenomenology of Dirac neutrinos, finding which of the textures are allowed by current experimental data. Finally, Section 8 presents the conclusions of this thesis.

All Feynman diagrams were drawn using the FeynGame software [42, 43].

2 The Electroweak Standard Model

In this section, we briefly review the general structure of the SM and study the main features of the electroweak sector, establishing the key ideas to be used throughout the thesis. The discussion in this section is strongly inspired by the Giunti and Kim's book [44].

2.1 Standard Model Structure

The Standard Model (SM) describes the strong, weak and electromagnetic interactions of elementary particles within the framework of quantum field theory. It is a gauge theory based on the local symmetry group:

$$SU(3)_C \times SU(2)_L \times U(1)_Y. \tag{2.1}$$

Here, the subscripts C, L and Y represent color, left-handed chirality and weak hypercharge, respectively. The group $SU(n)$ is the special unitary group of degree n, which is the Lie group of $n \times n$ unitary matrices with determinant 1, and it has $n^2 - 1$ generators. Each group uniquely defines the interactions, with its generators associated to vector gauge bosons. There are eight massless gluons that mediate strong interactions, corresponding to the eight generators of $SU(3)_C$. In Subsection 2.3, we will see that the electromagnetic and weak interactions must be treated together due to a mixing between the neutral gauge bosons of $SU(2)_L$ and $U(1)_Y$. After spontaneous symmetry breaking, given by

$$SU(2)_L \times U(1)_Y \rightarrow U(1)_{EM}, \tag{2.2}$$

we end with four gauge bosons mediating electroweak interactions, from which three are massive ($W^{\pm}, Z$) and one is massless (γ, the photon). The breaking pattern of Eq. (2.2) will be discussed in Subsection 2.4.

Strong and electroweak interactions can be studied separately in the SM. The reason is that the symmetry $SU(3)_C$ remains unbroken and does not mix with the $SU(2)_L \times U(1)_Y$ groups. This section will focus on the electroweak sector of the SM, where the problem of neutrino masses arises. The theory that describes strong interactions given through the color charge is called *quantum chromodynamics* (QCD). It has its own implications[1], and they will not be discussed here. For an introduction to QCD, the reader can be referred to, for example, [45, 46].

The symmetry group of the SM fixes the number and properties of the vector gauge bosons. Only one coupling constant is left as a free parameter for each of the groups $SU(3)_C$, $SU(2)_L$, and $U(1)_Y$, which are later determined by experiments. In contrast, the number and properties of the fermions and scalar gauge bosons are not constrained by the SM symmetry. What is constrained is that these must transform according to their group symmetries (they have to be representations of the groups) and must lead to cancellation of quantum anomalies (see Appendix A). The number of scalar bosons is chosen to implement the Higgs mechanism in a minimal way, and the number and properties of fermions are determined by experimental data. The known particle content in the SM is displayed in Figure 1, where particles are

---

[1]The main difference with respect to the electroweak sector is the strong character of the interaction at low energies, which does not allow perturbative approximations. The dynamics of QCD can be perturbatively solved only at high energies, where the effective coupling constant becomes small. This phenomenon is known as *asymptotic freedom*.
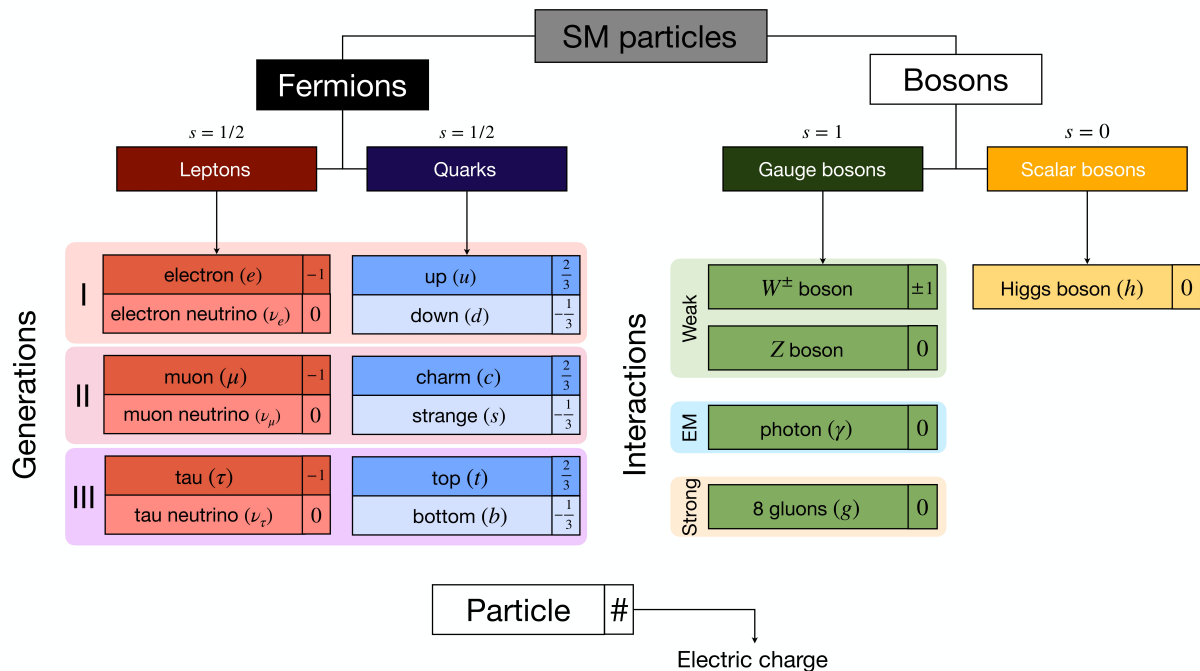
Figure 1: Scheme with the particle content of the SM, along with their spin and electromagnetic charges. The SM particles are divided into fermions and bosons. Each gauge boson carries a fundamental interaction, and each fermion is classified in three different generations.

distributed in families or generations, and classified according to their spin and charges.

Fundamental fermion particles follow Fermi-Dirac statistics and have a spin of $1/2$. The fermion sector is divided into two categories: quarks q and leptons ℓ. Quarks are affected by all the forces in the Standard Model (strong, weak, and electromagnetic), whereas leptons participate only in electroweak interactions. Quarks are the constituents of hadrons and do not exist as free particles; they possess both color and electric charge. Within leptons, there are charged leptons (e, μ, τ) and neutrinos $(\nu_e, \nu_\mu, \nu_\tau)$. Neutrinos are neutral under the electromagnetic interaction; hence, they interact only via the weak force. This organization is schematically represented in Fig. 2 resembling a Matryoshka doll, where weak interactions affect all particles, electromagnetic interactions exclude neutrinos, and strong interactions affect only quarks. As we will see in Subsection 2.2, the left-handed chiral components of the fermion fields are grouped into weak isospin doublets, while the right-handed components transform as singlets under the weak isospin group.

As we mentioned, quarks do not exist as free particles but in composite systems. This phenomenon is usually known as *color confinement*, a consequence of gluons having color charge. Quarks are confined in color-neutral composite particles called hadrons. Depending on the number of quarks, the hadrons are classified into baryons and mesons. A baryon is a color-neutral composite particle with three quarks (like the proton and neutron), and a meson has a quark-antiquark pair (like the pions).

The scalar boson, known as the Higgs particle (h), is neutral under the electromagnetic interaction. It comes from the Higgs mechanism, from which particles acquire mass. This mechanism is reviewed in Subsection 2.4.
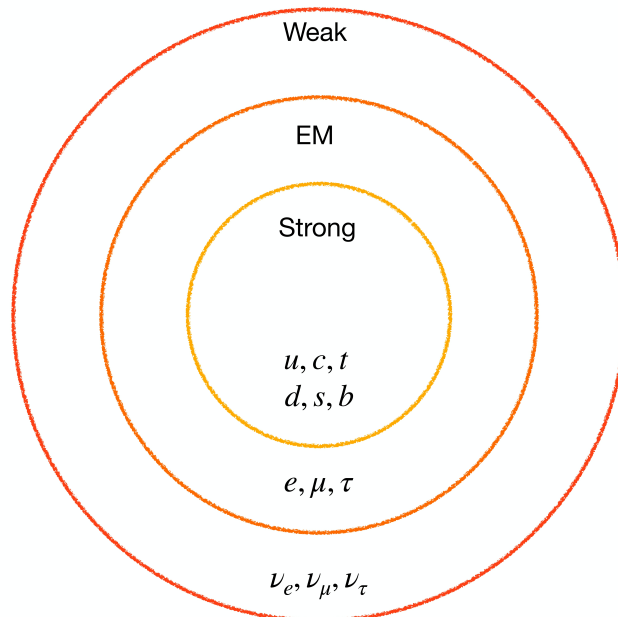
Figure 2: Fermion interaction scheme of the SM. Weak interactions affect all fermions, electromagnetic interactions do not affect neutrinos, and strong interactions affect only quarks.

In the fermion sector, the SM has 13 free parameters, including six quark masses, three charged lepton masses, three quark mixing angles, and one CP (charge-parity) violating phase. The gauge sector introduces three additional parameters arising from the coupling constants. Furthermore, QCD contributes a small parameter linked to the *strong CP problem*, while the Higgs sector introduces a Higgs mass and a *vacuum expectation value*, making a total of 19 independent free parameters when considering massless neutrinos. If the SM is minimally extended to incorporate massive neutrinos, more parameters are introduced, involving the three neutrino masses, three neutrino mixing angles, and an extra CP-violating phase. If neutrinos are Majorana particles, two extra Majorana phases must be considered.

2.2   Electroweak Standard Model Lagrangian

In order to study neutrino interactions, we review the electroweak part of the SM Lagrangian, which corresponds to the $SU(2)_L \times U(1)_Y$ part of the SM symmetry group.

The symmetry group $SU(2)_L$ is called *weak isospin* group. The left-handed chiral components of the fermion fields transform non-trivially under $SU(2)_L$, while the right-handed counterparts transform as singlets under weak isospin transformations. The group has three generators, represented by

$$I_a \qquad (a = 1, 2, 3), \tag{2.3}$$

which satisfy

$$[I_a, I_b] = i\, \varepsilon_{abc}\, I_c, \tag{2.4}$$

where ε_{abc} is the antisymmetric tensor with three indices, having $\varepsilon_{123} = 1$. In a two-dimensional representation of the group, the generators are $I_a = \tau_a/2$, where τ_1, τ_2, τ_3 are

the Pauli matrices.

The symmetry group $U(1)_Y$ is called *hypercharge* group. Its generator is the hypercharge operator Y, and it is connected to I_a by

$$Q = I_3 + Y, \tag{2.5}$$

where Q is the electric charge. Eq. (2.5) is known as the Gell-Mann - Nishijima relation [2] [47, 48], and implies the unification of weak and electromagnetic interactions.

To ensure local gauge invariance, it is necessary to introduce three vector gauge bosons W_a^μ ($a = 1, 2, 3$) associated with the three generators I_a of $SU(2)_L$ and one vector gauge boson B^μ associated with the generator Y of $U(1)_Y$. The covariant derivative D_μ, which replaces the standard derivative ∂_μ in the Lagrangian, is given by

$$D_\mu = \partial_\mu + ig\, \boldsymbol{W}_\mu \cdot \boldsymbol{I} + ig' B_\mu Y. \tag{2.6}$$

Here, the notation is

$$\boldsymbol{W}^\mu \equiv (W_1^\mu, W_2^\mu, W_3^\mu) \qquad \text{and} \qquad \boldsymbol{I} \equiv (I_1, I_2, I_3), \tag{2.7}$$

with the scalar product

$$\boldsymbol{W}^\mu \cdot \boldsymbol{I} \equiv \sum_{a=1}^{3} W_a^\mu I_a. \tag{2.8}$$

The covariant derivative in Eq. (2.6) has two coupling constants: g associated with the $SU(2)_L$ group, and g' associated with the $U(1)_Y$ group.

The fermion fields are accommodated into representations of the $SU(2)_L \times U(1)_Y$ group. The left-handed chiral components of the fermion fields form weak isospin doublets. Considering only the first generation of leptons and quarks for simplicity, we have

$$L_L = \begin{pmatrix} \nu_{eL} \\ e_L \end{pmatrix}, \qquad Q_L = \begin{pmatrix} u_L \\ d_L \end{pmatrix}. \tag{2.9}$$

With this choice of representation, we have

$$\boldsymbol{I}\, L_L = \frac{\boldsymbol{\tau}}{2} L_L, \qquad \boldsymbol{I}\, Q_L = \frac{\boldsymbol{\tau}}{2} Q_L, \tag{2.10}$$

where $\boldsymbol{\tau} = (\tau_1, \tau_2, \tau_3)$. Also,

$$Y\, L_L = Y_{L_L} L_L, \qquad Y\, Q_L = Y_{Q_L} Q_L, \tag{2.11}$$

where Y_{f_L} is the eigenvalue for the hypercharge. These values are presented in Table 1. The left-handed fermion fields transform as

$$L_L \to L_L' = \exp\left[i\,\boldsymbol{\theta}(x) \cdot \boldsymbol{I}^\ell + i\,\eta(x)\, Y^\ell\right] L_L \quad \text{and} \tag{2.12}$$

$$Q_L \to Q_L' = \exp\left[i\,\boldsymbol{\theta}(x) \cdot \boldsymbol{I}^q + i\,\eta(x)\, Y^q\right] Q_L. \tag{2.13}$$

---

[2]In the literature, it is also commonly defined as $Q = I_3 + Y'/2$. We will use Y, having $Y = Y'/2$. The inclusion of the $1/2$ factor in the hypercharge is a matter of convention.

In Eqs. (2.12) and (2.13), $\boldsymbol{\theta}(x)$ and $\eta(x)$ are 3 and 1 space-time dependent parameters respectively. The superscript ℓ and q in $\boldsymbol{I}$ and Y indicates the corresponding value of isospin and hypercharge for left-handed leptons and quarks.

In the SM, it is assumed that neutrino fields have only left-handed chiral components, implying that neutrinos are massless. However, it is now established that neutrinos have mass. The masses of neutrinos and their implications are reviewed in Section 3. For now, we will keep studying the SM with massless neutrinos. The right-handed components of the other fermions,

$$e_R, \quad u_R, \quad d_R, \tag{2.14}$$

are singlets under the weak isospin group. They transform as

$$f_R \to f_R' = \exp\left[i\,\eta(x)Y^f\right]f_R, \tag{2.15}$$

where Y^f is the hypercharge value for the corresponding right-handed fermion. Table 1 contains the values for the weak isospin, hypercharge and electric charge of the fermion doublets and singlets.

	Rep	I	I_3	Y	Q
lepton doublet	$\begin{pmatrix} \nu_{eL} \\ e_L \end{pmatrix}$	$1/2$	$\begin{pmatrix} 1/2 \\ -1/2 \end{pmatrix}$	$-1/2$	$\begin{pmatrix} 0 \\ -1 \end{pmatrix}$
lepton singlet	e_R	0	0	-1	-1
quark doublet	$\begin{pmatrix} u_L \\ d_L \end{pmatrix}$	$1/2$	$\begin{pmatrix} 1/2 \\ -1/2 \end{pmatrix}$	$1/6$	$\begin{pmatrix} 2/3 \\ -1/3 \end{pmatrix}$
quark singlets	u_R d_R	0 0	0 0	$2/3$ $-1/3$	$2/3$ $-1/3$

Table 1: Fermions in their representations of $SU(2)_L$ with their values for the weak isospin I, third component of weak isospin I_3, hypercharge Y and electric charge Q.

The electroweak SM Lagrangian is the most general renormalizable Lagrangian invariant under the local symmetry $SU(2)_L \times U(1)_Y$ constructed with the fermion fields, the gauge boson fields and a Higgs doublet $H(x)$ to be discussed in Subsection 2.4. Considering only

the first generation, the Lagrangian yields

$$
\begin{aligned}
\mathcal{L} = & \, i\overline{L_L}\,\slashed{D}\,L_L + i\overline{Q_L}\,\slashed{D}\,Q_L + \sum_{f=e,u,d} i\overline{f_R}\,\slashed{D}\,f_R \\
& - \frac{1}{4}\boldsymbol{W}_{\mu\nu}\boldsymbol{W}^{\mu\nu} - \frac{1}{4}B_{\mu\nu}B^{\mu\nu} \\
& + (D_\mu H)^\dagger (D^\mu H) - \mu^2 H^\dagger H - \lambda \left(H^\dagger H\right)^2 \\
& - y^e \left(\overline{L_L} H\, e_R + \overline{e_R}\, H^\dagger L_L\right) \\
& - y^d \left(\overline{Q_L} H\, d_R + \overline{d_R}\, H^\dagger Q_L\right) - y^u \left(\overline{Q_L}\, \widetilde{H}\, u_R + \overline{u_R}\, \widetilde{H}^\dagger Q_L\right),
\end{aligned}
\tag{2.16}
$$

where $\slashed{D} \equiv \gamma^\mu D_\mu$, and we define $\widetilde{H}$ as

$$
\widetilde{H} = i\tau_2\, H^*,
\tag{2.17}
$$

along with

$$
B_{\mu\nu} \equiv \partial_\mu B_\nu - \partial_\nu B_\mu,
\tag{2.18}
$$
$$
\boldsymbol{W}_{\mu\nu} \equiv \partial_\mu \boldsymbol{W}_\nu - \partial_\nu \boldsymbol{W}_\mu.
\tag{2.19}
$$

Defining

$$
U\left(\boldsymbol{\theta}(x), \eta(x)\right) = \exp\left[i\,\boldsymbol{\theta}(x)\cdot\boldsymbol{I} + i\,\eta(x)\,Y\right],
\tag{2.20}
$$

to maintain gauge invariance, the covariant derivative must transform as

$$
D_\mu \to D'_\mu = U\left(\boldsymbol{\theta}(x), \eta(x)\right) D_\mu\, U^{-1}\left(\boldsymbol{\theta}(x), \eta(x)\right),
\tag{2.21}
$$

implying the transformation for the gauge boson fields:

$$
\boldsymbol{W}_\mu \cdot \boldsymbol{I} \to \boldsymbol{W}'_\mu \cdot \boldsymbol{I} = U\left(\boldsymbol{\theta}(x), 0\right)\left[\boldsymbol{W}_\mu \cdot \boldsymbol{I} - \frac{i}{g}\partial_\mu\right] U^{-1}\left(\boldsymbol{\theta}(x), 0\right) \quad \text{and}
\tag{2.22}
$$

$$
B_\mu \to B'_\mu = B_\mu - \frac{1}{g'}\partial_\mu \eta(x).
\tag{2.23}
$$

2.3   Electroweak Interactions

Expanding the covariant derivative (2.6) in the Lagrangian (2.16), and omitting the kinetic terms, we obtain the electroweak interactions between the fermion and the boson fields:

$$
\begin{aligned}
\mathcal{L}_I = & -\frac{1}{2}\overline{L_L}\left(g\slashed{W}\cdot\boldsymbol{\tau} - g'\slashed{B}\right) L_L - \frac{1}{2}\overline{Q_L}\left(g\slashed{W}\cdot\boldsymbol{\tau} + \frac{1}{3}g'\slashed{B}\right) Q_L \\
& + g'\overline{e_R}\slashed{B}e_R - \frac{2}{3}g'\overline{u_R}\slashed{B}u_R + \frac{1}{3}g'\overline{d_R}\slashed{B}d_R.
\end{aligned}
\tag{2.24}
$$

Considering only the lepton sector, we have

$$
\mathcal{L}_{I,L} = -\frac{1}{2}\begin{pmatrix}\overline{\nu_{eL}} & \overline{e_L}\end{pmatrix}\begin{pmatrix} g\slashed{W}_3 - g'\slashed{B} & g\left(\slashed{W}_1 - i\slashed{W}_2\right) \\ g\left(\slashed{W}_1 + i\slashed{W}_2\right) & -g\slashed{W}_3 - g'\slashed{B}\end{pmatrix}\begin{pmatrix}\nu_{eL} \\ e_L\end{pmatrix} + g'\overline{e_R}\slashed{B}e_R.
\tag{2.25}
$$

The previous Lagrangian can be separated into a charged-current (CC) Lagrangian corresponding to the off-diagonal terms in Eq. (2.25), given by

$$
\mathcal{L}_{I,L}^{CC} = -\frac{g}{2}\left[\overline{\nu_{eL}}\left(\slashed{W}_1 - i\slashed{W}_2\right) e_L + \overline{e_L}\left(\slashed{W}_1 + i\slashed{W}_2\right)\nu_{eL}\right],
\tag{2.26}
$$

and a neutral-current (NC) Lagrangian corresponding to the diagonal terms:

$$\mathcal{L}_{I,L}^{NC} = -\frac{1}{2}\left[\overline{\nu_{eL}}\left(g\slashed{W}_3 - g'\slashed{B}\right)\nu_{eL} - \overline{e_L}\left(g\slashed{W}_3 + g'\slashed{B}\right)e_L - 2g'\overline{e_R}\slashed{B}e_R\right]. \tag{2.27}$$

Defining the field $W_\mu^\pm$ as

$$W_\mu^\pm \equiv \frac{W_\mu^1 \mp iW_\mu^2}{\sqrt{2}}, \tag{2.28}$$

the CC Lagrangian yields

$$\mathcal{L}_{I,L}^{CC} = -\frac{g}{2\sqrt{2}}\overline{\nu_e}\gamma^\mu\left(1 - \gamma^5\right)e\,W_\mu^+ + \text{h.c.}, \tag{2.29}$$

where we have applied the projection operator

$$f_L = P_L\,f \equiv \frac{1 - \gamma^5}{2}f \tag{2.30}$$

into the electron field. The bosons $W^\pm$ are known as the weak charged boson fields, carriers of the charged-current weak interactions.

Considering now the neutral-current Lagrangian, it is possible to perform a rotation of the fields W_3^μ and B^μ through an angle θ_W:

$$A^\mu = \sin\theta_W\,W_3^\mu + \cos\theta_W\,B^\mu, \tag{2.31}$$
$$Z^\mu = \cos\theta_W\,W_3^\mu - \sin\theta_W\,B^\mu. \tag{2.32}$$

Here, the boson A^μ is identified as the massless photon field, since the theory must include the electromagnetic interactions. The boson Z^μ is the neutral weak boson field, responsible of neutral-current weak interactions. The angle θ_W is known as the weak mixing angle, or Weinberg angle [1, 2]. Inserting Eqs. (2.31) and (2.32) into the CC Lagrangian, we obtain

$$\mathcal{L}_{I,L}^{NC} = -\frac{1}{2}\Bigg\{\overline{\nu_{eL}}\left[\left(g\cos\theta_W + g'\sin\theta_W\right)\slashed{Z} + \left(g\sin\theta_W - g'\cos\theta_W\right)\slashed{A}\right]\nu_{eL}$$
$$- \overline{e_L}\left[\left(g\cos\theta_W - g'\sin\theta_W\right)\slashed{Z} + \left(g\sin\theta_W + g'\cos\theta_W\right)\slashed{A}\right]e_L \tag{2.33}$$
$$- 2g'\overline{e_R}\left[-\sin\theta_W\slashed{Z} + \cos\theta_W\slashed{A}\right]e_R\Bigg\}.$$

Neutrinos are neutral particles. Therefore, they do not couple to the photon field. This implies the relation

$$g\sin\theta_W = g'\cos\theta_W \qquad \Rightarrow \qquad \tan\theta_W = \frac{g'}{g}. \tag{2.34}$$

Using Eq. (2.34), we finally obtain

$$\mathcal{L}_{I,L}^{NC} = -\frac{g}{2\cos\theta_W}\left[\overline{\nu_{eL}}\slashed{Z}\nu_{eL} - \left(1 - 2\sin^2\theta_W\right)\overline{e_L}\slashed{Z}e_L + 2\sin^2\theta_W\,\overline{e_R}\slashed{Z}e_R\right] + g\sin\theta_W\,\bar{e}\slashed{A}e. \tag{2.35}$$

We identify the electromagnetic coupling in the last term with

$$g \sin \theta_W = e, \tag{2.36}$$

where e is the elementary electric charge. Using again Eq. (2.34), the following relation holds:

$$g^2 + g'^2 = e^2. \tag{2.37}$$

The derivation of weak interactions for quarks is completely analogous. Also, the generalization for three generations is straightforward. For reference, the complete derivation can be found in [44]. Charged-current and neutral-current interactions, generalized to quarks and three generations, are given through the Lagrangian

$$
\begin{aligned}
\mathcal{L}_I = & -\frac{g}{2\sqrt{2}} \sum_i \overline{\Psi}_i \gamma^\mu \left(1 - \gamma^5\right) \left(T^+ W_\mu^+ + T^- W_\mu^-\right) \Psi_i \\
& - e \sum_i Q_i \overline{\Psi}_i \gamma^\mu \Psi_i A_\mu - \frac{g}{2\cos\theta_{\theta_W}} \sum_i \overline{\Psi}_i \gamma^\mu \left(g_V^i - g_A^i \gamma^5\right) \Psi_i Z_\mu,
\end{aligned} \tag{2.38}
$$

where T^+ and T^- are weak isospin raising and lowering operators, and the vector and axial-vector couplings g_V^i and g_A^i are given by

$$g_V^i \equiv t_{3L}(i) - 2Q_i \sin^2 \theta_W, \tag{2.39}$$

$$g_A^i \equiv t_{3L}(i). \tag{2.40}$$

In definitions (2.39) and (2.40), $t_{3L}(i)$ is the weak isospin of fermion i and Q_i is the charge of Ψ_i.

2.4 Higgs Mechanism and Electroweak Symmetry Breaking

The Higgs mechanism [49–51] provides masses for the $W^\pm$ and Z gauge bosons, as well as for the fermions. This mechanism is implemented by the Higgs doublet

$$H(x) = \begin{pmatrix} H^+(x) \\ H^0(x) \end{pmatrix}, \tag{2.41}$$

where $H^+(x)$ is a charged complex scalar field and $H^0(x)$ is a neutral complex scalar field. The gauge quantum numbers for the Higgs field are listed in Table 2. The Higgs doublet

		I	I_3	Y	Q
Higgs doublet	$H(x) \equiv \begin{pmatrix} H^+(x) \\ H^0(x) \end{pmatrix}$	$1/2$	$\begin{pmatrix} 1/2 \\ -1/2 \end{pmatrix}$	$1/2$	$\begin{pmatrix} 1 \\ 0 \end{pmatrix}$

Table 2: Higgs doublet with its values for the weak isospin I, third component of weak isospin I_3, hypercharge Y and electric charge Q.

transforms as

$$H \to H' = \exp\left[\frac{i}{2}\boldsymbol{\theta}(x) \cdot \boldsymbol{\tau} + \frac{i}{2}\eta(x)\right] H. \tag{2.42}$$

Taking the Higgs sector of the Lagrangian in Eq. (2.16), we have

$$\mathcal{L}_{\text{Higgs}} = (D_\mu H)^\dagger (D^\mu H) - V(H), \tag{2.43}$$

where the Higgs potential is given by

$$V(H) = \mu^2 H^\dagger H + \lambda \left(H^\dagger H\right)^2. \tag{2.44}$$

Whereas the coefficient λ must be positive to ensure that the potential $V(H)$ is bounded from below, the coefficient μ^2 can be assumed negative. Defining

$$v \equiv \sqrt{-\frac{\mu^2}{\lambda}}, \tag{2.45}$$

the Higgs potential can be rewritten as

$$V(H) = \lambda \left(H^\dagger H - \frac{v^2}{2}\right)^2, \tag{2.46}$$

where we have neglected a constant term $v^4/4$. The minimum of the potential is then achieved when

$$H^\dagger H \to \frac{v^2}{2}. \tag{2.47}$$

The minimum of the potential corresponds to the vacuum, namely, the lowest energy state. Fermions and vector bosons must possess a vanishing value in the vacuum to preserve Lorentz invariance. Similarly, charged scalar must also have a vanishing value in the vacuum, since the vacuum is electrically neutral. However, neutral scalar fields can possess a nonzero value for the vacuum, which is called the *vacuum expectation value* or *VEV*. Therefore, the Higgs field acquires a VEV $\langle H \rangle$ given by

$$\langle H \rangle = \frac{1}{\sqrt{2}} \begin{pmatrix} 0 \\ v \end{pmatrix}. \tag{2.48}$$

In the vacuum, the symmetry $SU(2)_L \times U(1)_Y$ is spontaneously broken by the VEV $\langle H \rangle$, since it transforms non trivially:

$$\begin{aligned}
I_1 \langle H \rangle &= \frac{\tau_1}{2} \langle H \rangle = \frac{1}{2\sqrt{2}} \begin{pmatrix} v \\ 0 \end{pmatrix} \neq 0, \\
I_2 \langle H \rangle &= \frac{\tau_2}{2} \langle H \rangle = -\frac{i}{2\sqrt{2}} \begin{pmatrix} v \\ 0 \end{pmatrix} \neq 0, \\
I_3 \langle H \rangle &= \frac{\tau_3}{2} \langle H \rangle = -\frac{1}{2\sqrt{2}} \begin{pmatrix} 0 \\ v \end{pmatrix} \neq 0, \\
Y \langle H \rangle &= \frac{1}{2} \langle H \rangle = \frac{1}{2\sqrt{2}} \begin{pmatrix} 0 \\ v \end{pmatrix} \neq 0.
\end{aligned} \tag{2.49}$$

On the other hand,

$$Q\langle H \rangle = (I_3 + Y)\langle H \rangle = 0, \tag{2.50}$$

which implies that the vacuum is invariant under gauge transformations belonging to the group $U(1)_{EM}$:

$$e^{iQ}\langle H \rangle = \langle H \rangle. \tag{2.51}$$

The invariance under this symmetry ensures the existence of a massless gauge boson associated with the $U(1)_{EM}$ group, which is identified with the photon. Consequently, we have the spontaneous symmetry breaking (SSB) represented by

$$SU(2)_L \times U(1)_Y \xrightarrow{\text{SSB}} U(1)_{EM}. \tag{2.52}$$

The breaking of the $SU(2)_L \times U(1)_Y$ symmetry to a $U(1)_{EM}$ is known as *Electroweak Symmetry Breaking* (EWSB).

In the unitary gauge, in which the physical states appear explicitly, the Higgs doublet can be defined as

$$H(x) = \frac{1}{\sqrt{2}} \begin{pmatrix} 0 \\ v + h(x) \end{pmatrix}, \tag{2.53}$$

where $h(x)$ is the physical Higgs boson, corresponding to excitations of the neutral Higgs field above the vacuum. Inserting Eq. (2.53) in the Lagrangian (2.43), using the covariant derivative (2.6) and expanding terms, we finally obtain

$$
\begin{aligned}
\mathcal{L}_{\text{Higgs}} =& \frac{1}{2} \left(\partial h \right)^2 - \lambda v^2 h^2 - \lambda v h^3 - \frac{\lambda}{4} h^4 + \frac{g^2 v^2}{4} W_\mu^- W^{\mu+} + \frac{g^2 v^2}{8 \cos^2 \theta_W} Z_\mu Z^\mu \\
&+ \frac{g^2 v}{2} W_\mu^- W^{\mu+} h + \frac{g^2 v}{4 \cos^2 \theta_W} Z_\mu Z^\mu h \\
&+ \frac{g^2}{4} W_\mu^- W^{\mu+} h^2 + \frac{g^2}{8 \cos^2 \theta_W} Z_\mu Z^\mu h^2.
\end{aligned}
\tag{2.54}
$$

The second term in Eq. (2.54) is the mass term for the Higgs field, given by

$$m_h = \sqrt{2\lambda v^2}. \tag{2.55}$$

The first observation of the Higgs particle was carried out in [52, 53]. Using experimental data, the values for the Higgs mass and the VEV v yield

$$m_h = 125.25 \pm 0.17 \text{ GeV}, \qquad \text{and} \qquad v = 246.22 \text{ GeV}. \tag{2.56}$$

The fifth and sixth terms give the masses for the $W^\pm$ and Z bosons:

$$m_W = \frac{gv}{2}, \qquad m_Z = \frac{gv}{2 \cos \theta_W}. \tag{2.57}$$

Their values were first obtained experimentally in [54, 55], giving[3]

$$M_Z = 91.1875 \pm 0.0021 \text{ GeV} \qquad \text{and} \qquad M_W = 80.376 \pm 0.033 \text{ GeV}. \tag{2.58}$$

2.5 Charged lepton masses

Fermion masses arises as a consequence of the Higgs mechanism through the Yukawa interactions between the fermions and the Higgs doublet.

---

[3]These values correspond to the pole masses.

A fermion mass term is built with the coupling of a left-handed with a right-handed field[4]. The Dirac mass terms are of the form

$$\bar{f}\, f = \overline{f_L} f_R + \overline{f_R} f_L,$$ (2.59)

which are forbidden by gauge symmetry given that left-handed and right-handed fields transform differently under $SU(2)_L \times U(1)_Y$. Lepton masses come from the fourth line of the Lagrangian (2.16), which, generalized to three generations, is

$$\mathcal{L}_{H,L} = -\sum_{\alpha,\beta=e,\mu,\tau} Y'^{\ell}_{\alpha\beta}\, \overline{L'_{\alpha L}}\, H\, \ell'_{\beta R} + \text{h.c.}$$ (2.60)

The matrix Y'^{ℓ} of Yukawa couplings is, in general, a non-diagonal complex 3×3 matrix. In the unitary gauge, with the Higgs acquiring a VEV v, Eq. (2.60) becomes

$$\mathcal{L}_{H,L} = -\left(\frac{v+h}{\sqrt{2}}\right) \sum_{\alpha,\beta=e,\mu,\tau} Y'^{\ell}_{\alpha\beta}\, \overline{\ell'_{\alpha L}}\, \ell'_{\beta R} + \text{h.c.}$$ (2.61)

The term proportional to v is a mass term for the charged lepton, while the term proportional to h represent a coupling to the Higgs boson. Since Y'^{ℓ} is in general non-diagonal, fields e', μ', τ' do not have definite masses. To have definite masses, is necessary to diagonalize the matrix Y'^{ℓ}. Defining the arrays

$$\boldsymbol{\ell}'_L = \begin{pmatrix} e'_L \\ \mu'_L \\ \tau'_L \end{pmatrix} \qquad \text{and} \qquad \boldsymbol{\ell}'_R = \begin{pmatrix} e'_R \\ \mu'_R \\ \tau'_R \end{pmatrix},$$ (2.62)

the Higgs-lepton Yukawa Lagrangian can be written as

$$\mathcal{L}_{H,L} = -\left(\frac{v+h}{\sqrt{2}}\right) \overline{\boldsymbol{\ell}'_L}\, Y'^{\ell}\, \boldsymbol{\ell}'_R + \text{h.c.}$$ (2.63)

The Yukawa matrix Y'^{ℓ} can be diagonalized as

$$V_L^{\ell\dagger}\, Y'^{\ell}\, V_R^{\ell} = Y^{\ell}, \quad \text{with} \quad Y^{\ell}_{\alpha\beta} = y^{\ell}_{\alpha}\, \delta_{\alpha\beta} \quad (\alpha,\beta = e,\mu,\tau),$$ (2.64)

with y^{ℓ}_{α} real and positive. Here, V_L^{ℓ} and V_R^{ℓ} are 3×3 unitary matrices. Defining the transformations

$$\boldsymbol{\ell}_L = V_L^{\ell\dagger}\, \boldsymbol{\ell}'_L \equiv \begin{pmatrix} e_L \\ \mu_L \\ \tau_L \end{pmatrix}, \qquad \boldsymbol{\ell}_R = V_R^{\ell\dagger}\, \boldsymbol{\ell}'_R \equiv \begin{pmatrix} e_R \\ \mu_R \\ \tau_R \end{pmatrix},$$ (2.65)

we can write the diagonalized Lagrangian as

$$\begin{aligned}
\mathcal{L}_{H,L} &= -\left(\frac{v+h}{\sqrt{2}}\right) \overline{\boldsymbol{\ell}_L}\, Y^{\ell}\, \boldsymbol{\ell}_R + \text{h.c.} \\
&= -\left(\frac{v+h}{\sqrt{2}}\right) \sum_{\alpha=e,\mu,\tau} y^{\ell}_{\alpha}\, \overline{\ell_{\alpha L}} \ell_{\alpha R} + \text{h.c.}
\end{aligned}$$ (2.66)

---

[4]The coupling between two right-handed or two left-handed fields is identically zero since $m\overline{\Psi_R}\Psi_R = m\overline{\Psi}P_L\, P_R\Psi = 0 = m\overline{\Psi_L}\Psi_L$, by the property $P_L\, P_R = 0$.

Using the Dirac fields

$$\ell_\alpha = \ell_{\alpha L} + \ell_{\alpha R} \qquad (\alpha = e, \mu, \tau), \tag{2.67}$$

we obtain

$$\mathcal{L}_{H,L} = - \sum_{\alpha = e, \mu, \tau} \frac{y_\alpha^\ell v}{\sqrt{2}} \, \overline{\ell_\alpha} \ell_\alpha - \sum_{\alpha = e, \mu, \tau} \frac{y_\alpha^\ell}{\sqrt{2}} \, \overline{\ell_\alpha} \ell_\alpha h. \tag{2.68}$$

Therefore, the masses for the charged leptons are given by

$$m_\alpha = \frac{y_\alpha^\ell v}{\sqrt{2}} \qquad (\alpha = e, \mu, \tau). \tag{2.69}$$

The masses m_α can be considered as free parameters of the SM and are obtained experimentally. With those results, the Yukawa coefficients y_α^ℓ can be extracted. From Eq. (2.69), it can be seen that the trilinear coupling between the charged leptons and the Higgs boson is proportional to the charged lepton mass.

Now we analyze the charged and neutral interactions under transformations (2.65). The CC Lagrangian for leptons is

$$\mathcal{L}_{I,L}^{CC} = - \frac{g}{2\sqrt{2}} \sum_{\alpha = e, \mu, \tau} \overline{L_\alpha'} \gamma^\mu \left(1 - \gamma^5\right) \left(T^+ W_\mu^+ + T^- W_\mu^-\right) L_\alpha'. \tag{2.70}$$

Defining the array

$$\boldsymbol{\nu}_L' \equiv \begin{pmatrix} \nu_{eL}' \\ \nu_{\mu L}' \\ \nu_{\tau L}' \end{pmatrix}, \tag{2.71}$$

the Lagrangian (2.70) can be written as

$$\begin{aligned}
\mathcal{L}_{I,L}^{CC} &= - \frac{g}{2\sqrt{2}} \, \overline{\boldsymbol{\nu}_L'} \gamma^\mu \, \boldsymbol{\ell}_L' \, W_\mu^+ + \text{h.c.} \\
&= - \frac{g}{2\sqrt{2}} \, \overline{\boldsymbol{\nu}_L'} \gamma^\mu \left(V_L^\ell \, \boldsymbol{\ell}_L\right) W_\mu^+ + \text{h.c.}
\end{aligned} \tag{2.72}$$

We can transform the massless neutrino fields as

$$\boldsymbol{\nu}_L = V_L^{\ell\dagger} \, \boldsymbol{\nu}_L' \equiv \begin{pmatrix} \nu_{eL} \\ \nu_{\mu L} \\ \nu_{\tau L} \end{pmatrix}. \tag{2.73}$$

Therefore, the CC Lagrangian yields

$$\begin{aligned}
\mathcal{L}_{I,L}^{CC} &= - \frac{g}{2\sqrt{2}} \, \overline{\boldsymbol{\nu}_L} \gamma^\mu \, \boldsymbol{\ell}_L \, W_\mu^+ + \text{h.c.} \\
&= - \frac{g}{2\sqrt{2}} \sum_{\alpha = e, \mu, \tau} \overline{\nu_{\alpha L}} \, \gamma^\mu \, \ell_{\alpha L} \, W_\mu^+ + \text{h.c.}
\end{aligned} \tag{2.74}$$

The neutrino fields ν_e, ν_μ, ν_τ are called *flavor neutrino fields*, since each of them couples with the corresponding charged lepton in the charged weak interaction given by Eq. (2.74). In the SM, with the assumption of massless neutrinos, these fields are also mass eigenstates. In

Section 3, we will see that this is not longer true for massive neutrinos, implying neutrino oscillations.

In the case of neutral interactions, it can be shown that the NC Lagrangian for leptons remains the same after transformations (2.65) and (2.73).

The case for quark masses is slightly different from the lepton case, since all quarks possess a right-handed component and are massive, in contrast to neutrino fields. This difference implies the existence of mixing between mass and flavor eigenstates in the quark sector, described by the CKM matrix [56, 57]. Rather than reviewing quark masses, we will focus on the scenario with a right-handed neutrino in Section 3.

As can be seen from Eq. (2.74), weak interactions between leptons conserve a quantum number called *flavor lepton number*. The assignment is shown in Table 3. Furthermore,

Fields	L_e	L_μ	L_τ
(ν_e, e^-)	+1	0	0
(ν_μ, μ^-)	0	+1	0
(ν_τ, τ^-)	0	0	+1

Table 3: Flavor lepton number assignment. For antiparticles, the corresponding number is -1.

lepton number, defined as $L = 1$ for leptons and $L = -1$ for antileptons, is conserved. This conservation is related to the invariance of the Lagrangian under a global $U(1)_\ell$ symmetry[5]. Something similar happens in processes involving baryons, where a global symmetry $U(1)_B$ can be associated to baryon number conservation. If a baryon number is assigned as $B = 1$ for baryons and $B = -1$ for antibaryons, then B is conserved in weak interactions. However, this symmetry is anomalous in the SM, which means that while it is preserved at the classical level, it is broken at the quantum level.

From these two conserved numbers, it follows that another symmetry, $U(1)_{B-L}$, exists, where $B-L$ represents the difference between baryon number and lepton number. Unlike $U(1)_\ell$ and $U(1)_B$, this symmetry can be anomaly free when three right-handed neutrinos are considered. For further discussion regarding anomalies in symmetries, see Appendix A.

In BSM physics, the non-conservation of lepton number plays an important role, as we will see in following sections.

---

[5]Note that we have used ℓ instead of L for the lepton number symmetry group, to avoid confusion with left-chirality.

3 Basics of Neutrino Physics

In this section, we shortly review the neutrino interactions in the SM, which were introduced in the previous section. We now consider massive neutrinos, extending the SM with right-handed neutrinos and introducing Majorana mass terms. We also study an important consequence of the existence of neutrino masses: neutrino mixing and oscillations. For a more complete review concerning neutrinos in general, see for example [44, 58].

3.1 Neutrinos in the SM

As discussed in the previous section, neutrinos are spin $1/2$ fermions that have neither color nor electric charge. Therefore, they are singlets of the subgroup $SU(3)_C \times U(1)_{EM}$. Neutrinos are part of the lepton doublets

$$L_{L\ell} = \begin{pmatrix} \nu_\ell \\ \ell \end{pmatrix}_L,$$ (3.1)

where f_L is the left-handed component of the fermion f, with $f_L = P_L\, f \equiv \frac{1-\gamma_5}{2}\, f$. Neutrinos that appear in these doublets are called *active neutrinos*, *left-handed neutrinos* or *light neutrinos*. In the SM, there is one active neutrino for each charged lepton, $\ell = e, \mu, \tau$, and no right-handed neutrinos. Active neutrinos only interact through weak forces with the exchange of Z and $W^\pm$ bosons. These interactions, invariant under $SU(2)_L$, are given by

$$\mathcal{L}_{CC} = -\frac{g}{\sqrt{2}} \sum_\ell \bar{\nu}_{L\ell}\, \gamma^\mu\, \ell_L^-\, W_\mu^+ + \text{h.c.} \qquad \text{and}$$ (3.2)

$$\mathcal{L}_{NC} = -\frac{g}{2\cos\theta_W} \sum_\ell \bar{\nu}_{L\ell}\, \gamma^\mu\, \nu_{L\ell}\, Z_\mu.$$ (3.3)

Here, g is the coupling constant of $SU(2)$ and θ_W is the Weinberg angle, as reviewed in Section 2. Eq. (3.2) corresponds to weak charged-current interactions (CC) where neutrinos interact with their associated charged leptons, and Eq. (3.3) represents neutral-current interactions (NC) where neutrinos interact with themselves. From the latter, the decay width of the Z boson into light neutrinos can be obtained. Thus, a measurement of the total decay width can indicate the number of active neutrinos. In Z decays produced in electron-positron collisions by the ALEPH, DELPHI, L3 and OPAL experiments at LEP and the SLD experiment at SLC, both reported in [54], such measurements give the result

$$N_\nu = 2.9840 \pm 0.0082.$$ (3.4)

The corresponding plot is displayed in Fig. 3, where the hadron production cross section measurements are shown around the Z resonance. Predicted cross sections for 2, 3 and 4 neutrinos are plotted considering SM couplings and negligible masses for fermions. Therefore, in the SM and in any extension of it, there should be three, and only three, light left-handed neutrinos, provided that

$$m_\nu < \frac{m_Z}{2}.$$ (3.5)

3.2 Neutrino Masses

The absence of right-handed neutrinos in the SM forbids mass terms for light neutrinos at the Lagrangian level. This led to the construction of the SM with the assumption of
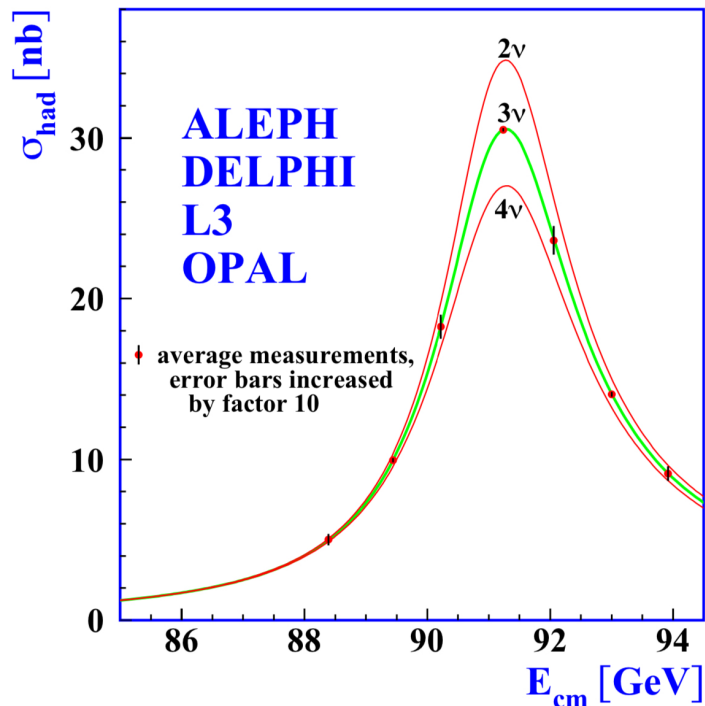
Figure 3: Hadron production cross section measurements around the Z resonance. The predicted cross sections for two, three and four neutrinos are shown. Plot from [54].

massless neutrino fields. However, recent experimental evidence, including the PLANCK collaboration [12], the KATRIN experiment [35, 36] and the observation of neutrino oscillations [23–34], indicates that at least two neutrinos must carry a mass of the order of 1 eV. The arising question is how this mass can be obtained within the SM framework. A minimal way to accomplish neutrino masses is adding a right-handed neutrino to the SM, obtaining the *minimally extended Standard Model*. Such addition allows two possible mass terms: Dirac masses and Majorana masses.

3.2.1 Dirac Fermion Masses

By adding right-handed neutrinos to the SM, it is possible to obtain neutrino masses from the Higgs mechanism. This extension consists in the introduction of right-handed components $\nu_{\alpha R}$ of the neutrino fields ($\alpha = e, \mu, \tau$).

With these new fields, Dirac mass terms can be constructed as

$$Y_{ij}^{\nu} \, \overline{L^i} \, \widetilde{H} \, \nu_R^j, \tag{3.6}$$

where $\widetilde{H}$ was first introduced in Eq. (2.17), with $\widetilde{H} = i\tau_2 H^*$. This transformation gives a Higgs doublet with hypercharge $Y = -1/2$. Since L^i and $\widetilde{H}$ have the same weak and hypercharge quantum numbers, ν_R must be neutral under both the weak and electromagnetic force to maintain gauge invariance. Therefore, ν_R is a gauge singlet under the SM, and it is usually referred as *sterile neutrino*, as its only interaction is gravitational.

It is important to note that these sterile neutrinos do not play a role in SM quantum anomalies (see Appendix A). Hence, the number of right-handed neutrino fields added is

28

not limited by anomaly cancellation constraints on the SM symmetry groups[6]. However, because of neutrino oscillation experiments, at least two right-handed neutrinos are needed to reproduce experimental data.

With the insertion of three right-handed neutrinos, the SM Higgs-lepton Yukawa Lagrangian in Eq. (2.60) is extended, giving

$$\mathcal{L}_{H,L} = - \sum_{\alpha,\beta=e,\mu,\tau} Y'^{\ell}_{\alpha\beta} \, \overline{L_{\alpha L}} \, H \, \ell'_{\beta R} - \sum_{\alpha,\beta=e,\mu,\tau} Y'^{\nu}_{\alpha\beta} \, \overline{L_{\alpha L}} \, \widetilde{H} \, \nu'_{\beta R} + \text{h.c.}, \tag{3.7}$$

where Y'^{ν} is a new matrix of Yukawa couplings. After SSB, the Lagrangian can be written as

$$\mathcal{L}_{H,L} = - \left(\frac{v+h}{\sqrt{2}}\right) \left[\overline{\boldsymbol{\ell}'_L} Y'^{\ell} \boldsymbol{\ell}'_R + \overline{\boldsymbol{\nu}'_L} Y'^{\nu} \boldsymbol{\nu}'_R\right] + \text{h.c.}, \tag{3.8}$$

with the arrays $\boldsymbol{\ell}'_L, \boldsymbol{\ell}'_R$ and $\boldsymbol{\nu}'_L$ defined in Eqs. (2.62) and (2.71), and the new array for right-handed neutrinos given by

$$\boldsymbol{\nu}'_R = \begin{pmatrix} \nu'_{eR} \\ \nu'_{\mu R} \\ \nu'_{\tau R} \end{pmatrix}. \tag{3.9}$$

The Yukawa matrix Y'^{ν} can be diagonalized as

$$V_L^{\nu\dagger} Y'^{\nu} V_R^{\nu} = Y^{\nu}, \quad \text{with} \quad Y^{\nu}_{kj} = y^{\nu}_k \delta_{kj} \quad (k,j=1,2,3), \tag{3.10}$$

with y^{ν}_k real and positive, and V_L^{ν} and V_R^{ν} being 3×3 unitary matrices. Defining the transformations

$$\boldsymbol{n}_L = V_L^{\nu\dagger} \boldsymbol{\nu}_L \equiv \begin{pmatrix} \nu_{1L} \\ \nu_{2L} \\ \nu_{3L} \end{pmatrix}, \qquad \boldsymbol{n}_R = V_R^{\nu\dagger} \boldsymbol{\nu}_R \equiv \begin{pmatrix} \nu_{1R} \\ \nu_{2R} \\ \nu_{3R} \end{pmatrix}, \tag{3.11}$$

together with transformations (2.65) we can write the diagonalized Lagrangian as

$$\begin{aligned}
\mathcal{L}_{H,L} &= - \left(\frac{v+h}{\sqrt{2}}\right) \left[\overline{\boldsymbol{\ell}_L} Y^{\ell} \boldsymbol{\ell}_R + \overline{\boldsymbol{n}_L} Y^{\nu} \boldsymbol{n}_R\right] + \text{h.c.} \\
&= - \left(\frac{v+h}{\sqrt{2}}\right) \left[\sum_{\alpha=e,\mu,\tau} y^{\ell}_{\alpha} \, \overline{\ell_{\alpha L}} \ell_{\alpha R} + \sum_{k=1}^{3} y^{\nu}_k \, \overline{\nu_{kL}} \nu_{kR}\right] + \text{h.c.}
\end{aligned} \tag{3.12}$$

Using the Dirac fields of Eq. (2.67) and

$$\nu_k = \nu_{kL} + \nu_{kR} \qquad (k=1,2,3), \tag{3.13}$$

we obtain

$$\mathcal{L}_{H,L} = - \sum_{\alpha=e,\mu,\tau} \frac{y^{\ell}_{\alpha} v}{\sqrt{2}} \, \overline{\ell}_{\alpha} \ell_{\alpha} - \sum_{k=1}^{3} \frac{y^{\nu}_k v}{\sqrt{2}} \, \overline{\nu}_k \nu_k - \sum_{\alpha=e,\mu,\tau} \frac{y^{\ell}_{\alpha}}{\sqrt{2}} \, \overline{\ell}_{\alpha} \ell_{\alpha} \, h - \sum_{k=1}^{3} \frac{y^{\nu}_k}{\sqrt{2}} \, \overline{\nu}_k \nu_k \, h. \tag{3.14}$$

---

[6]As we discuss in Appendix A, if an additional symmetry is considered, for example, $U(1)_{B-L}$, then the number and charges of right-handed neutrinos can be constrained to maintain an anomaly free symmetry.

Therefore, neutrino masses are given by

$$m_k = \frac{y_k^\nu \, v}{\sqrt{2}} \qquad (k = 1, 2, 3). \tag{3.15}$$

With this derivation, neutrino masses are proportional to the Higgs VEV, v, in the same way that the rest of particles in the SM do. However, the masses of neutrinos are much smaller than those of quarks and charged leptons. For example, the mass of the lightest charged lepton, the electron, is $m_e \approx 0.511$ MeV. Given that $v = 246.22$ GeV, this implies a Yukawa coefficient of $y_e \sim 10^{-6}$. Now, considering a neutrino with mass $m_\nu \sim 10^{-12}$ GeV, its Yukawa coefficient would be $y^\nu \sim 10^{-15}$. In the minimally extended Standard Model, there is no explanation for the very small values of y_k^ν.

3.2.2 Majorana Neutrinos and Majorana Mass Term

Quantum Field Theory must be invariant under CPT transformations (charge conjugation, parity and time reversal)[7]. As such, the theory must contain the CPT conjugate of a neutrino field with spin $\pm 1/2$ and momentum $\vec{p}$, which corresponds to an antineutrino:

$$CPT \, |\nu \, (\vec{p}, \pm 1/2)\rangle = |\bar{\nu} \, (\vec{p}, \mp 1/2)\rangle. \tag{3.16}$$

Other fermions in the Standard Model are distinguishable from their respective CPT conjugates because of electric charge. However, in the case of neutrinos, there is no way to distinguish a neutrino and an antineutrino unless there is an additional quantum number. If this extra symmetry exists, then neutrinos and antineutrinos are distinguishable and they are *Dirac* particles. A natural example of this extra symmetry is lepton number, introduced in Subsection 2.5. If this is not the case, then neutrinos are the same as their antineutrinos and therefore they are defined as *Majorana* particles.

We define the charge conjugation transformation $\mathcal{C}$ as

$$\psi \xrightarrow{\mathcal{C}} C \, \overline{\psi}^T \equiv \psi^c, \tag{3.17}$$

which transforms a particle into its antiparticle. The matrix C is the charge conjugation matrix, represented in the Dirac basis with

$$C = -i\gamma^0\gamma^2, \tag{3.18}$$

where γ^i are the Dirac matrices. The charge conjugated field ψ^c transforms with the opposite chirality of ψ:

$$P_{L,R}\,\psi = \psi_{L,R} \xrightarrow{\mathcal{C}} \left(\psi_{L,R}^c\right) = (\psi^c)_{R,L} = P_{R,L}\,\psi^c. \tag{3.19}$$

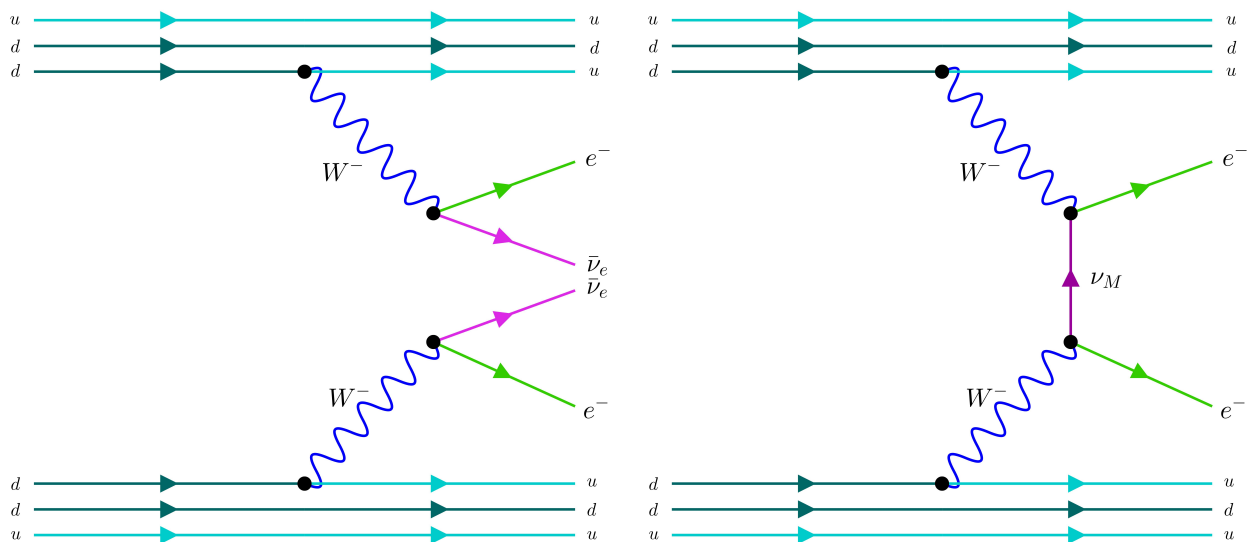Defining a Majorana field as

$$\psi_M = \psi_L + \psi_L^c, \tag{3.20}$$

the Majorana condition reads

$$\psi_M = \psi_M^c. \tag{3.21}$$

If neutrinos are Majorana fields, then a Majorana mass term can be constructed using only left-handed neutrinos as

$$m_L \, \overline{\nu_L^c} \nu_L + \text{h.c.} \tag{3.22}$$

---

[7]A proof can be found in [59]. For a rigorous proof, see [60].

(a) Ordinary neutrino double beta decay ($2\nu\beta\beta$). (b) Neutrinoless double beta decay ($0\nu\beta\beta$).

Figure 4: In 4a, ordinary neutrino double beta decay with two electrons and two electron antineutrinos emitted from the decaying nucleus. In 4b, neutrinoless double beta decay, where only electrons are emitted. This process violates lepton number by two, and it is only possible if neutrinos are Majorana particles.

This term is Lorentz-invariant, since ν_L^c transforms as a right-handed field. If a lepton number $L = 1$ is assigned to neutrinos, Eq. (3.22) violates it by two units, i.e, $\Delta L = 2$. Furthermore, it also violates $U(1)_Y$ and $SU(2)_L$, but preserves $U(1)_{EM}$ [8]. Hence, if it exists, then it should be derived from a theory beyond the SM.

If right-handed neutrinos are considered, the most general mass expression including Dirac and Majorana terms is written as

$$m_D\, \overline{\nu_R}\nu_L + \frac{1}{2}m_L\, \overline{\nu_L^c}\nu_L + \frac{1}{2}m_R\, \overline{\nu_R^c}\nu_R + \text{h.c.,} \tag{3.23}$$

where m_D has the form of Eq. (3.15). The possibilities for this mass term are

- $m_L = m_R = 0$: Dirac neutrinos with mass m_D.

- $m_D = 0$: ν_L and ν_R are both Majorana neutrinos with masses m_L and m_R, respectively.

- $m_D \neq 0$ and at least $m_R \neq 0$ or $m_L \neq 0$: neutrinos are Majorana, and their masses are obtained diagonalizing the mass matrix. As we will see in Subsection 4.2, the case for $m_L = 0$ and $m_R \neq 0$ corresponds to the so-called *seesaw mechanism*.

If neutrinos are Majorana particles, there is a possibility to measure the neutrinoless double beta decay process [37], displayed in Fig. 4. However, this process has never been observed despite experimental efforts [38–41]. Consequently, when neutrino masses are studied with SM extensions, both natures, Majorana and Dirac, are still considered.

---

[8]Note that in the case of a Majorana mass term for sterile neutrinos $m_R\, \overline{\nu_R^c}\nu_R$ the gauge symmetries of the SM are preserved.

3.3 Neutrino Mixing and Oscillations

In 1957, Bruno Pontecorvo initially introduced the idea of neutrino oscillations, exploring neutrino–antineutrino mixing inspired by the oscillation behavior observed in neutral kaons [61, 62]. In 1962, Maki, Nakagawa, and Sakata proposed that interaction and propagation eigenstates in neutrinos could be different [63]. The notion that oscillations result from interference among distinct massive neutrinos was subsequently developed by Pontecorvo [64].

In the Homestake experiment [65], during the late 1960s, using a detector based on the reaction

$$\nu_e + {}^{37}\mathrm{Cl} \to e^- + {}^{37}\mathrm{Ar}, \tag{3.24}$$

it was observed a deficit in the flux of electron neutrinos from the sun with respect to the prediction of the SM and the Solar Standard Model. This discrepancy was known as the *solar neutrino problem*. The results were confirmed later in 1989 by the Kamiokande experiment [66] with Cherenkov effect based detectors. In these, the neutrino-electron scattering process

$$\nu_e + e \to \nu_e + e, \tag{3.25}$$

produces charged electrons propagating through water and emitting cones of light, detected by photomultiplier tubes (PMTs). However, the origin for this deficit was not explained until the detection of solar neutrinos in flavor-sensitive processes by the Sudbury Neutrino Observatory [25] in 2002. It was possible to distinguish outcomes from different neutrino flavors with the CC, NC and electron scattering (ES) reactions using deuterium:

$$\begin{aligned}
\mathrm{CC} &: \nu_e + d \to p + p + e, \\
\mathrm{NC} &: \nu_{e,\mu,\tau} + d \to p + n + \nu_{e,\mu,\tau}, \\
\mathrm{ES} &: \nu_{e,\mu,\tau} + e \to e + \nu_{e,\mu,\tau}.
\end{aligned} \tag{3.26}$$

The three neutrino flavors interact through the exchange of a Z boson, whereas neutrino electrons also interact by the exchange of W bosons. With this experiment, it was confirmed that solar neutrinos were oscillating, finally explaining the flux deficit.

On the other hand, the detection of atmospheric neutrinos led to a similar puzzle regarding neutrino fluxes. Atmospheric neutrinos are produced from collisions of cosmic rays with nuclei in the atmosphere. This production is dominated by the processes

$$\begin{aligned}
\pi^+ &\to \mu^+ + \nu_\mu \\
&\hookrightarrow \mu^+ \to e^+ + \overline{\nu_\mu} + \nu_e.
\end{aligned} \tag{3.27}$$

A similar decay occurs for π^- particles. From this chain, a ratio for the fluxes of muon neutrinos and electron neutrinos ν_μ/ν_e of 2 to 1 is expected. However, the Super-Kamiokande experiment [24] found a dependence of the muon neutrino flux with the zenith angle, with the number of upward-going muon neutrinos (generated on the other side of the Earth) with a deficit respect to downward-going muon neutrinos. This was explained again with neutrino oscillations, since these depend on the travelled distance.

Reactor anti-neutrino disappearance was first reported by the KamLAND collaboration [26]. Later, disappearance of reactor electron antineutrinos was also observed in the Double Chooz

experiment [30] using two detectors at different distances from the reactor. In this short-baseline oscillation experiment, the reactor mixing angle, to be introduced in Subsection 3.3.3, was measured. This results were confirmed by the Daya Bay [31] and RENO [32] reactor neutrino observatories.

Furthermore, neutrino oscillations in neutrino beams have been also detected, for example by the K2K [27], MINOS [28] and Super-Kamiokande experiments.

3.3.1 Neutrino mixing

Oscillation of neutrinos arise from the mixing between their mass and flavor eigenstates. This mixing is a consequence of the mismatch between the three neutrino states that interact with the charged leptons and the three propagating neutrino states of definite mass. That is, neutrinos are absorbed and emitted through weak processes in flavor eigenstates, but travel as mass eigenstates. Both basis are related by means of a unitary mixing matrix, similar to the Cabibbo-Kobayashi-Maskawa (CKM) mixing matrix in the quark sector [56, 57]. The linear combinations are then

$$|\nu_\alpha\rangle = \sum_i U_{\alpha i} |\nu_i\rangle, \tag{3.28}$$

$$|\nu_i\rangle = \sum_\alpha U_{i\alpha}^* |\nu_\alpha\rangle. \tag{3.29}$$

Here, $|\nu_\alpha\rangle$ is a neutrino with definite flavor $\alpha = e, \mu, \tau$, $|\nu_i\rangle$ is a neutrino with definite mass m_i where $i = 1, 2, 3$, and U is the lepton mixing matrix or PMNS matrix (Pontecorvo–Maki–Nakagawa–Sakata). When three active neutrinos are considered, the matrix is 3×3:

$$U_{\text{PMNS}} \equiv U = \begin{pmatrix} U_{e1} & U_{e2} & U_{e3} \\ U_{\mu 1} & U_{\mu 2} & U_{\mu 3} \\ U_{\tau 1} & U_{\tau 2} & U_{\tau 3} \end{pmatrix}. \tag{3.30}$$

Using the PDG parametrization [9], the PMNS matrix is written as

$$U = \begin{pmatrix} 1 & 0 & 0 \\ 0 & c_{23} & s_{23} \\ 0 & -s_{23} & c_{23} \end{pmatrix} \begin{pmatrix} c_{13} & 0 & s_{13}e^{-i\delta} \\ 0 & 1 & 0 \\ -s_{13}e^{i\delta} & 0 & c_{13} \end{pmatrix} \begin{pmatrix} c_{12} & s_{12} & 0 \\ -s_{12} & c_{12} & 0 \\ 0 & 0 & 1 \end{pmatrix}$$
$$= \begin{pmatrix} c_{12}c_{13} & s_{12}c_{13} & s_{13}e^{-i\delta} \\ -s_{12}c_{23} - c_{12}s_{23}s_{13}e^{i\delta} & c_{12}c_{23} - s_{12}s_{23}s_{13}e^{i\delta} & s_{23}c_{13} \\ s_{12}s_{23} - c_{12}c_{23}s_{13}e^{i\delta} & -c_{12}s_{23} - s_{12}c_{23}s_{13}e^{i\delta} & c_{23}c_{13} \end{pmatrix}, \tag{3.31}$$

where $c_{ij} = \cos\theta_{ij}$ and $s_{ij} = \sin\theta_{ij}$ respectively. The phase δ is also known as Dirac phase, and accounts for CP violation. If Majorana neutrinos are considered, then extra phases enter in the PMNS matrix as

$$U = \begin{pmatrix} c_{12}c_{13} & s_{12}c_{13} & s_{13}e^{-i\delta} \\ -s_{12}c_{23} - c_{12}s_{23}s_{13}e^{i\delta} & c_{12}c_{23} - s_{12}s_{23}s_{13}e^{i\delta} & s_{23}c_{13} \\ s_{12}s_{23} - c_{12}c_{23}s_{13}e^{i\delta} & -c_{12}s_{23} - s_{12}c_{23}s_{13}e^{i\delta} & c_{23}c_{13} \end{pmatrix} \begin{pmatrix} e^{i\alpha_1/2} & 0 & 0 \\ 0 & e^{i\alpha_2/2} & 0 \\ 0 & 0 & 1 \end{pmatrix}. \tag{3.32}$$

The phases α_1 and α_2 are non-vanishing only if neutrinos are Majorana particles, and they do not contribute to oscillation phenomena.

3.3.2 Oscillation Probability

We want to know the time evolution of a neutrino. This is achieved with the evolution operator as

$$|\nu_i(t)\rangle = e^{-iE_i t}|\nu_i(0)\rangle. \tag{3.33}$$

In the ultra-relativistic limit, in which $p_i \gg m_i$, and assuming that all states i have the same momenta, we derive

$$E_i = \sqrt{p_i^2 + m_i^2} \simeq p_i + \frac{m_i^2}{2p_i} \approx E + \frac{m_i^2}{2E}, \tag{3.34}$$

where E is the energy of the particle viewed as a wavepacket. In the ultra-relativistic limit, we can take $t \sim L$:

$$|\nu_i(t)\rangle = e^{-iEL}\, e^{-i\left(\frac{m_i^2 L}{2E}\right)}|\nu_i(0)\rangle. \tag{3.35}$$

The probability of an initial neutrino of flavour α oscillating to a flavour β at a time t is given by

$$P_{\alpha\to\beta} = \left|\langle\nu_\beta|\nu_\alpha(t)\rangle\right|^2 = \left|\sum_i U_{\alpha i}^* U_{\beta i} e^{-i\frac{m_i^2 L}{2E}}\right|^2, \tag{3.36}$$

where we have used Eq. (3.28). Note that the exponential term e^{-iEL} in Eq. (3.35) disappears in the transition probability. The final expression yields

$$
\begin{aligned}
P_{\alpha\to\beta} = \delta_{\alpha\beta} &- 4\sum_{i>j} \mathrm{Re}\left[U_{\alpha i}^* U_{\beta i} U_{\alpha j} U_{\beta j}^*\right] \sin^2\left(\frac{\Delta m_{ij}^2 L}{4E}\right) \\
&+ 2\sum_{i>j} \mathrm{Im}\left[U_{\alpha i}^* U_{\beta i} U_{\alpha j} U_{\beta j}^*\right] \sin\left(\frac{\Delta m_{ij}^2 L}{2E}\right),
\end{aligned} \tag{3.37}
$$

with $\Delta m_{ij}^2 = m_i^2 - m_j^2$. It is evident from here that, in order to have oscillations, at least two neutrinos must be massive.

Neutrino oscillations violate flavor lepton number, but total lepton number is still conserved.

3.3.3 Oscillation Parameters

Neutrino oscillations depend on three mixing angles θ_{ij}, a CP violation phase δ and the squared mass differences Δm_{ij}^2. Oscillation experiments can be categorized based on the source of the observed neutrinos, namely solar, atmospheric, and reactor neutrino experiments. Each of these experiments has measured specific parameters, which further serve to define their names: θ_{12} and Δm_{12}^2 are also called solar parameters ($\Delta m_{12}^2 \equiv \Delta m_{\mathrm{sol}}^2$), θ_{23} and Δm_{23}^2 are atmospheric parameters ($\Delta m_{23}^2 \equiv \Delta m_{\mathrm{atm}}^2$), and θ_{13} is the nuclear mixing angle.

There are two possible hierarchies for neutrino masses, shown in Fig. 5. In normal ordering (NO), the hierarchy is $m_1 < m_2 < m_3$. In Inverted Ordering (IO), is $m_3 < m_2 < m_1$.

The best fit values for neutrino oscillation parameters are presented in Table 4, obtained from the Valencia global fit collaboration [68]. See [69] for the global fit of the NuFIT collaboration.
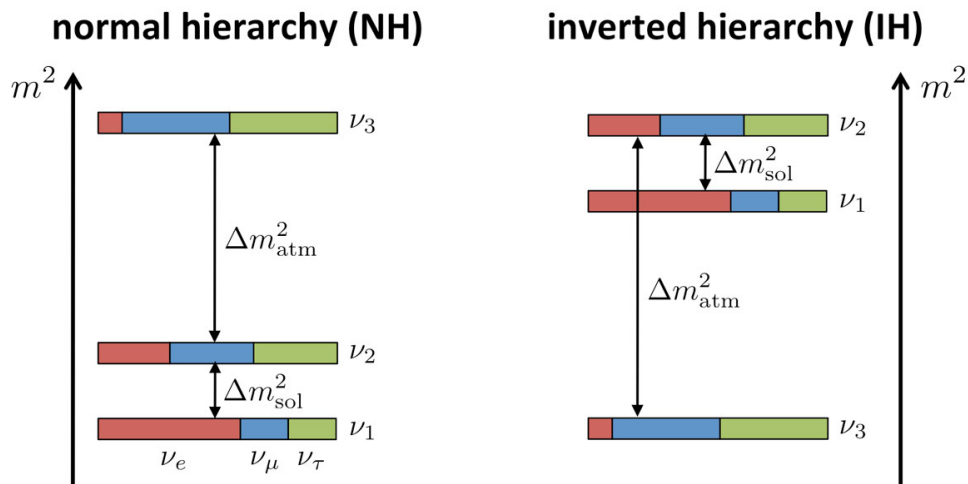
Figure 5: Possible orderings of the neutrino mass eigenstates. The contribution of each flavour is represented by colours: electron, muon and tau are given in red, blue and green, respectively. Figure from [67].

Parameters	Best Fit $\pm 1\sigma$	3σ Range
$\Delta m_{21}^2 : [10^{-5}\text{eV}^2]$	$7.50^{+0.22}_{-0.20}$	$6.94 - 8.14$
$\|\Delta m_{31}^2\| : [10^{-3}\text{eV}^2]$ (NO)	$2.55^{+0.02}_{-0.03}$	$2.47 - 2.63$
$\|\Delta m_{31}^2\| : [10^{-3}\text{eV}^2]$ (IO)	$2.45^{+0.02}_{-0.03}$	$2.37 - 2.53$
$\sin^2 \theta_{12}/10^{-1}$	3.18 ± 0.16	$2.71 - 3.69$
$\sin^2 \theta_{23}/10^{-1}$ (NO)	5.74 ± 0.14	$4.34 - 6.10$
$\sin^2 \theta_{23}/10^{-1}$ (IO)	$5.78^{+0.10}_{-0.17}$	$4.33 - 6.08$
$\sin^2 \theta_{13}/10^{-2}$ (NO)	$2.200^{+0.069}_{-0.062}$	$2.000 - 2.405$
$\sin^2 \theta_{13}/10^{-2}$ (IO)	$2.225^{+0.064}_{-0.070}$	$2.018 - 2.424$
δ_{CP}/π (NO)	$1.08^{+0.13}_{-0.12}$	$0.71 - 1.99$
δ_{CP}/π (IO)	$1.58^{+0.15}_{-0.16}$	$1.11 - 1.96$

Table 4: Global fit for neutrino oscillation parameters, given by [68].

(a) Long range probability.

(b) Short range probability.
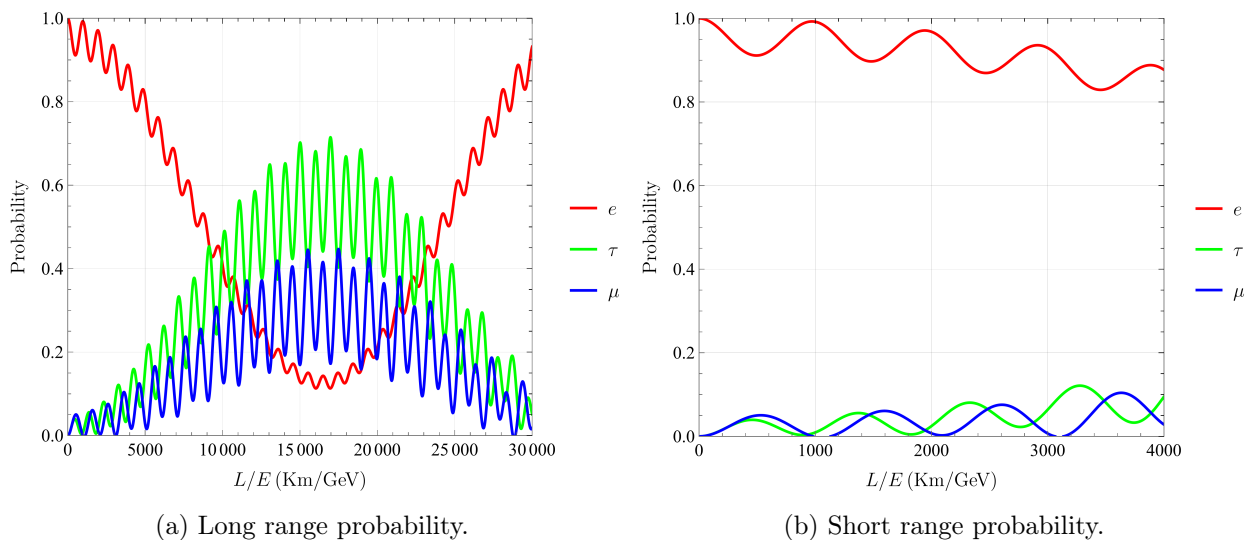
Figure 6: Probability of an initial electron neutrino ν_e transforming into $\nu_{e,\mu,\tau}$ (red, blue and green) in vacuum vs. L/E. In 6a, the probability is shown for long range ratios, whereas in 6b is displayed for short range.

The probability of an initial electron neutrino transforming into another flavor (or the same flavor) in vacuum is displayed in Fig. 6. The horizontal axis corresponds to the relation L/E in Km/GeV. The oscillation parameters used for the probability are those of the best fit [68]. In disappearance and appearance experiments, a deficit in the neutrino flux of a determined flavor is measured. This can be understood with the probability plots, where, for example, at a value of $L/E \sim 15000$ Km/GeV, electron neutrinos are less likely to be observed compared to other distances.

Neutrino oscillations also occur in matter [70], with a change in the probability due to NC and CC interactions of ν_e with electrons, and NC reactions for ν_μ and ν_τ. Then, for example, in solar neutrino detectors, neutrino oscillations inside the Sun must be considered for the calculation of probabilities. A review about neutrino oscillations in matter can be found in [71, 72].

4 Neutrino Mass Generation

Neutrino masses represent BSM physics. Originally postulated massless, it is until experiments observed oscillations that we know that neutrinos should carry a mass. However, its generation together with a natural explanation for their smallness is currently unknown.

We review the most popular mechanisms to generate Majorana neutrino masses. These represent UV realizations of the Weinberg operator to be introduced below. Each model has its own implications and phenomenology, briefly discussed throughout this section.

4.1 Dim-5 Weinberg Operator

If we allow non-renormalizable operators in the SM, a dim-5 neutrino mass term can be constructed using only SM fields. This effective operator violates lepton number, is unique and has the form

$$\mathcal{O}_W^{(5)} = \frac{c_{\alpha\beta}}{\Lambda} \overline{L_\alpha^c} L_\beta \widetilde{H}^* \widetilde{H}^\dagger + \text{h.c.}, \tag{4.1}$$

with $\widetilde{H} = i\sigma^2 H^*$, $c_{\alpha\beta}$ a model-dependent coefficient and Λ the scale of new physics. This operator was first proposed by Weinberg in 1979 [73], so it is called the *dim-5 Weinberg Operator*, and its Feynman diagram is shown in Figure 7. After electroweak symmetry
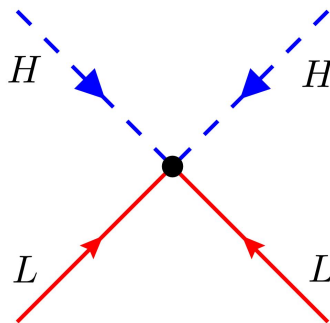
Figure 7: Feynman diagram of the dim-5 Weinberg operator. This interaction is effective, and therefore non-renormalizable.

breaking, the Weinberg operator gives rise to Majorana neutrino masses:

$$\mathcal{O}_W^{(5)} \to \frac{v^2}{2\Lambda} c_{\alpha\beta} \overline{\nu_\alpha^c} \nu_\beta, \tag{4.2}$$

with v the VEV of the SM Higgs. Therefore, the neutrino mass scale is approximately

$$m_\nu \sim c_{\alpha\beta} \frac{v^2}{\Lambda}. \tag{4.3}$$

Considering a SM VEV of $v \sim 10^2$ GeV, the upper bound for neutrino masses leads to $c_{\alpha\beta}/\Lambda \sim 10^{-14}$ GeV^{-1}. Assuming a coefficient $c_{\alpha\beta} \sim O(1)$, the scale for new physics is given by $\Lambda \sim 10^{14}$ GeV, being far from current experimental energy limits. However, if we consider a more suppressed $c_{\alpha\beta}$, then the scale Λ can be lowered, being potentially accessible

(a) Seesaw type-I.   (b) Seesaw type-II.   (c) Seesaw type-III.
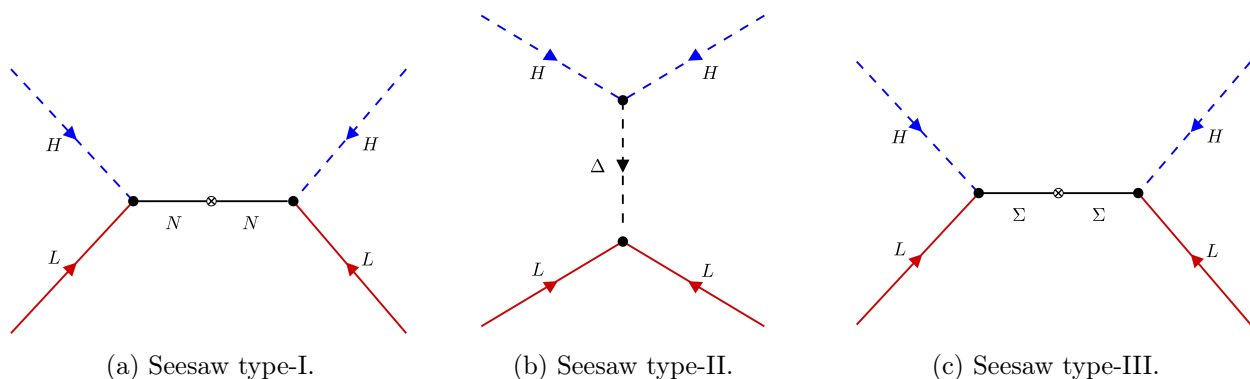
Figure 8: The three canonical types of the seesaw mechanism, which are UV realizations of the dim-5 Weinberg operator at tree-level. In type-I, a singlet fermion N is introduced, whereas in type-II and type-III a triplet scalar Δ and a triplet fermion Σ are introduced, respectively.

to experiments. Such suppression can be achieved considering a radiative mass generation mechanism in which $c_{\alpha\beta} \propto (\frac{1}{16\pi^2})^n$, where n is the number of loops.

Having a mass dimension of five, the Weinberg operator is a non-renormalizable effective operator. To generate masses coming from this operator, a UV realization is needed, where Eq. (4.1) is constructed using renormalizable and gauge invariant operators. This is achieved considering extensions of the SM, with the addition of new fields and symmetries. There are several UV realizations proposed in the literature, both at tree-level and radiative. In the next sections, we review the seesaw mechanism and the Scotogenic model, which correspond to tree-level and one-loop level completions respectively.

4.2 Tree-level Realizations: Seesaw Mechanism

The most straightforward way to complete the Weinberg operator is at tree-level. Taking (4.1) and recalling that $\widetilde{H} = i\sigma^2 H^*$, by Fierz transformations we have the equalities

$$\left(\overline{L_\alpha^c}\widetilde{H}^*\right)\left(\widetilde{H}^\dagger L_\beta\right) = \frac{1}{2}\left(\overline{L_\alpha^c}\sigma^i L_\beta\right)\left(\widetilde{H}^\dagger \sigma^i \widetilde{H}^*\right) = -\left(\overline{L_\alpha^c}\sigma^i \widetilde{H}^*\right)\left(\widetilde{H}^\dagger \sigma^i L_\beta\right), \qquad (4.4)$$

where we have used

$$\left(\sigma^i\right)_{ab}\left(\sigma^i\right)_{cd} = 2\,\delta_{ad}\,\delta_{bc} - \delta_{ab}\,\delta_{cd}, \qquad (4.5)$$

with a, b, c, d being SU(2) indices. In Eq. (4.4), the first term can be completed with the coupling of LH to a fermion singlet under the SM, the second term with a scalar triplet with hypercharge 1 and the last to a fermion triplet with zero hypercharge. Each one of these cases defines a different type of the seesaw mechanism, with the corresponding diagram shown in Fig. 8.

4.2.1 Type-I Seesaw

As we reviewed in Section 3.2, neutrino masses can be generated by adding a right-handed neutrino ν_R with mass m_R to the SM. The UV completion of the Weinberg operator with just right-handed neutrinos corresponds to the type-I seesaw mechanism [74, 75]. To reproduce neutrino oscillations data, we need at least two copies of this right-handed neutrino.

Recalling the mass terms of Eq. (3.23), if we consider the case $m_L = 0$, the relevant Lagrangian for neutrino masses can be rewritten as

$$\mathcal{L}_{\nu_I} = \frac{1}{2} \begin{pmatrix} \overline{\nu_L^c} & \overline{\nu_R} \end{pmatrix} \mathcal{M}_\nu \begin{pmatrix} \nu_L \\ \nu_R^c \end{pmatrix} + \text{h.c.}, \tag{4.6}$$

with the neutrino mass matrix given by

$$\mathcal{M}_\nu = \begin{pmatrix} 0 & m_D \\ m_D & m_R \end{pmatrix}. \tag{4.7}$$

Considering the limit $m_R \gg m_D$[9], the eigenvalues for the neutrino mass matrix can be approximated to

$$m_1 \approx -m_D \cdot m_R^{-1} \cdot m_D, \tag{4.8}$$

$$m_2 \approx m_R. \tag{4.9}$$

Therefore, masses for a light and a heavy neutrino, m_1 and m_2, are obtained. The origin for the term "seesaw" comes from the relation between these masses: as one gets larger, the other gets smaller.

If the Dirac mass term is given through a Yukawa coupling y, i.e,

$$y \, \overline{L} H \nu_R \tag{4.10}$$

then $m_D = v \, y / \sqrt{2}$ after SSB, and

$$m_1 \approx \frac{v^2 \, y^2}{2 m_R}. \tag{4.11}$$

While the smallness of neutrino masses can be achieved with this mechanism, imposing $m_1 \sim 1 \, \text{eV}$ and $y \sim \mathcal{O}(1)$ implies $m_2 \sim 10^{13} \, \text{GeV}$. A smaller value for y could also be considered natural. However, taking $y^2 \sim 10^{-4}$, makes $m_2 \sim 10^9 \, \text{GeV}$, which is still far beyond experimental limits for detection.

4.2.2 Type-II Seesaw

In the type-II seesaw, a scalar triplet with hypercharge 1 is added to the SM [76–79]. This triplet is $\Delta = (\Delta^{++}, \Delta^+, \Delta^0)$ and it is usually expressed in the double representation of $SU(2)_L$ as

$$\Delta = \begin{pmatrix} \Delta^+/\sqrt{2} & \Delta^{++} \\ \Delta^0 & -\Delta^+/\sqrt{2} \end{pmatrix}. \tag{4.12}$$

The relevant Lagrangian terms are

$$\mathcal{L}_{\nu_{II}} = \left(Y_\Delta \, \overline{L^c} \Delta L - \mu \, \widetilde{H}^\dagger \Delta^\dagger H + \text{h.c} \right) + M_\Delta^2 \, \Delta^\dagger \Delta. \tag{4.13}$$

The simultaneous presence of Y_Δ and μ implies lepton number violation by two units, having as possibilities $L = -2$ or $L = 0$ for Δ. Additionally, the presence of the μ term induces

---

[9]For example, having $m_D \sim \mathcal{O}(m_e, m_\mu, m_\tau)$ and $m_R \sim \mathcal{O}(10^{14} \, \text{GeV})$, which is the scale of new physics derived from the Weinberg operator considering couplings of $\mathcal{O}(1)$.

a VEV $\langle \Delta \rangle \neq 0$ when $\langle H \rangle \neq 0$. This can be derived from the tadpole equations of the potential terms in (4.13). After SSB, we have

$$\left. \frac{\partial V}{\partial v_\Delta} \right|_{\Psi=0} = 0 \quad \Rightarrow \quad v_\Delta = \frac{\mu\, v^2}{\sqrt{2} M_\Delta^2}. \tag{4.14}$$

Therefore, the smallness of the neutrino masses depends of the smallness of the VEV v_Δ, with

$$m_\nu = Y_\Delta \frac{v_\Delta}{\sqrt{2}}. \tag{4.15}$$

The seesaw mechanism here is dictated by the dependence of v_Δ with M_Δ: the larger the mass of Δ, the smaller the mass of the neutrinos.

4.2.3 Type-III Seesaw

The type-III seesaw [80] is similar to the type-I, but now the added fermion is a triplet $\Sigma = (\, \Sigma^+,\, \Sigma^0,\, \Sigma^-\,)$ with zero hypercharge. The Lagrangian is

$$\mathcal{L}_{\nu_{III}} = \frac{1}{2} \begin{pmatrix} \overline{\nu_L^c} & \overline{\Sigma}^0 \end{pmatrix} \mathcal{M}_\nu \begin{pmatrix} \nu_L \\ \Sigma^{0c} \end{pmatrix} + \text{h.c.}, \tag{4.16}$$

with the corresponding mass matrix

$$\mathcal{M}_\nu = \begin{pmatrix} 0 & m_D \\ m_D & m_\Sigma \end{pmatrix}. \tag{4.17}$$

While it has the same structure as the seesaw type-I, the gauge indices are contracted differently because of the triplet structure. The neutrino masses have an analogous expression given by

$$m_1 \approx m_D \cdot m_\Sigma^{-1} \cdot m_D. \tag{4.18}$$

The main difference between the type-I and type-III seesaws is the phenomenology associated to the charged components of Σ. Note that Σ^+ and Σ^- do not participate in the mass mechanism, as can be seen from Eq. (4.16).

4.3 A One-Loop Realization: Scotogenic Model

The dim-5 Weinberg operator can also be generated through radiative mechanisms. From these, the first proposed models were the Zee model [81] and the Zee-Babu model [82, 83] at one- and two-loop level respectively. Another one-loop mechanism is the Scotogenic model [84]. Here we will discuss the latter, being closely related to the models to be introduced in Sections 5 and 6.

The Scotogenic[10] model is one of the most popular neutrino mass models, because it links neutrino masses with dark matter. This model consists of a one-loop UV completion of the Weinberg Operator (4.1) given an extra Z_2 discrete symmetry (also known as parity symmetry, with ± 1 as possible charges). This extension of the SM reads

$$SU(3)_C \times SU(2)_L \times U(1)_Y \times Z_2, \tag{4.19}$$

---

[10] From ancient Greek, "scoto" means "darkness", while "genic" means "generated".

where the Z_2 symmetry is preserved after EWSB [85]. The particle content of the model is presented in table 5. As a UV realization of the Weinberg operator, new fields are added: three Majorana neutrinos N_i singlets under the SM, and an inert scalar doublet η. These new particles are odd (negative charge) under Z_2, while the SM particles are even (positive charge).

	Fields	$SU(2)_L \otimes U(1)_Y$	Z_2
Fermions	L_i	$(\mathbf{2}, -1/2)$	$+1$
	e_{R_i}	$(\mathbf{1}, -1)$	$+1$
	N_i	$(\mathbf{1}, 0)$	-1
Scalars	H^+, H^0	$(\mathbf{2}, 1/2)$	$+1$
	η^+, η^0	$(\mathbf{2}, 1/2)$	-1

Table 5: Particle content in the Scotogenic Model [84], with $i \in \{1, 2, 3\}$.

Because of the extra Z_2 symmetry, Dirac mass terms of the form $f_{ij} \bar{\nu}_i H N_j$ are forbidden, and neutrinos remain massless at tree-level. The relevant Yukawa interactions are given by

$$\mathcal{L}_Y = f_{ij} \left(H^- \nu_i + \overline{H}^0 \ell_i \right) \ell_j^c + y_{ij} \left(\nu_i \eta^0 - \ell_j \eta^+ \right) N_j + \text{h.c.,} \tag{4.20}$$

while the scalar potential of the model is

$$\begin{aligned} V = &\mu_H^2 \, H^\dagger H + \mu_\eta^2 \, \eta^\dagger \eta + \frac{1}{2}\lambda_1 \left(H^\dagger H \right)^2 + \frac{1}{2}\lambda_2 \left(\eta^\dagger \eta \right) + \lambda_3 \left(H^\dagger H \right) \left(\eta^\dagger \eta \right) \\ &+ \lambda_4 \left(H^\dagger \eta \right) \left(\eta^\dagger H \right) + \frac{1}{2}\lambda_5 \left[\left(H^\dagger \eta \right)^2 + \text{h.c.} \right]. \end{aligned} \tag{4.21}$$

The one-loop mechanism is constructed with the terms

$$\frac{1}{2} M_i \, \overline{N_i^c} N_i + \text{h.c.,} \tag{4.22}$$

$$\frac{1}{2}\lambda_5 (H^\dagger \eta)^2 + \text{h.c.} \tag{4.23}$$

Operators (4.22) and (4.23) violate lepton number by two units, whether if a lepton number is assigned to N_i or to η. From the potential, the masses for the particles are given by

$$m^2(\sqrt{2} \, H_R^0) = 2\lambda_1 v^2, \tag{4.24}$$

$$m^2(\eta^\pm) = m_2^2 + \lambda_3 v^2, \tag{4.25}$$

$$m^2(\sqrt{2} \, \eta_R^0) = m_2^2 + (\lambda_3 + \lambda_4 + \lambda_5)v^2 \equiv m_R^2, \tag{4.26}$$

$$m^2(\sqrt{2} \, \eta_I^0) = m_2^2 + (\lambda_3 + \lambda_4 - \lambda_5)v^2 \equiv m_I^2. \tag{4.27}$$

The mass mechanism of the Scotogenic model is shown in Fig. 9. In the mass basis, the

Rolando Martínez Ramírez
IF-UNAM
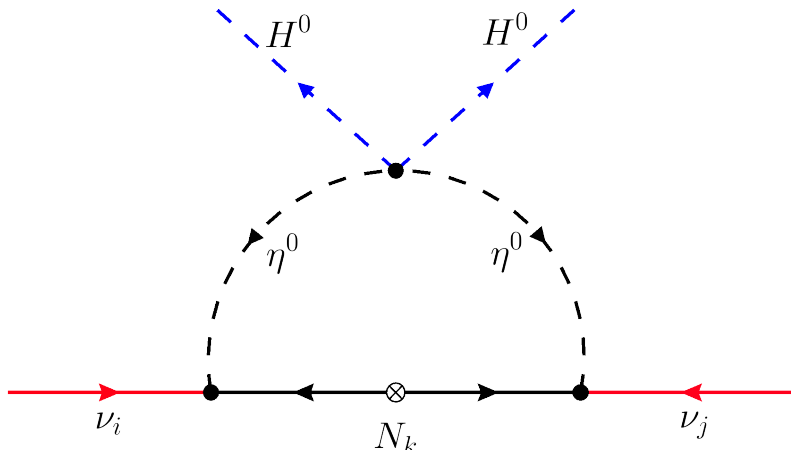**Neutrino Masses: Radiative Models and Phenomenology**

Figure 9: Feynman diagram of the one-loop neutrino mass generation mechanism in the Scotogenic Model [84].

diagram is calculable and yields

$$(\mathcal{M}_\nu)_{ij} = \sum_k \frac{y_{ik} y_{jk} M_k}{32\pi^2} \left[\frac{m_R^2}{m_R^2 - M_k^2} \ln \frac{m_R^2}{M_k^2} - \frac{m_I^2}{m_I^2 - M_k^2} \ln \frac{m_I^2}{M_k^2} \right]. \tag{4.28}$$

From Eqs. (4.26) and (4.27), the mass splitting between the scalar and the pseudoscalar is given by the coupling λ_5 as

$$m_R^2 - m_I^2 = 2\lambda_5 v^2. \tag{4.29}$$

If we consider

$$2\lambda_5 v^2 \ll \frac{m_R^2 + m_I^2}{2} = m_0^2, \tag{4.30}$$

and the limit where $M_k^2 \approx m_0^2$, expression (4.28) reduces to

$$(\mathcal{M}_\nu)_{ij} \approx \frac{\lambda_5 v^2}{32\pi^2} \sum_k \frac{y_{ik} y_{jk}}{M_k}. \tag{4.31}$$

Comparing to the seesaw type-I in Eq. (4.11), neutrino masses get an additional suppression given by the factor $\lambda_5/16\pi^2$. Considering $\lambda_5 \sim y^2 \sim 10^{-4}$ [11], the scale is then reduced from 10^9 GeV in the seesaw type-I to just 10^3 GeV in the Scotogenic model, feasible for experimental exploration.

4.3.1 Dark matter in the Scotogenic Model

In the model, there is a dark matter candidate. Due to the Z_2 symmetry, a decay of a dark particle into only SM matter is forbidden by charge conservation. Therefore, the lightest particle odd under Z_2 will be stable. This is represented schematically in Figure 10. In the Scotogenic model, there can be a scalar or a fermionic dark matter candidate, namely, the lightest particle between η and the three fermions N_i.

---

[11]Considering the *naturalness* definition of G. 't Hooft [86], a small value for λ_5 could be considered natural since when $\lambda_5 \to 0$, lepton number is conserved, increasing the symmetry of the model.
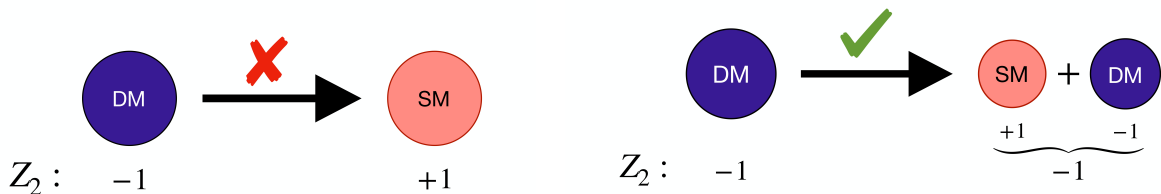
(a) Not allowed decay of dark particles into purely SM particles.

(b) Allowed decay of dark particles into SM and lighter dark particles.
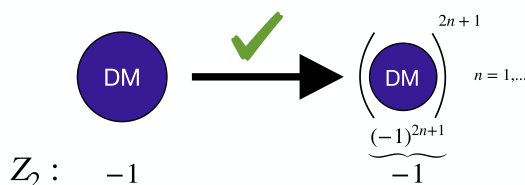
(c) Allowed decay of dark particles into an even number of lighter dark particles.

Figure 10: Diagram of dark matter stability under a Z_2 symmetry. A dark particle can not decay into purely SM particles because of charge conservation. However, it is possible for a dark particle to decay into SM and a lighter dark particle, or an even number of lighter dark particles. Therefore, the lightest dark particle is stable, and it is a dark matter candidate.

Considering the fermionic case, and assuming $M_1 < M_2 < M_3 < m_{\eta^\pm}$, the following decays are possible:

$$\eta^\pm \rightarrow \ell^\pm N_{1,2,3}, \tag{4.32}$$

followed by

$$N_3 \rightarrow \ell^\pm \ell^\mp N_{1,2} \qquad \text{and} \tag{4.33}$$
$$N_2 \rightarrow \ell^\pm \ell^\mp N_1 \tag{4.34}$$

through the exchange of $\eta^\pm$. In the scalar case, in which all M_k are greater than the mass of η, the following decays could be observed:

$$N_{1,2,3} \rightarrow \ell^\pm \eta^\mp, \tag{4.35}$$
$$\eta^\mp \rightarrow \eta^0 + W^\mp, \tag{4.36}$$

where the W boson becomes a lepton or quark pair through weak interaction.

The model also allows for Lepton Flavor Violation (LFV) processes trough Yukawa interaction with η. These will be of interest for our one-loop and two-loop model of Sections 5 and 6. More discussion regarding this phenomenological implication will be postponed until then.

4.4 Z_n and $U'(1)$ Models

In the Scotogenic model, the Z_2 symmetry is imposed by hand, allowing radiative neutrino masses and a stable dark matter candidate. However, other symmetries can be proposed for the same purpose, resulting in a different phenomenology.

Consider the finite cyclic group Z_n, whose elements are powers of a particular element ω with $\omega^n = \omega^0 = 1$. Under this group, particle fields transform as

$$\psi \to \omega^k \psi, \tag{4.37}$$

where ω is the n-th root of unity:

$$\omega = e^{\frac{2\pi i}{n}}. \tag{4.38}$$

In Eq (4.37), k represent the Z_n charge of ψ, and its power dictates if ψ is odd or even under the symmetry. In the Z_2 case:

$$\begin{aligned}
\omega^0 = \omega^2 &= +1, \\
\omega^1 &= -1.
\end{aligned} \tag{4.39}$$

Different Z_n symmetries can be used to build new models according to the particle content and desired phenomenology. The motivation is to forbid unwanted terms and to ensure stability for dark matter. Distinct Z_n have implications in the particle nature of neutrinos, allowing Dirac or Majorana mass terms [87]. As example, a two-loop model with a Z_3 symmetry is presented in [88].

A Z_n symmetry can also be obtained from spontaneously breaking of a $U'(1)$ symmetry [89]. This is the case for extension models of the form

$$SU(3)_C \times SU(2)_L \times U(1)_Y \times U'(1), \tag{4.40}$$

where the extra $U'(1)$ can be taken from some symmetry already present in the SM. A natural selection is the accidental $U(1)_\ell$ lepton number symmetry. With this possibility, the symmetry Z_n that was previously imposed without further explanation now is motivated from the breaking of an apparent symmetry of the SM [87, 90, 91]:

$$SU(2)_L \times U(1)_Y \times U(1)_\ell \to U(1)_{EM} \times Z_n. \tag{4.41}$$

A consequence of taking a $U'(1)$ symmetry is the presence of extra bosons, derived from the SSB process. When a global $U(1)$ symmetry is considered, a Goldstone boson is generated, which usually receives the name of *majoron* [79, 92].

Another possibility is the $U(1)_{B-L}$ symmetry. The special feature of this symmetry is that it can be anomaly free with the addition of right-handed neutrinos (see Appendix A) so it can be gauged to obtain a richer phenomenology, including the existence of a gauge boson. This is the case of Z' models.

In next sections, we propose a neutrino mass model with a Z_4 symmetry spontaneously broken to a Z_2, and another with a $U(1)_{B-L}$ spontaneously broken to a Z_3 symmetry.

5 One-Loop Mass Generation Model

In this section, we introduce a new proposal for a radiative Majorana neutrino mass model. We extend the SM with a discrete Z_4 symmetry, spontaneously broken to Z_2. We include three singlet fermions, along with a doublet and a singlet scalar. The lightest of these particles will represent a dark matter candidate, stabilized by the preserved Z_2 symmetry. Additionally, we include a singlet scalar which gets mixed with the Higgs particle and opens annihilation channels for dark matter. This model will generate neutrino masses through a one-loop mechanism. We explore the model, including a brief discussion regarding dark matter phenomenology when the dark matter candidate is a fermion.

5.1 The Model

We work in an extension of the SM given as

$$SU(3)_C \times SU(2)_L \times U(1)_Y \times Z_4, \tag{5.1}$$

where we have imposed an extra Z_4 symmetry. The matter content of the model is shown in Table 6. In the fermionic sector, we add three fermions N_k singlets of the SM, with

	Fields	$SU(2)_L \otimes U(1)_Y$	Z_4	Z_2
Fermions	L_j	$(\mathbf{2}, -1/2)$	1	1
	e_{R_j}	$(\mathbf{1}, -1)$	1	1
	N_k	$(\mathbf{1}, 0)$	i	-1
Scalars	H	$(\mathbf{2}, 1/2)$	1	1
	η	$(\mathbf{2}, 1/2)$	i	-1
	σ	$(\mathbf{1}, 0)$	i	-1
	ϕ	$(\mathbf{1}, 0)$	-1	1

Table 6: Particle content of the model with $j \in \{e, \mu, \tau\}$ and $k \in \{1, 2, 3\}$. All the fields listed are $SU(3)_C$ singlets. Fields with charges i under Z_4 correspond to dark matter candidates. The scalar field ϕ is real.

imaginary charge $e^{\frac{2\pi i}{4}} = i$ under Z_4. In the scalar sector, we add a scalar doublet η with the same hypercharge as the Higgs boson and a scalar σ singlet under the SM. Both fields transform as i under Z_4. Additionally, we include a real singlet scalar ϕ with a -1 charge under Z_4. The extra symmetry of the model is spontaneously broken to Z_2:

$$SU(2)_L \times U(1)_Y \times Z_4 \to U(1)_{EM} \times Z_2. \tag{5.2}$$

Therefore, fields with imaginary charge i under Z_4 will be protected by a residual Z_2 symmetry after SSB, with the lightest particle being a dark matter candidate.

Before SSB, the scalar potential is given by

$$
\begin{aligned}
V =& \mu_H^2 \left(H^\dagger H \right) + \mu_\eta^2 \left(\eta^\dagger \eta \right) + \mu_\sigma^2 \left(\sigma^* \sigma \right) + \mu_\phi^2 \left(\phi^2 \right) \\
& + \lambda_1 \left(H^\dagger H \right)^2 + \lambda_2 \left(H^\dagger H \right) \left(\eta^\dagger \eta \right) + \lambda_3 \left(H^\dagger \eta \right) \left(\eta^\dagger H \right) + \lambda_4 \left(H^\dagger H \right) \left(\sigma^* \sigma \right) + \lambda_5 \left(H^\dagger H \right) \phi^2 \\
& + \lambda_6 \left(\eta^\dagger \eta \right)^2 + \lambda_7 \left(\eta^\dagger \eta \right) \left(\sigma^* \sigma \right) + \lambda_8 \left(\eta^\dagger \eta \right) \phi^2 + \lambda_9 \left(\sigma^* \sigma \right)^2 + \lambda_{10} \left(\sigma^* \sigma \right) \phi^2 \\
& + \lambda_{11} \phi^4 + \left[\xi \left(H^\dagger \eta \right) \sigma \phi + \kappa_1 \left(H^\dagger \eta \right) \sigma^* + \kappa_2 \sigma^2 \phi + \text{h.c.} \right],
\end{aligned}
$$

$$(5.3)$$

where

$$
H = \begin{pmatrix} H^+ \\ H^0 \end{pmatrix}, \qquad \eta = \begin{pmatrix} \eta^+ \\ \eta^0 \end{pmatrix}. \tag{5.4}
$$

In Eq. (5.3), we have taken ξ, κ_1 and κ_2 as real coefficients. The relevant Yukawa terms of the model are

$$
\mathcal{L}_Y = Y_p \, \overline{L} \, \widetilde{\eta} \, N + Y_v \, \overline{N^c} \, N \, \phi + \text{h.c.} \tag{5.5}
$$

The charges under Z_4 forbid Dirac mass terms at tree-level, similarly to the Scotogenic model. Therefore, a Majorana mass term is built at one-loop level, as shown in Figure 11.
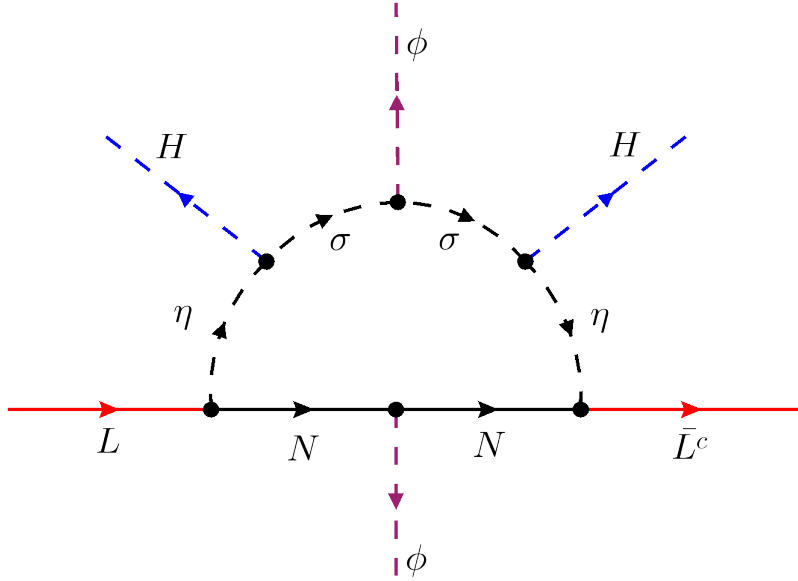
Figure 11: One-loop Feynman diagram for neutrino mass generation in our model, which is a radiative UV realization of the Weinberg operator. After SSB, Majorana neutrino masses are generated. The particles inside the loop are dark matter candidates.

5.2 Mass Spectrum

We perform a change to the mass basis to get the mass spectrum. To achieve this, we first put the scalar fields explicitly in terms of their real and imaginary parts, and let them acquire

a VEV as

$$H^0 \rightarrow \frac{1}{\sqrt{2}} \left(v_H + h_R^0 + i\, h_I^0 \right),$$

$$\eta^0 \rightarrow \frac{1}{\sqrt{2}} \left(v_\eta + \eta_R^0 + i\, \eta_I^0 \right),$$

$$\sigma \rightarrow \frac{1}{\sqrt{2}} \left(v_\sigma + \sigma_R + i\, \sigma_I \right),$$

$$\phi \rightarrow \frac{1}{\sqrt{2}} \left(v_\phi + \phi_R \right).$$

$$(5.6)$$

Recall that ϕ is a real scalar field. In Eqs. (5.6), v_H is the SM Higgs VEV of Eq. (2.56). We find the tadpole equations given by

$$\left. \frac{\partial V}{\partial v_\Psi} \right|_{\Psi=0} = 0, \tag{5.7}$$

where $\Psi = \{H^0, \eta^0, \sigma, \phi\}$ and v_Ψ is each one of their VEVs. Eq. (5.7) will give us four tadpole equations, one for each v_Ψ. A possible solution for v_η and v_σ tadpole equations is setting directly $v_\eta = v_\sigma = 0$. Considering this scenario, the other equations are

$$v_H: \quad v_H^3\, \lambda_1 + \frac{1}{2} v_H\, v_\phi^2\, \lambda_5 + v_H\, \mu_H^2 = 0,$$

$$v_\phi: \quad v_\phi^3\, \lambda_{11} + \frac{1}{2} v_H^2\, v_\phi\, \lambda_5 + v_\phi\, \mu_\phi^2 = 0. \tag{5.8}$$

Solving in terms of μ^2 yields

$$\mu_H^2 = -v_H^2\, \lambda_1 - \frac{1}{2} v_\phi^2\, \lambda_5$$

$$\mu_\phi^2 = -v_\phi^2\, \lambda_{11} - \frac{1}{2} v_H^2\, \lambda_5. \tag{5.9}$$

The mass matrices $\mathcal{M}$ are obtained with

$$\mathcal{M}_{ij} = \left. \frac{\partial^2 V}{\partial \Psi_i \partial \Psi_j} \right|_{\Psi=0}, \tag{5.10}$$

where, again, Ψ is each one of the scalar fields. We will find three different matrices, one for the visible sector[12] (with h_R^0 and ϕ_R), one for the scalar dark sector (η_R^0 and σ_R) and one for the pseudoscalar dark sector (η_I^0 and σ_I). The Higgs pseudoscalar h_I^0 will be the Goldstone boson of the SM Higgs mechanism.

After substituting Eqs. (5.9), the mass matrix for the visible sector is given by

$$\mathcal{M}_{\text{Visible}} = \begin{pmatrix} 2\, v_H^2\, \lambda_1 & v_H\, v_\phi\, \lambda_5 \\ v_H\, v_\phi\, \lambda_5 & 2\, v_\phi^2\, \lambda_{11} \end{pmatrix}. \tag{5.11}$$

The mass matrix is diagonalized by a 2×2 rotation matrix

$$\mathcal{O}_{\text{Visible}} = \begin{pmatrix} \cos\theta_V & \sin\theta_V \\ -\sin\theta_V & \cos\theta_V \end{pmatrix}, \tag{5.12}$$

---

[12]We call *dark sector* to every particle with imaginary charge i under Z_4 in this model. From the dark sector, only the lightest particle is dark matter. We call *visible sector* to any particle not belonging to the dark sector, including SM particles.

where

$$\tan(2\theta_V) = \frac{v_H \, v_\phi \, \lambda_5}{v_\phi^2 \, \lambda_{11} - v_H^2 \, \lambda_1}. \tag{5.13}$$

Thus, the rotation between the interaction and mass eigenstates V_1 and V_2 is given by

$$\begin{pmatrix} V_1 \\ V_2 \end{pmatrix} = \mathcal{O}_{\text{Visible}} \begin{pmatrix} h_R^0 \\ \phi_R \end{pmatrix}. \tag{5.14}$$

The masses for these eigenstates are

$$m_{V_1}^2 = \left(v_H^2 \, \lambda_1 + v_\phi^2 \, \lambda_{11} - \sqrt{(v_H^2 \, \lambda_1 - v_\phi^2 \, \lambda_{11})^2 + (v_H \, v_\phi \, \lambda_5)^2} \right), \tag{5.15}$$

$$m_{V_2}^2 = \left(v_H^2 \, \lambda_1 + v_\phi^2 \, \lambda_{11} + \sqrt{(v_H^2 \, \lambda_1 - v_\phi^2 \, \lambda_{11})^2 + (v_H \, v_\phi \, \lambda_5)^2} \right). \tag{5.16}$$

We identify one of these mass eigenstates as the physical Higgs field, with $m_h = 125.25$ GeV.

For the scalar dark sector, the mass matrix is given by

$$\mathcal{M}_{DM_X} = \begin{pmatrix} a & b_X \\ b_X & c_X \end{pmatrix}, \tag{5.17}$$

where

$$\begin{aligned}
a &= \frac{1}{2} \left[v_H^2 \, (\lambda_2 + \lambda_3) + v_\phi^2 \, \lambda_8 + 2 \, \mu_\eta^2 \right], \\
b_X &= \frac{1}{2} v_H \left(\sqrt{2} \, \kappa_1 + \zeta_X \, v_\phi \, \xi \right), \\
c_X &= \frac{1}{2} \left[\zeta_X \, 2\sqrt{2} \, v_\phi \, \kappa_2 + v_\phi^2 \, \lambda_{10} + v_H^2 \, \lambda_4 + 2 \, \mu_\sigma^2 \right].
\end{aligned} \tag{5.18}$$

Here, $X = \{R, I\}$ indicates real and imaginary, with $\zeta_R = 1$ and $\zeta_I = -1$. Similar to the visible case, the mass matrices are diagonalized by a 2×2 rotation matrix given by

$$\mathcal{O}_{DM_X} = \begin{pmatrix} \cos\theta_X & \sin\theta_X \\ -\sin\theta_X & \cos\theta_X \end{pmatrix}, \tag{5.19}$$

where

$$\tan(2\,\theta_X) = \frac{2\,b_X}{c_X - a}. \tag{5.20}$$

The rotation between the interaction and mass eigenstates X_1 and X_2[13] is

$$\begin{pmatrix} X_1 \\ X_2 \end{pmatrix} = \mathcal{O}_{DM_X} \begin{pmatrix} \eta_X^0 \\ \sigma_X \end{pmatrix}. \tag{5.21}$$

The masses for these eigenstates are

$$m_{X_1}^2 = \frac{1}{2} \left(a + c_X - \sqrt{(a - c_X)^2 + 4\,b_X^2} \right), \tag{5.22}$$

$$m_{X_2}^2 = \frac{1}{2} \left(a + c_X + \sqrt{(a - c_X)^2 + 4\,b_X^2} \right). \tag{5.23}$$

---

[13]Therefore, the notation is R_1 and R_2 for the scalars, and I_1 and I_2 for the pseudoscalars.
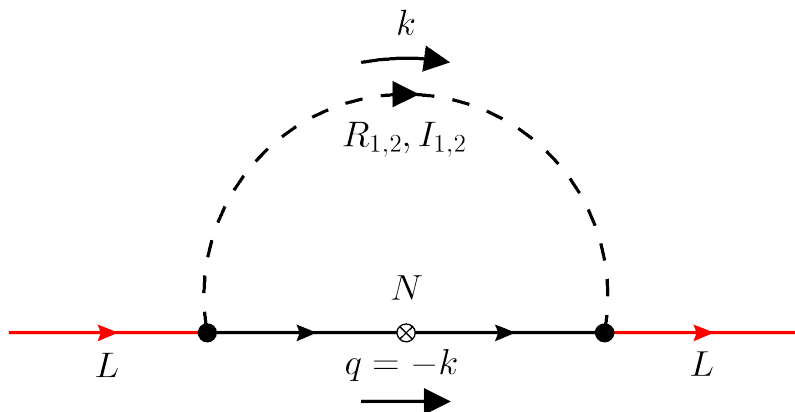
Figure 12: One-loop Feynman diagram in the mass basis, where the scalar fields are mixed and H^0 and ϕ have acquired a VEV.

Therefore,

$$m_{X_2}^2 = m_{X_1}^2 + \Delta m_X^2, \tag{5.24}$$

where Δm_X^2 is the mass splitting between the two scalars, given by

$$\Delta m_X^2 = \sqrt{(a - c_X)^2 + 4\, b_X^2}. \tag{5.25}$$

The mass for the charged scalar particle $\eta^\pm$ is

$$m_{\eta^\pm}^2 = \frac{1}{2} \left(v_H^2\, \lambda_2 + v_\phi^2\, \lambda_8 \right) + \mu_\eta^2. \tag{5.26}$$

Regarding the fermionic sector, the mass of the fermions N_k are given through SSB by

$$m_{N_k} = \sqrt{2}\, (Y_v)_{kk}\, v_\phi. \tag{5.27}$$

We work in a basis where fermions N_k do not mix with each other, implying a diagonal Yukawa matrix Y_v.

5.3   Neutrino Masses and Numerical Analysis

After scalar fields get mixed through Eq. (5.14) and Eq. (5.21), the resulting one-loop Feynman diagram in the mass basis is shown in Fig. 12. The propagator is now one of each of the mixed scalar fields $R_{1,2}$ and pseudoscalars $I_{1,2}$. The amplitude for this diagram in the vanishing external momentum limit reads

$$\mathcal{M} = V^A \int \frac{d^4 k}{(2\pi)^4} \frac{m_{N_k}}{(k^2 - m_A^2)(k^2 - m_{N_k}^2)}, \tag{5.28}$$

where V^A are vertex coefficients arising from the couplings in $Y_p\, \overline{L}\, \widetilde{\eta}\, N$. Linear momentum terms vanish when integrated. The integral (5.28) is the one-loop scalar Passarino-Veltman

49

function B_0 [93], whose solution is Eq. (C.14), given in the Appendix C. The total integral amplitude yields

$$(\mathcal{M}_\nu)_{\alpha\beta} = \sum_i^3 \frac{(Y_p)_{\alpha i} (Y_p)_{i\beta}}{32\pi^2} M_{N_i} \sum_{A=1}^4 V_A(\theta_X) V_A^*(\theta_X) \left[\frac{m_A^2 \log m_A^2 - M_{N_i}^2 \log M_{N_i}^2}{m_A^2 - M_{N_i}^2} \right] \tag{5.29}$$

with

$$m_1 = m_{R_1}, \qquad m_2 = m_{I_1}, \qquad m_3 = m_{R_2}, \qquad m_4 = m_{I_2}; \tag{5.30}$$

and

$$V_1 = \cos(\theta_R), \qquad V_2 = -i\cos(\theta_I), \qquad V_3 = -\sin(\theta_R) \qquad \text{and} \qquad V_4 = i\sin(\theta_I). \tag{5.31}$$

The neutrino mass matrix can be rewritten as

$$(M_\nu)_{\alpha\beta} = \left(Y_p^T \Lambda Y_p \right)_{\alpha\beta}, \tag{5.32}$$

where the Λ matrix is

$$\Lambda = \begin{pmatrix} \Lambda_1 & 0 & 0 \\ 0 & \Lambda_2 & 0 \\ 0 & 0 & \Lambda_3 \end{pmatrix}, \qquad \text{with}$$

$$\Lambda_i = \frac{1}{32\pi^2} M_{N_i} \sum_{A=1}^4 V_A(\theta_X) V_A^*(\theta_X) \left[\frac{m_A^2 \log m_A^2 - M_{N_i}^2 \log M_{N_i}^2}{m_A^2 - M_{N_i}^2} \right]. \tag{5.33}$$

The neutrino mass matrix is diagonalized with

$$U_{\text{PMNS}}^T M_\nu U_{\text{PMNS}} = \hat{m}_\nu \equiv \begin{pmatrix} m_1 & 0 & 0 \\ 0 & m_2 & 0 \\ 0 & 0 & m_3 \end{pmatrix}. \tag{5.34}$$

where the mixing matrix U_{PMNS} is given in Eq. (3.30)[14]. Using the Casas-Ibarra parametrization [94], the Yukawa matrix $(Y_p)_{i\alpha}$ can be written as

$$Y_p = \sqrt{\Lambda}^{-1} R \sqrt{\hat{m}_\nu} U_{\text{PMNS}}^\dagger, \tag{5.35}$$

where R is a complex orthogonal matrix such that $R^T R = 1$. Using this parametrization, we are allowed to use neutrino oscillation data as input to determine the Yukawa matrix values.

It is possible to make a numerical scan in order to obtain numerical results for the model parameters. First, we obtain the Yukawa matrix with Eq. (5.35), assuming normal ordering, a light mass of $m_{\nu 1} = 10^{-3}$ eV, and assigning the best-fit value for oscillation parameters in U_{PMNS} from Table 4. This ensures that our Yukawa couplings can reproduce correctly neutrino masses and oscillation data. The values assigned as inputs for the masses, mixing angles and some couplings in the model are shown in Table 7, where we have introduced a mass splitting between the scalar and pseudoscalar fields as

$$\Delta M^2 = m_{I_2}^2 - m_{R_2}^2. \tag{5.36}$$

---

[14]Majorana phases will be neglected in the computations.

Parameter	Input
λ_6, λ_9	1
$\lambda_2, \lambda_4, \lambda_7$	10^{-4}
μ_η^2, μ_σ^2	100 GeV^2
$\cos(\theta_R), \cos(\theta_V)$	$[0.75, 0.99]$
m_{R_1}	$[300, 2000]$ GeV
Δm_R^2	$[10, 100]^2$ GeV^2
Δm_I^2	$[10, 100]^2$ GeV^2
ΔM^2	$[10, 100]^2$ GeV^2
m_ϕ	$[300, 2000]$ GeV
$m_{\eta^\pm}$	$[300, 2000]$ GeV
m_{N_i}	$[10, \min(m_{R_{1,2}}, m_{I_{1,2}}, m_{\eta^\pm})]$ GeV

Table 7: Input parameters for the one-loop model.

We will analyze the case of a fermionic dark matter candidate, namely, N_i. Thus, in order to maintain N_i as the stable dark matter candidate of the model, the maximum possible value for its mass is the minimum value between all the other odd scalar fields. The mixing angles θ_X and θ_V are selected to be small, indicating minimal mixing between the mass and flavor eigenstates of the scalar and pseudoscalar particles in the model. The input parameter values completely determine the spectrum parameter, defining a benchmark point from which phenomenology of the model can be studied.

The condition for a potential to be bounded from below imposes additional constraints in the parameter spectrum [95, 96]. For potential (5.3), these conditions read

$$\lambda_{1,6,9,11} > 0, \qquad \lambda_2 \geq -2\sqrt{\lambda_1 \lambda_6}, \qquad \lambda_4 \geq -2\sqrt{\lambda_1 \lambda_9}, \qquad \lambda_5 \geq -2\sqrt{\lambda_1 \lambda_{11}},$$
$$\lambda_7 \geq -2\sqrt{\lambda_6 \lambda_9}, \qquad \lambda_8 \geq -2\sqrt{\lambda_6 \lambda_{11}}, \qquad \lambda_{10} \geq -2\sqrt{\lambda_9 \lambda_{11}}, \qquad \lambda_2 + \lambda_3 \geq -2\sqrt{\lambda_1 \lambda_6}.$$
$$(5.37)$$

With these inputs and constraints, a correlation between the Yukawa values and the fermion mass m_N is displayed in Fig 13. We can see that the Yukawa couplings in the model can be less suppressed than those of a tree-level seesaw mechanism, achieving small neutrino masses in a more natural way.
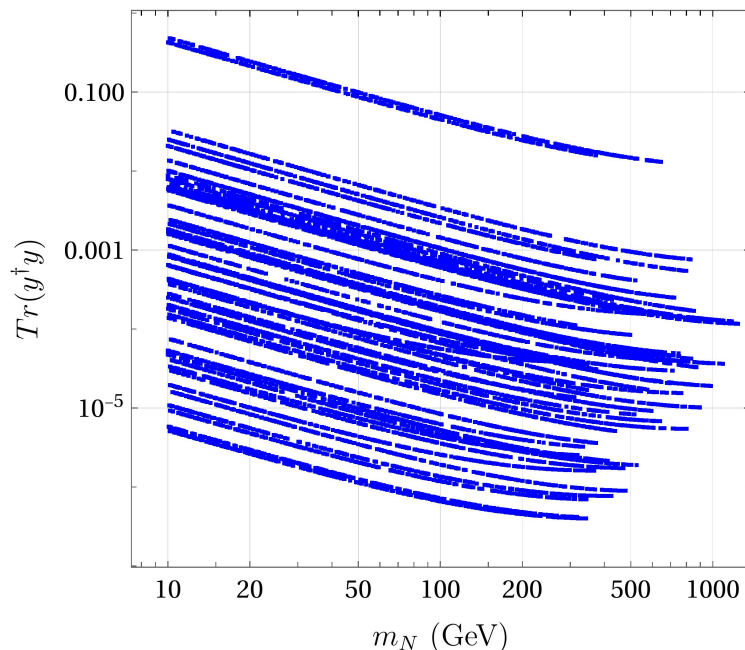
Figure 13: Fermion mass vs $\text{Tr}(Y^\dagger Y)$ in the one-loop model.

5.4   Dark Matter Phenomenology

We consider fermionic dark matter, with N_i the lightest particle. The annihilation channels are shown in Figure 14. The Yukawa interaction $Y_p \bar{L} \widetilde{\eta} N$ gives rise to LFV processes, namely, $\ell_\alpha \to \ell_\beta \gamma$ and $\ell_\alpha \to 3\ell_\beta$, where $\ell_\alpha = \{e, \mu, \tau\}$. These processes are constrained by experimental limits[15], which impose the Yukawa coupling Y_p to be small ($Y_p \ll 1$) [97]. Therefore, the annihilation via t-channel (Fig. 14a) becomes suppressed, inducing dark matter overabundance [98, 99]. The addition of the real singlet scalar ϕ allows another two channels for NN annihilation through the interaction $Y_v \overline{N^c} N \phi$, shown in Figs. 14b and 14c. These annihilation channels contribute to the dark matter relic abundance without being constrained by LFV upper limits. Two similar models are discussed in [97] and [100], but with an additional Majoron field coming from spontaneous lepton number breaking.

In our model, there is the possibility of *cannibalism* effect [101], which allows three particles to annihilate into two. In such a $3 \to 2$ process, mass is turned into kinetic energy of the outgoing particles, heating the dark sector [102]. In this model, this can be achieved through

$$3N \to N + \phi, \tag{5.38}$$

whose diagram is shown in Fig. 15.

---

[15]The LFV Feynman diagrams and experimental bounds are displayed in Section 6, in Figs. 19,20,21, and Table 10, respectively.
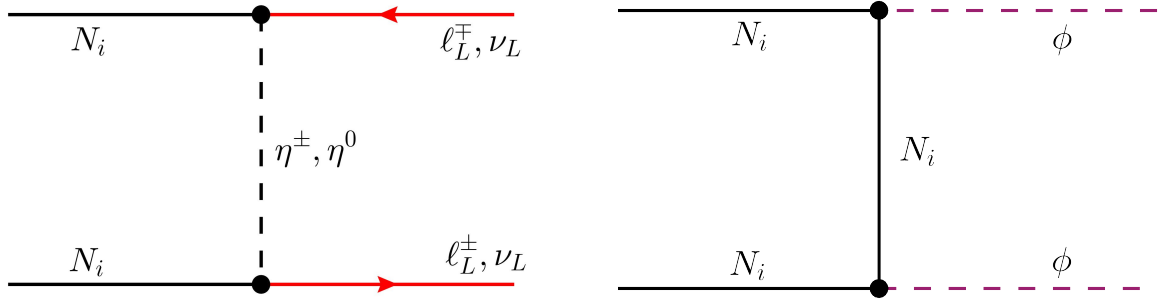
(a) *t*-channel for dark matter annihilation through η into SM leptons.

(b) *t*-channel for dark matter annihilation to ϕ fields.
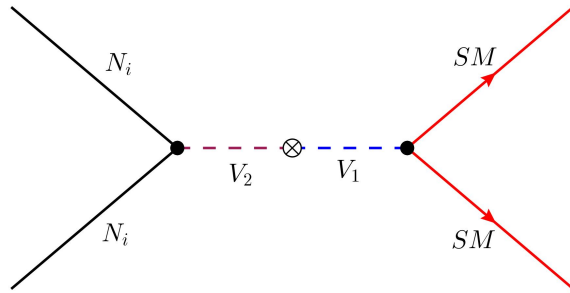
(c) *s*-channel for dark matter annihilation through the Higgs portal into SM particles.

Figure 14: Fermionic dark matter annihilation channels.
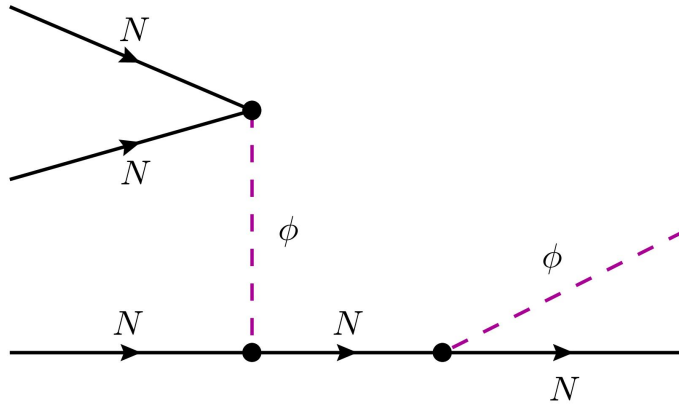
Figure 15: Cannibal process in which three particles annihilate into two: $3N \to N + \phi$.

An extra condition $m_{N_i} > m_\phi/2$ has to be imposed to kinematically allow such process. If allowed, it contributes also to the dark matter relic density, leading to a different cosmological history.

A numerical scan of the relic abundance versus the dark matter mass m_{N_i} can be made. The input parameters should fulfill the constraints given by Eq. (5.37), neutrino oscillation data, LFV processes and electroweak precision [103, 104]. There are two regions of interest to be explored:

- $m_{N_i} < m_\phi$: *forbidden* region.

- $m_{N_i} > m_\phi$: *secluded* region.

In the forbidden region, the t-channel of Fig. 14b is kinematically suppressed. Inside this region, when $1.5\,m_{N_i} < m_\phi < 2\,m_{N_i}$, the cannibal process of Fig. 15 becomes relevant. There are also two *resonant regions* with $m_{N_i} \sim m_{V_1}/2$ and $m_{N_i} \sim m_{V_2}/2$, where dark matter annihilates more efficiently.

Using the computer tools `SARAH (versions 4.15.2 and 4.11.0)`[16] [106], `SPheno (4.0.2)` [107, 108] and `micrOmegas (5.3.41)` [109] we can obtain a numerical value for the relic density for different benchmark points. First, the model is implemented in `SARAH`, a `Mathematica` package that provides analytical information about the model. With `SARAH` it is possible to obtain a source code for `SPheno`, where the analytical expressions are evaluated numerically given input values. Several observables can also be obtained in `SPheno` with the `FlavorKit` extension [108], such as LFV branching ratios. Finally, `SARAH` also generates a source code for `micrOmegas`[17], which is a routine that calculates the relic density for the numerical outputs obtained with `SPheno`.

We perform a numerical scan considering N_1 as the dark matter candidate, and fixing $m_\phi = 30\,\text{GeV}$. We consider the input values in table 8. The Yukawa couplings $(Y_p)_{ij}$ are fixed to reproduce neutrino oscillation data and to be allowed by LFV constraints. Other parameters have been fixed, having $\xi = 10^{-13}, \lambda_{11} = 0.1$ and the Higgs mixing coupling with ϕ as $\lambda_5 = 0.01$. The parameter λ_1 is solved in each iteration for $m_H = 125.25\,\text{GeV}$ and m_ϕ. The Yukawa couplings $(Y_v)_{22}$ and $(Y_v)_{33}$ are chosen to be > 1, ensuring heavy fermions. To perform the scan, we have used an approximate numerical solution given in [110].

Parameter	Input
$\lambda_{2,3,4,6,7,9},\ \kappa_2$	$[10^{-6}, 1]$
λ_8	$[10^{-2}, 1]$
λ_{10}	$[10^{-6}, 10^{-2}]$
κ_1	$[10^{-6}, 10^{-3}]$
μ_η^2, μ_σ^2	$[10^6, 10^7]\ \text{GeV}^2$
$(Y_v)_{11}$	$[0.06, 0.45]$
v_ϕ	$[5, 300]\ \text{GeV}$

Table 8: Input parameters for relic density scan

---

[16]For a pedagogical `SARAH` tutorial, see [105].

[17]We have used `SARAH (4.15.2)` for `micrOmegas (5.3.41)` and `SARAH (4.11.0)` for `SPheno (4.0.2)`, ensuring compatibility between distinct versions of the programs.

The corresponding plot is shown in Fig. 16. The horizontal lines represent the value of the relic density observed by PLANCK in 2018 with a 3σ range [12]:

$$\Omega_{N_1}h^2 = 0.120 \pm 0.0036. \tag{5.39}$$

Points falling within this range are printed in red color. Points below the line, printed in blue, indicate underabundant dark matter, implying that contributions from another dark matter candidate are required to reproduce the correct relic density value. The green vertical line represents $m_{N_1} = 30\,\text{GeV}$. The region to the left of this line is the forbidden region, while the region to the right is the secluded region. At $m_{N_1} \sim m_\phi/2 = 15\,\text{GeV}$ we observe the first resonance region, where dark matter annihilates efficiently resulting in low values for the relic density. The second resonance occurs at $m_{N_1} \sim m_h/2 \approx 62\,\text{GeV}$, as depicted in the plot.
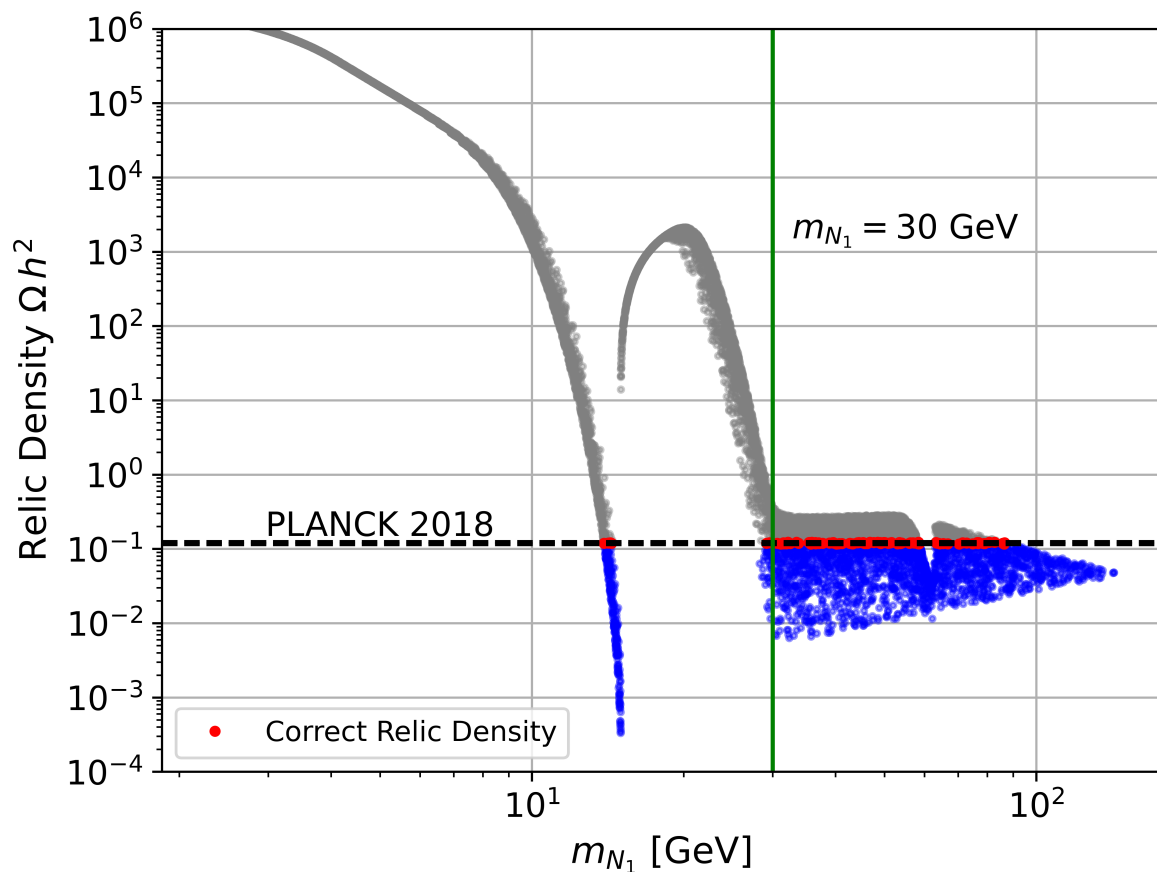
Figure 16: Cannibal process in which three particles annihilate into two: $3N \to N + \phi$.

5.5   One-loop Model Summary

We have proposed a neutrino mass model that generates neutrino masses at one-loop level. This extension of the SM consists of a discrete Z_4 symmetry spontaneously broken to Z_2, with the addition of three singlet fermions N_i, a scalar doublet η, and a scalar singlet σ, constituting the dark sector of the model. Additionally, we have included a scalar singlet ϕ, enabling two extra annihilation channels for dark matter when considering a fermionic dark matter candidate.

We have derived the mass spectrum for the model and included a numerical analysis where points reproduce neutrino oscillation data. Furthermore, we have discussed the possibilities for the dark matter relic density contributions in a fermionic dark candidate scenario, generating a numerical scan which includes the forbidden and secluded regions, with points reproducing correctly the dark matter relic density and also underabundant dark matter.

Additional relic density scans, the analysis of the cannibal process and a discussion regarding the cosmological history within the model represent future goals and possibilities, which are still work in progress at the moment of the realization of this thesis.

6 Two-Loop Mass Generation Model

In this section, we introduce another proposal for a radiative neutrino mass model, in which a two-loop mechanism generates Majorana neutrino masses. Given an extra suppression factor of $(\frac{1}{16\pi^2})^2$ due to the two loops, the Yukawa couplings can have a greater value than in a one-loop mechanism to reproduce the light neutrino masses.

In this model, the SM is extended with a $U(1)_{B-L}$ gauge symmetry, spontaneously broken to Z_3. We include three singlet fermions, a doublet, and a singlet scalar as the dark matter sector. The lightest of these particles will represent a dark matter candidate, protected by the preserved Z_3 symmetry. We include three fermions along with singlet scalar fields to have an anomaly free $U(1)_{B-L}$ symmetry, as explained below. We derive the mass spectrum of the model and study some of its phenomenological implications, such as Lepton Flavor Violation processes.

6.1 Model and Mass Spectrum

We extend the SM with a gauged symmetry $U(1)_{B-L}$ spontaneously broken into a discrete symmetry Z_3:

$$SU(2)_L \times U(1)_Y \times U(1)_{B-L} \rightarrow U(1)_{EM} \times Z_3. \tag{6.1}$$

The particle content of the model is given in Table 9. The vector-like singlet fermions $\chi_{L,R}$,

	Fields	$SU(2)_L \otimes U(1)_Y$	$U(1)_{B-L}$	Z_3
Fermions	L_i	$(\mathbf{2}, -1/2)$	-1	1
	e_{R_i}	$(\mathbf{1}, -1)$	-1	1
	$\chi_{(L,R)_j}$	$(\mathbf{1}, 0)$	$-1/3$	ω^2
	N_k	$(\mathbf{1}, 0)$	$(-4, -4, 5)$	1
Scalars	H	$(\mathbf{2}, 1/2)$	0	1
	η	$(\mathbf{2}, 1/2)$	$2/3$	ω^2
	ρ	$(\mathbf{1}, 0)$	$2/3$	ω^2
	$\phi_1, \phi_2, \phi_6, \phi_8$	$(\mathbf{1}, 0)$	$(1, 2, 6, 8)$	1

Table 9: Particle content of the model with $i \in \{e, \mu, \tau\}$, $j \in \{1, 2, 3\}$ and $k \in \{-4, -4, 5\}$, corresponding to each one of the charges $(-4, -4, 5)$. All the fields listed are $SU(3)_C$ singlets. Particles with non-trivial charges under Z_3 correspond to dark matter candidates.

the doublet scalar η and the singlet scalar ρ are dark matter candidates, having non-trivial charges under Z_3. The N_k charges $(-4, -4, 5)$ are assigned to cancel anomalies for the extra symmetry $U(1)_{B-L}$ (see Appendix A). Consequently, fields ϕ_1 and ϕ_8 are included to give masses to N_k, avoiding extra radiation contributions to the universe constrained by cosmological observations. However, an accidental $U(1)'$ symmetry emerges when ϕ_1 and ϕ_8 are added. This symmetry is undesired since it generates an extra Goldstone boson in the theory. To avoid such accidental symmetry, we include ϕ_6. An alternative to this addition would be considering soft-breaking terms in the Lagrangian, which consist of terms with couplings of positive mass dimension breaking softly[18] the $U(1)'$ symmetry.

---

[18]The idea of *softly* breaking a symmetry is to break it at low-energies with an explicit term in the Lagrangian, but with the symmetry conserved at high-energy limits. We will not discuss further in this thesis. For an example, see [111] in the context of supersymmetry.
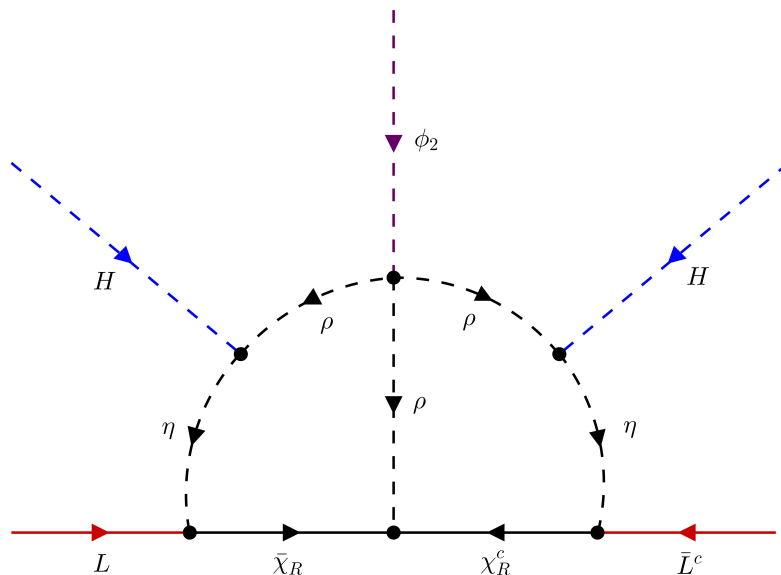
Figure 17: Two-loop Feynman diagram for neutrino mass generation in our model. After SSB, Majorana neutrino masses are generated. Particles inside the loops are dark matter candidates.

The assigned $U(1)_{B-L}$ charges forbid tree- and one loop-level neutrino masses. The renormalizable scalar potential of the model is given by

$$
\begin{aligned}
\mathcal{L}_V = & \sum_i \mu_i^2 \, \mathbf{\Phi}_i^\dagger \mathbf{\Phi}_i + \frac{1}{2} \sum_{i,j} \lambda_{ij} \left(\mathbf{\Phi}_i^\dagger \mathbf{\Phi}_i \right) \left(\mathbf{\Phi}_j^\dagger \mathbf{\Phi}_j \right) + \lambda \left(H^\dagger \eta \right) \left(\eta^\dagger H \right) \\
& + \left(\xi_1 \, \rho^3 \phi_2^* + \xi_2 \, \phi_6^* \phi_2^3 + \xi_3 \, \phi_8^* \phi_6 \phi_1^2 + \kappa_1 \, H^\dagger \eta \rho^* + \kappa_2 \, \phi_1^2 \phi_2^* + \kappa_3 \, \phi_8 \phi_6^* \phi_2^* + \text{h.c.} \right),
\end{aligned}
\tag{6.2}
$$

where

$$
\mathbf{\Phi} \in \{ H, \eta, \rho, \phi_1, \phi_2, \phi_6, \phi_8 \},
\tag{6.3}
$$

and

$$
H = \begin{pmatrix} H^+ \\ H^0 \end{pmatrix}, \qquad \eta = \begin{pmatrix} \eta^+ \\ \eta^0 \end{pmatrix}.
\tag{6.4}
$$

The explicit scalar potential is displayed in Appendix B. The relevant Yukawa interactions are

$$
\mathcal{L}_Y \subset (Y_1)_{\alpha i} \, \overline{L_\alpha} \, \widetilde{\eta} \, \chi_{R_i} + (Y_2)_{ij} \, \rho \, \overline{\chi_{R_i}}^c \chi_{R_j} + m_\chi \, \overline{\chi_{L_i}} \chi_{R_j} + \text{h.c.},
\tag{6.5}
$$

where $\alpha = 1, 2, 3$. We consider three copies of the fermion χ_R with no mixing between them. So we have $i = j = 1, 2, 3$. A mass term for χ is given as

$$
m_\chi \, \overline{\chi_{L_i}} \, \chi_{R_j} + \text{h.c.}
\tag{6.6}
$$

The two-loop diagram for neutrino masses is presented in Fig. 17. To obtain the neutrino masses, we perform a change to the mass basis.

The scalar dark sector composed by the scalars η_r^0 and ρ_r, and the pseudoscalars η_i^0 and ρ_i, get mixed in the mass basis. After obtaining their mass matrices (see Appendix B), we

found that the scalar and pseudoscalar dark bosons are degenerate. Therefore, we have two equal 2×2 mass matrices given by

$$\mathcal{M}_{DM}^R = \mathcal{M}_{DM}^I = \mathcal{M}_{DM} = \begin{pmatrix} a & b \\ b & c \end{pmatrix}, \tag{6.7}$$

with

$$a = \frac{1}{2} \left[v_{\phi_1}^2 \, \lambda_{11} + v_{\phi_6}^2 \, \lambda_{12} + v_{\phi_2}^2 \, \lambda_{13} + v_{\phi_8}^2 \, \lambda_{14} + v_H^2 \, (\lambda_2 + \lambda_3) \right] + \mu_\eta^2,$$

$$b = \frac{v_H \, \kappa_2}{\sqrt{2}}, \tag{6.8}$$

$$c = \frac{1}{2} \left[v_{\phi_1}^2 \, \lambda_{16} + v_{\phi_6}^2 \, \lambda_{17} + v_{\phi_2}^2 \, \lambda_{18} + v_{\phi_8}^2 \, \lambda_{19} + v_H^2 \lambda_4 \right] + \mu_\rho^2.$$

The mass matrix is diagonalized by a 2×2 rotation matrix

$$\mathcal{O}_{DM} = \begin{pmatrix} \cos\theta & \sin\theta \\ -\sin\theta & \cos\theta \end{pmatrix}, \tag{6.9}$$

where we have just one mixing angle given by

$$\tan 2\theta = \frac{2b}{a - c}. \tag{6.10}$$

Thus, a rotation between the interaction and mass eigenstates R_1, R_2, I_1 and I_2 can be done with

$$\begin{pmatrix} R_1 \\ R_2 \end{pmatrix} = \mathcal{O}_{DM} \begin{pmatrix} \eta_r^0 \\ \rho_r \end{pmatrix} \qquad \text{and} \qquad \begin{pmatrix} I_1 \\ I_2 \end{pmatrix} = \mathcal{O}_{DM} \begin{pmatrix} \eta_i^0 \\ \rho_i \end{pmatrix}. \tag{6.11}$$

The mass for these eigenstates are

$$m_{R_1}^2 = m_{I_1}^2 = \frac{1}{2} \left(a + c + \sqrt{(a - c)^2 + 4b^2} \right),$$

$$m_{R_2}^2 = m_{I_2}^2 = \frac{1}{2} \left(a + c - \sqrt{(a - c)^2 + 4b^2} \right). \tag{6.12}$$

Therefore

$$m_{R_1}^2 = m_{R_2}^2 + \Delta m^2, \tag{6.13}$$

where Δm^2 is the mass splitting between the two scalars, given by $\Delta m^2 = \sqrt{(a - c)^2 + 4b^2}$. The mass of the charged scalar $\eta^\pm$ is

$$m_{\eta^\pm}^2 = \sqrt{a - \frac{1}{2} v_H^2 \lambda_3}, \tag{6.14}$$

where a is defined in eq. (6.8). Finally, the two-loop diagram in the mass basis is shown in Fig. 18.

6.2 Integral Amplitude

The scalar propagators in Fig. 18 can be one of the four mass eigenstates. To calculate the total diagram amplitude, we need to sum each possible combination. The amplitude for an
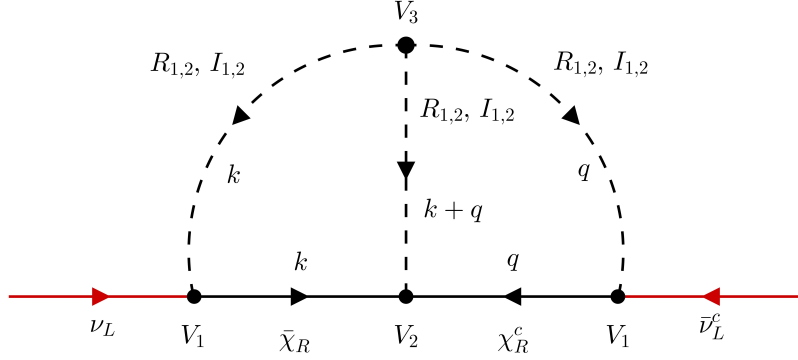
Figure 18: Two-loop diagram in the mass basis. Here, $R_{1,2}$ and $I_{1,2}$ are the scalar and pseudoscalar mass eigenstates, respectively. The total amplitude corresponds to the sum of all the field combinations in the diagram. Vertex and momentum labels are also shown, in the vanishing external momentum limit.

ABC configuration is

$$i\mathcal{M}^{ABC} = V^{ABC} \times I_{ABC}$$

$$= V^{ABC} \times \int \frac{d^4k}{(2\pi)^4} \int \frac{d^4q}{(2\pi)^4} \frac{(\slashed{k} + m_\chi)(\slashed{q} + m_\chi)}{(k^2 - m_A^2)(k^2 - m_\chi^2)(q^2 - m_C^2)(q^2 - m_\chi^2)[(k+q)^2 - m_B^2]}.$$
$$(6.15)$$

Here, $\{A, B, C\}$ represent the left, middle and right propagators emerging from vertex V_3, and they can be any of $\{R_1, R_2, I_1, I_2\}$. The coefficient V^{ABC} corresponds to the vertex products in the diagram.

The three relevant interactions are $(Y_1)_{\alpha i}\, \bar{L}_\alpha\, \tilde{\eta}\, \chi_{R_i}$, $(Y_2)_{ij}\, \rho\, \chi^c_{R_i}\, \chi_{R_j}$ and $\xi_1\, \rho^3 \phi_2^*$, each one with its complex conjugate term. Dropping the matrix structure of the Yukawa couplings for now, we have:

$\mathbf{V_1} : y_1 \bar{L}\, \tilde{\eta}\, \chi_R + \text{h.c.}$

$$\longrightarrow y_1 \bar{\nu}_L \eta^{0*} \chi_R + \text{h.c.} \xrightarrow{\text{mass basis}} \frac{y_1 \bar{\nu}_L}{\sqrt{2}} \left(c_\theta R_1 - s_\theta R_2 - i c_\theta I_1 + i s_\theta I_2 \right) \chi_R + \text{h.c.}, \qquad (6.16)$$

$\mathbf{V_2} : y_2\, \rho\, \chi^c_R\, \chi_R + \text{h.c.}$

$$\xrightarrow{\text{mass basis}} \frac{y_2}{\sqrt{2}} \left(s_\theta R_1 + c_\theta R_2 + i s_\theta I_1 + i c_\theta I_2 \right) \bar{\chi}^c_R \chi_R + \text{h.c.}, \qquad (6.17)$$

$\mathbf{V_3} : \xi_1\, \rho^3 \phi_2^* + \text{h.c.}$

$$\xrightarrow{SSB} \xi_1 \left(\frac{\rho_r + i\rho_i}{\sqrt{2}} \right)^3 \frac{v_{\phi_2}}{\sqrt{2}} + \text{h.c.} \xrightarrow{\text{Mass Basis}} \frac{\xi_1}{4} \left[(s_\theta R_1 + c_\theta R_2) + i (s_\theta I_1 + c_\theta I_2) \right]^3 v_{\phi_2} + \text{h.c.}$$

$$= \xi_1 v_{\phi_2} \left(\frac{1}{2} s_\theta^3 R_1^3 + \frac{1}{2} c_\theta^3 R_2^3 + \frac{3}{2} s_\theta^2 c_\theta R_1^2 R_2 + \frac{3}{2} c_\theta^2 s_\theta R_2^2 R_1 - \frac{3}{2} s_\theta^3 I_1^2 R_1 - \frac{3}{2} s_\theta^2 c_\theta I_1^2 R_2 \right.$$

$$\left. - \frac{3}{2} c_\theta^2 s_\theta I_2^2 R_1 - \frac{3}{2} c_\theta^3 I_2^2 R_2 - 3 c_\theta^2 s_\theta I_1 I_2 R_2 - 3 s_\theta^2 c_\theta I_1 I_2 R_1 \right). \qquad (6.18)$$

Therefore, depending on the field combination, the vertex coefficient will change accordingly,

60

given by

$$V^{ABC} = \frac{y_1^2\, y_2\, \xi_1 v_{\phi_2}}{2\sqrt{2}} \left[V_1^A(\theta) \times V_2^B(\theta) \times V_1^C(\theta) \times V_3^{ABC}(\theta) \right]. \tag{6.19}$$

Note that all terms in the V_3 vertex are real, which means that diagrams with an odd number of pseudoscalar fields I are zero, i.e., $V_3^{IR^2} = V_3^{I^3} = 0$.

Now we evaluate I_{ABC}. We have

$$I_{ABC} = \int \frac{d^4k}{(2\pi)^4} \int \frac{d^4q}{(2\pi)^4} \frac{(\slashed{k} + m_\chi)(\slashed{q} + m_\chi)}{(k^2 - m_A^2)(k^2 - m_\chi^2)(q^2 - m_C^2)(q^2 - m_\chi^2)[(k+q)^2 - m_B^2]}. \tag{6.20}$$

The numerator can be written as a trace, giving

$$\begin{aligned}
\mathrm{Tr}\{(\gamma^\mu k^\mu + m_\chi)(\gamma^\nu q^\nu + m_\chi)\} &= k^\mu q^\nu \,\mathrm{Tr}\{\gamma^\mu \gamma^\nu\} + \mathrm{Tr}\{m_\chi^2\} \\
&= 4\, k^\mu q^\nu \eta^{\mu\nu} + 4\, m_\chi^2 \\
&= 4\, k \cdot q + 4\, m_\chi^2 \\
&= 4\left\{ \frac{1}{2}[(k+q)^2 - k^2 - q^2] + m_\chi^2 \right\}
\end{aligned} \tag{6.21}$$

Thus, the integral I_{ABC} is:

$$I_{ABC} = \frac{4}{(16\pi^2)^2} \left[m_\chi^2 I_{ABC}^{(1)} + \frac{1}{2}\left(I_{ABC}^{[(k+q)^2]} - I_{ABC}^{(k^2)} - I_{ABC}^{(q^2)} \right) \right]. \tag{6.22}$$

These integrals can be written in terms of "master integrals" which solution is known, given in appendix C. After a rescaling in m_B^2, we obtain that

$$\frac{1}{m_B^2} I_{ABC}^{(1)} = \frac{1}{m_B^2} \frac{1}{(t_{AB} - r_B)(t_{CB} - r_B)} \left\{ -\hat{g}(t_{AB}, t_{CB}) + \hat{g}(r_B, t_{CB}) + \hat{g}(t_{AB}, r_B) - \hat{g}(r_B, r_B) \right\}, \tag{6.23}$$

$$\begin{aligned}
I_{ABC}^{(k^2)} = \Bigg\{ & \frac{1}{t_{CB} - r_B}[-\hat{g}(r_B, t_{CB}) + \hat{g}(r_B, r_B)] \\
& + \frac{t_{AB}}{(t_{AB} - r_B)(t_{CB} - r_B)}[-\hat{g}(t_{AB}, t_{CB}) + \hat{g}(t_{AB}, r_B) + \hat{g}(r_B, t_{CB}) - \hat{g}(r_B, r_B)] \Bigg\},
\end{aligned} \tag{6.24}$$

$$\begin{aligned}
I_{ABC}^{(q^2)} = \Bigg\{ & \frac{1}{t_{AB} - r_B}[-\hat{g}(t_{AB}, r_B) + \hat{g}(r_B, r_B)] \\
& + \frac{t_{CB}}{(t_{AB} - r_B)(t_{CB} - r_B)}[-\hat{g}(t_{AB}, t_{CB}) + \hat{g}(t_{AB}, r_B) + \hat{g}(r_B, t_{CB}) - \hat{g}(r_B, r_B)] \Bigg\},
\end{aligned} \tag{6.25}$$

$$I_{ABC}^{[(k+q)^2]} = \left\{ \hat{B}_0'(0, r_B, t_{AB})\, \hat{B}_0'(0, r_B, t_{CB}) + \frac{-\hat{g}(t_{AB}, t_{CB}) + \hat{g}(t_{AB}, r_B) + \hat{g}(r_B, t_{CB}) - \hat{g}(r_B, r_B)}{(t_{AB} - r_B)(t_{CB} - r_B)} \right\}. \tag{6.26}$$

LFV Process	Branching Ratio Present Bound
$\mu \to e\gamma$	4.2×10^{-13} [112]
$\tau \to e\gamma$	3.3×10^{-8} [113]
$\tau \to \mu\gamma$	4.4×10^{-8} [113]
$\mu \to 3e$	1.0×10^{-12} [114]
$\tau \to 3e$	2.7×10^{-8} [115]
$\tau \to 3\mu$	2.1×10^{-8} [115]

Table 10: Current experimental upper bounds for the branching ratio of LFV observables.

Here,

$$r_B = \left(\frac{m_\chi}{m_B}\right)^2, \qquad t_{AB} = \left(\frac{m_A}{m_B}\right)^2, \qquad t_{CB} = \left(\frac{m_C}{m_B}\right)^2. \tag{6.27}$$

Combining all terms, we have the final result for the neutrino mass matrix:

$$(M_\nu)_{\alpha\beta} = \sum_i^3 \frac{4\,(Y_1)_{i\alpha}\,(Y_2)_{ii}\,(Y_1)_{i\beta}\,\xi_1 v_{\phi_2}}{2\sqrt{2}\,(16\pi^2)^2}$$
$$\times \sum_{ABC} \left(V_1^A\,V_2^B\,V_1^C\,V_3^{ABC}\right) \left[\frac{(m_\chi^2)_i}{m_B^2}\,I_{ABC}^{(1)} + \frac{1}{2}\left(I_{ABC}^{[(k+q)^2]} - I_{ABC}^{(k^2)} - I_{ABC}^{(q^2)}\right)\right], \tag{6.28}$$

with $\{A, B, C\}$ all combinations of R_1, R_2, I_1 and I_2.

6.3 Lepton Flavor Violation Processes

The previously analyzed model allows for processes with Lepton Flavor Violation (LFV), in which the flavor lepton number for the charged leptons, displayed in Table 3, is violated. While neutrino oscillations can be understood as a flavor-violating process, this type of phenomenon has not been observed for charged leptons. The experimental searches for LFV processes such as $\ell_\alpha \to \ell_\beta\gamma$ and $\ell_\alpha \to 3\ell_\beta$ have resulted in upper bounds on their branching ratios, as showed in table 10. In this section we analyze those processes in the context of the two-loop model, following the reference [98].

As in the one-loop model of Section 5, the neutrino mass matrix in eq. (6.28) can be rewritten as

$$(M_\nu)_{\alpha\beta} = \left(Y_1^T \Lambda Y_1\right)_{\alpha\beta}, \tag{6.29}$$
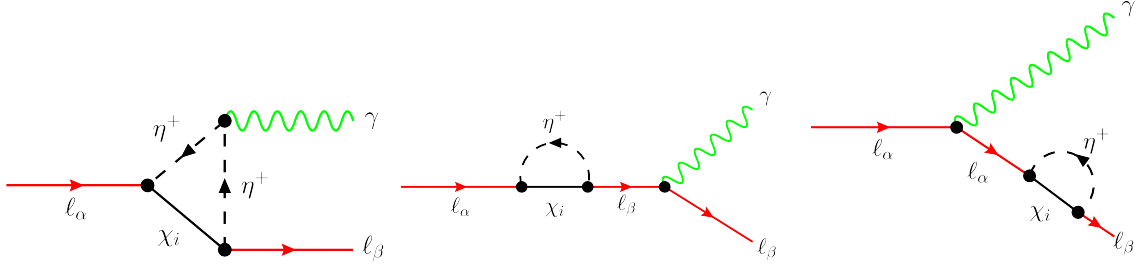
Figure 19: Diagrams contributing to LFV process $\ell_\alpha \to \ell_\beta \gamma$.

where the Λ matrix is

$$
\Lambda = \begin{pmatrix} \Lambda_1 & 0 & 0 \\ 0 & \Lambda_2 & 0 \\ 0 & 0 & \Lambda_3 \end{pmatrix}, \qquad \text{with}
$$

$$
\Lambda_i = \frac{4\,(Y_2)_{ii}\,\xi_1 v_{\phi_2}}{2\sqrt{2}\,(16\pi^2)^2} \times \sum_{ABC} \left(V_1^A\, V_2^B\, V_1^C\, V_3^{ABC} \right) \left[\frac{(m_\chi^2)_i}{m_B^2}\, I_{ABC}^{(1)} + \frac{1}{2}\left(I_{ABC}^{[(k+q)^2]} - I_{ABC}^{(k^2)} - I_{ABC}^{(q^2)} \right) \right].
$$
(6.30)

After using again the Casas-Ibarra parametrization, the Yukawa matrix $(Y_1)_{i\alpha}$ can be written as

$$
Y_1 = \sqrt{\Lambda}^{-1} R \sqrt{\hat{m}_\nu}\, U_{\text{PMNS}}^\dagger.
$$
(6.31)

6.3.1 $\ell_\alpha \to \ell_\beta \gamma$

The process can be described by the effective Lagrangian

$$
\mathcal{L}_{\text{eff}} = \left(\frac{\mu_{\alpha\beta}}{2} \right) \bar{\ell}_\beta \sigma^{\mu\nu} \ell_\alpha F_{\mu\nu},
$$
(6.32)

where $\mu_{\beta\alpha}$ is a transition magnetic moment. The Feynman diagrams contributing to $\ell_\alpha \to \ell_\beta \gamma$ at lowest order are shown in Fig. 19. It is convenient to define $\mu_{\beta\alpha}$ in terms of the dipole form factor A_D as

$$
\mu_{\beta\alpha} = e\, m_\alpha A_D / 2,
$$
(6.33)

where terms proportional to m_β have been neglected. Here, e is the electromagnetic coupling, with $\alpha_{\text{em}} = e^2/(4\pi)$. The 1-loop contributions lead to [98]:

$$
A_D = \sum_{i=1}^{3} \frac{(Y_1)_{i\beta}^*\,(Y_1)_{i\alpha}}{2(4\pi)^2} \frac{1}{m_{\eta^+}^2} F_2(\zeta_i)
$$
(6.34)

where $\zeta_i \equiv m_{\chi_i}^2/m_{\eta^+}^2$ and the function $F_2(x)$ is given in appendix D. The branching ratio for $\ell_\alpha \to \ell_\beta \gamma$ yields

$$
\text{Br}(\ell_\alpha \to \ell_\beta \gamma) = \frac{3(4\pi)^3\,\alpha_{em}}{4\,G_F^2}\, |A_D|^2\, \text{Br}(\ell_\alpha \to \ell_\beta \nu_\alpha \bar{\nu}_\beta),
$$
(6.35)

with G_F the Fermi constant.

6.3.2 $\ell_\alpha \to 3\,\ell_\beta$

This process, denoted more accurately as $\ell_\alpha \to \ell_\beta \bar{\ell}_\beta \ell_\beta$, has four types of contributions at lowest order. These are γ-penguins, Z-penguins, Higgs penguins and box diagrams. Higgs-penguins diagrams are suppressed by the small Yukawa coupling of leptons μ and e, so they will be neglected. The contributing Feynman diagrams are displayed in Fig. 20 and Fig. 21.
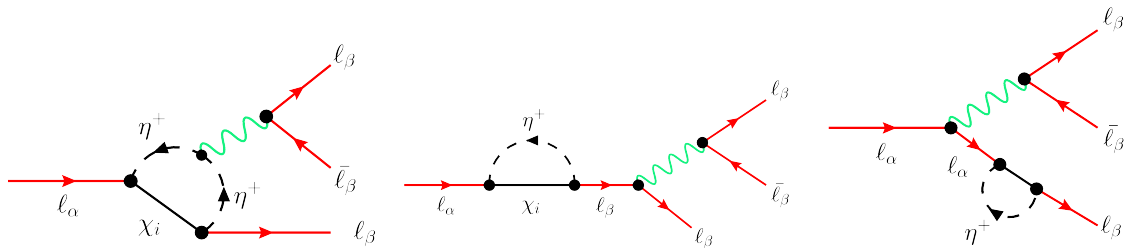
Figure 20: Penguin diagrams contributing to LFV process $\ell_\alpha \to 3\ell_\beta$. The boson exchange can be either a photon or a Z boson.
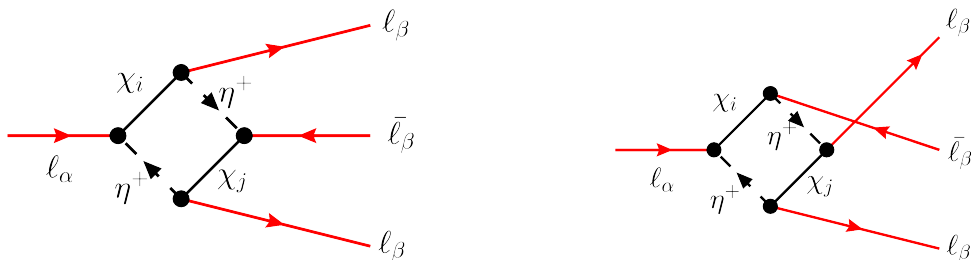
Figure 21: Box diagrams contributing to LFV process $\ell_\alpha \to 3\ell_\beta$.

Following the notation of [98], which is itself inspired in [116, 117], we label the momenta as $\ell_\alpha(p) \to \ell_\beta(k_1)\bar{\ell}_\beta(k_2)\ell_\beta(k_3)$. Then, neglecting factors suppressed by charged lepton masses, the γ-penguin diagrams in Fig. 20 give

$$
\begin{aligned}
i\mathcal{M}_\gamma =\,& ie^2 A_{ND}\, \bar{u}(k_1)\gamma^\mu P_L\, u(p)\bar{u}(k_3)\gamma_\mu v(k_2) \\
& + ie^2 \frac{m_\alpha}{q^2} A_D\, \bar{u}(k_1)\sigma^{\mu\nu}q_\nu P_R\, u(p)\bar{u}(k_3)\gamma_\mu v(k_2) - (k_1 \leftrightarrow k_3),
\end{aligned}
\tag{6.36}
$$

where $q \equiv k_1 - p$ is the photon momentum. The coefficient A_{ND} corresponds to photonic non-dipole contributions and is given by

$$
A_{ND} = \sum_{i=1}^{3} \frac{(Y_1)^*_{i\beta}(Y_1)_{i\alpha}}{6(4\pi)^2}\frac{1}{m_{\eta^+}^2}\, G_2(\zeta_i),
\tag{6.37}
$$

where the loop function $G_2(x)$ is defined in appendix D. Considering now the Z-penguin diagrams, the amplitude can be written as

$$
i\mathcal{M}_Z = \frac{iF}{m_Z^2}\bar{u}(k_1)\gamma^\mu P_R\, u(p)\bar{u}(k_3)\gamma_\mu \left(g_L^\ell P_L + g_R^\ell P_R\right) v(k_2) - (k_1 \leftrightarrow k_3),
\tag{6.38}
$$

64

where

$$g_L^\ell = \frac{g_2}{\cos\theta_W}\left(\frac{1}{2} - \sin^2\theta_W\right) \qquad \text{and} \qquad g_R^\ell = -\frac{g_2}{\cos\theta_W}\left(\sin^2\theta_W\right), \tag{6.39}$$

are the couplings between the Z boson and the charged leptons, with g_2 the $SU(2)_L$ gauge coupling and θ_W the weak mixing angle. The coefficient F is given by

$$F = \sum_{i=1}^{3} \frac{(Y_1)_{i\beta}\,(Y_1)_{i\alpha}}{2(4\pi)^2}\frac{m_\alpha m_\beta}{m_{\eta^+}^2}\frac{g_2}{\cos\theta_W}F_2(\zeta_i). \tag{6.40}$$

For $\ell_\alpha \to 3\,\ell_\beta$, Z-penguins diagrams are suppressed by the product of masses $m_\alpha m_\beta$, so the main contributions come from γ-penguins and box diagrams. For the latter, the amplitude reads

$$i\mathcal{M}_{\text{box}} = ie^2 B\left[\bar{u}(k_3)\gamma^\mu P_L\,v(k_2)\right]\left[\bar{u}(k_1)\gamma_\mu P_L\,u(p)\right]. \tag{6.41}$$

The coefficient B is defined as

$$B = \frac{1}{e^2(4\pi)^2 m_{\eta^+}^2}$$

$$\times \sum_{i,j=1}^{3}\left[\frac{1}{2}D_1\left(\zeta_i,\zeta_j\right)(Y_1)_{j\beta}^*(Y_1)_{j\beta}(Y_1)_{i\beta}^*(Y_1)_{j\alpha} + \sqrt{\zeta_i\zeta_j}\,D_2\left(\zeta_i,\zeta_j\right)(Y_1)_{j\beta}^*(Y_1)_{j\beta}^*(Y_1)_{i\beta}(Y_1)_{i\alpha}\right], \tag{6.42}$$

where the loop functions $D_1\left(\zeta_i,\zeta_j\right)$ and $D_2\left(\zeta_i,\zeta_j\right)$ are given in Appendix D.

Finally, the branching ratio is

$$\text{Br}\left(\ell_\alpha \to \ell_\beta\bar{\ell}_\beta\ell_\beta\right) = \frac{3(4\pi)^2\alpha_{\text{em}}^2}{8\,G_F^2}\left[|A_{ND}|^2 + |A_D|^2\left(\frac{16}{3}\log\left(\frac{m_\alpha}{m_\beta}\right) - \frac{22}{3}\right) + \frac{1}{6}|B|^2\right.$$

$$+ \frac{1}{3}\left(2|F_{RR}|^2 + |F_{RL}|^2\right) + \left(-2A_{ND}A_D^* + \frac{1}{3}A_{ND}B^* - \frac{2}{3}A_D B^* + \text{h.c.}\right)\bigg]$$

$$\times \text{Br}\left(\ell_\alpha \to \ell_\beta\nu_\alpha\bar{\nu}_\beta\right), \tag{6.43}$$

where

$$F_{RR} = \frac{F\,g_R^\ell}{g_2^2\sin^2\theta_W\,m_Z^2} \qquad \text{and} \qquad F_{RL} = \frac{F\,g_L^\ell}{g_2^2\sin^2\theta_W\,m_Z^2}. \tag{6.44}$$

6.3.3 Parameter Scan

Once we have defined the required functions, we can make a scan in the parameters to obtain the branching ratios in our model. First, we obtain the Yukawa matrix with eq. (6.31), assuming normal ordering, a light mass of $m_{\nu 1} = 10^{-3}$ eV, and assigning a random value for oscillation parameters in the 3σ range from table 4. This ensures that our Yukawa couplings can reproduce correctly neutrino masses and oscillation data. The values assigned for the other free parameters in the model are shown in table 11. In order to maintain χ as the dark matter candidate of the model, the maximum possible value for its mass is the minimum value of the mass of the scalar particle R_2. The parameter θ is selected to be small, indicating minimal mixing between the mass and flavor eigenstates of the scalar and pseudoscalar particles in the model.

Parameter	Input
m_{ν_1}	$10^{-12}\,\mathrm{GeV}$
Y_2	0.001
$\xi_1\,v_{\phi_2}$	$1\,\mathrm{GeV}$
λ_3	-0.003
θ	$[0.01, 0.7]$
m_{R_2}	$[1, 5]\,\mathrm{TeV}$
Δm	$[10, 100]\,\mathrm{GeV}$
m_χ	$[10, \min(m_{R_2})]\,\mathrm{GeV}$

Table 11: Input parameters for the scan of the branching ratios.

In Fig. 22, the branching ratios for $\ell_\alpha \to \ell_\beta \gamma$ and $\ell_\alpha \to 3\,\ell_\beta$ are plotted as function of m_χ. For the chosen input parameters, all the branching ratios are below the experimental limits specified in Table 10. The couplings Y_2 and $\xi_1 v_{\phi_2}$ can be lowered or increased to obtain more or less suppressed results. Fig. 23 shows the correlation between the branching ratio and the Yukawa entries for $\mu \to e\gamma$ and $\mu \to 3e$. As the Yukawa coupling Y_1 decrease, the branching ratio gets more suppressed. The values for the branching ratio of $\ell_\alpha \to 3\ell_\beta$ are more constrained with respect to $\ell_\alpha \to \ell_\beta \gamma$.
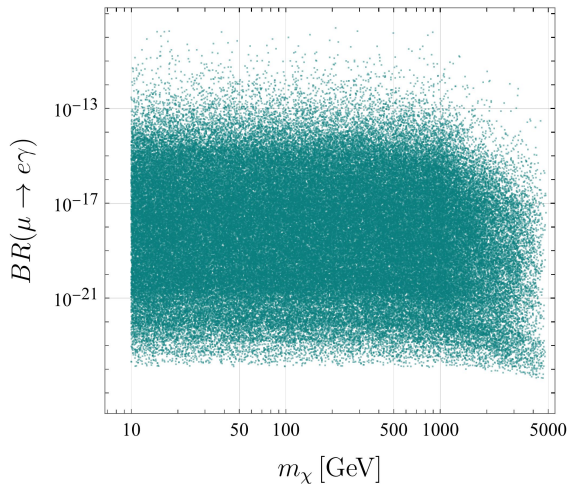
(a) Branching ratio $\mu \to e\gamma$ vs m_χ.
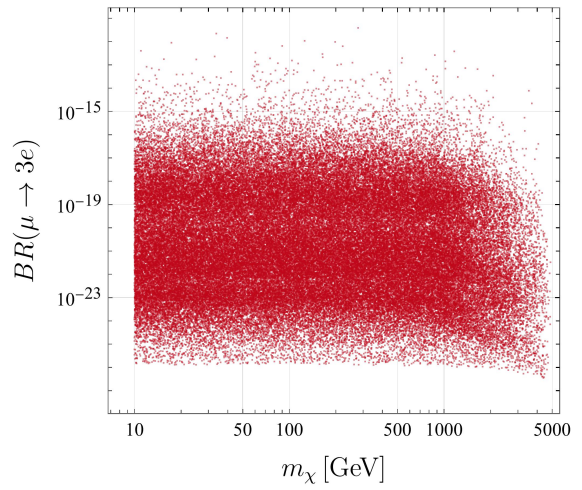
(b) Branching ratio $\mu \to 3e$ vs m_χ.
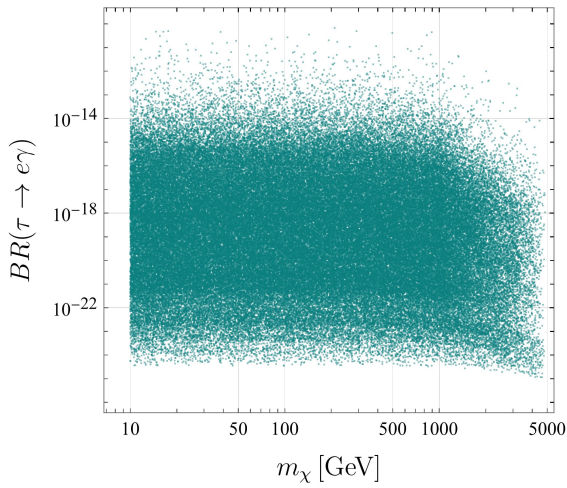
(c) Branching ratio $\tau \to e\gamma$ vs m_χ.
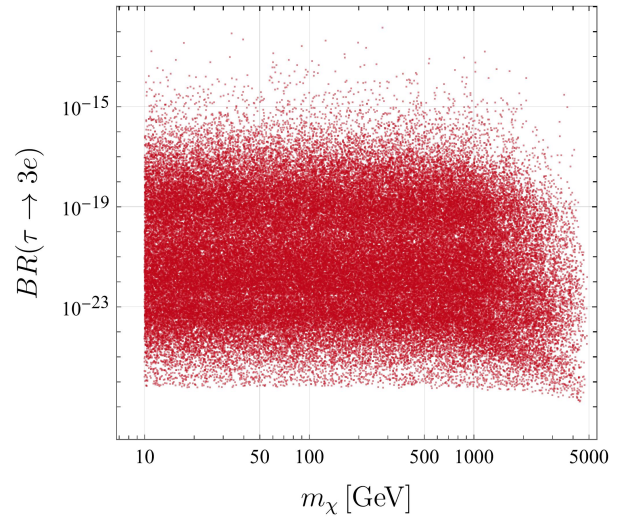
(d) Branching ratio $\tau \to 3e$ vs m_χ.
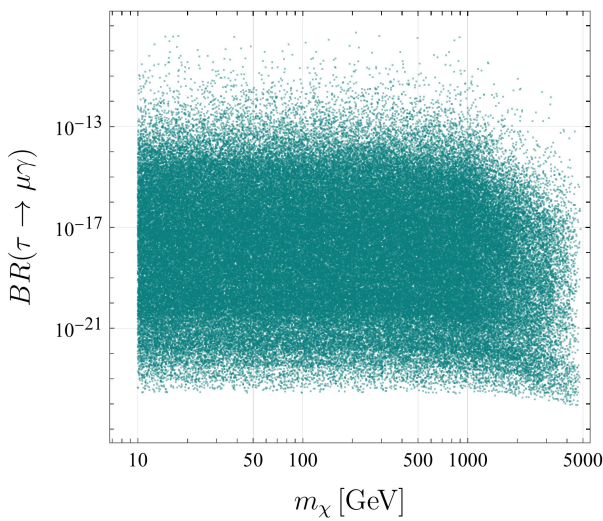
(e) Branching ratio $\tau \to \mu\gamma$ vs m_χ.
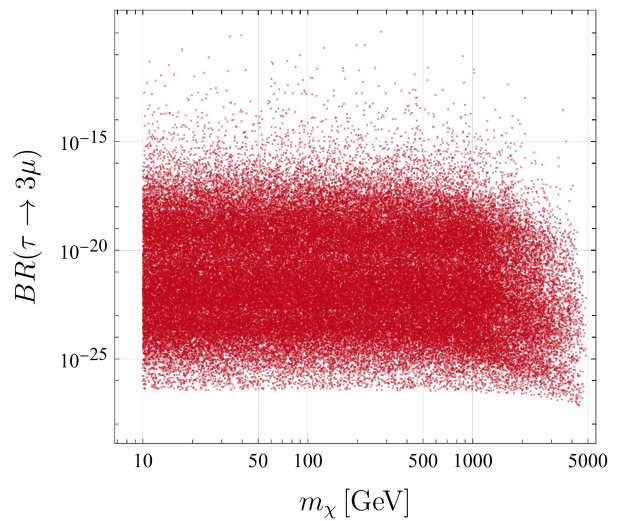
(f) Branching ratio $\tau \to 3\mu$ vs m_χ.

Figure 22: Branching Ratios for LFV processes $\ell_\alpha \to \ell_\beta \gamma$ and $\ell_\alpha \to 3\ell_\beta$ vs fermion mass m_χ.

67
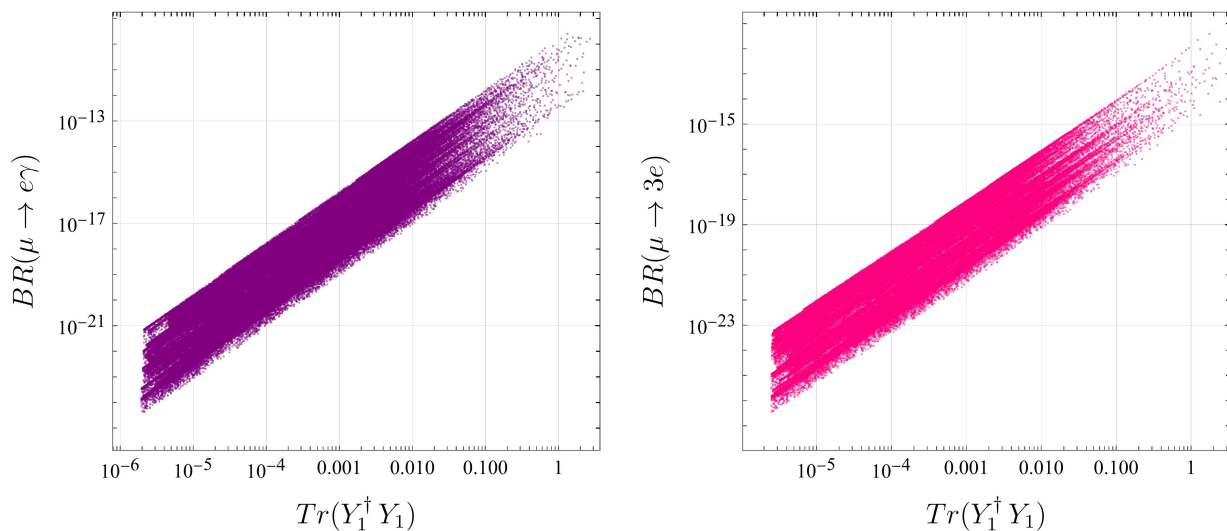
(a) Branching ratio $\mu \to e\gamma$ vs $\mathrm{Tr}\,(Y_1^\dagger Y_1)$.

(b) Branching ratio $\mu \to 3e$ vs $\mathrm{Tr}\,(Y_1^\dagger Y_1)$.

Figure 23: Branching Ratios for LFV processes vs the trace of the product of the Yukawa matrix.

6.4   Two-loop Model Summary and Perspectives

In this section, we have proposed a radiative neutrino mass model, generating Majorana neutrino masses at two-loop order. This extension consists of a gauge $U(1)_{B-L}$ symmetry spontaneously broken to Z_3, which stabilizes the dark matter. We have included three singlet fermions χ_j, one doublet scalar η and one singlet scalar ρ constituting the dark sector of the model. We also have included a singlet scalar ϕ_2 which participates in the neutrino mass mechanism, and the three singlet fermions $N_{(-4,-4,5)}$ along with the singlet scalars $\phi_{1,8}$ to ensure an anomaly free symmetry, and to give masses to N_k avoiding radiation contributions to the universe. An additional singlet scalar ϕ_6 is included to break an accidental $U(1)$ symmetry.

We have derived the mass spectrum for the model, obtaining degenerate masses for the scalar and pseudoscalar fields. We have made a numerical analysis regarding LFV processes. We obtained that these processes are suppressed in the model given our numerical scan.

The dark matter and Z' phenomenology discussion of the model is still pending. The implementation of the model in `SARAH`, `SPheno` and `micrOmegas` to make a complete numerical analysis represent future perspectives to be explored. In particular, it is of interest a numerical scan including constraints of the dark matter relic density in a fermionic or scalar dark matter scenario.

An alternative option under consideration is to consider $N_{(-1,-1,-1)}$ instead of $N_{(-4,-4,5)}$ to avoid the scalar fields $\phi_{1,6,8}$. This choice would allow mass terms at tree level, resulting in a seesaw type-I mechanism along with the two-loop mechanism contributing to neutrino masses. However, the seesaw type-I can be suppressed considering small couplings and heavy masses for N, thereby making the two-loop mechanism the primary contribution.

This project with its perspectives is still work in progress at the moment of the realization of the present thesis.

7 Dirac Neutrinos Phenomenology with Texture Zeros

In the previous section, a new model assuming Majorana neutrinos was proposed and some of its phenomenological implications were studied. A different approach to study neutrinos phenomenology is making approximations or assumptions directly in the neutrino mass matrix in a model-independent way. By this means, correlations between the parameters in the matrix can be obtained. One example is the zero textures approach, in which some entries of the neutrino mass matrix are set to zero, deriving correlations between oscillation parameters. This can be applied either to Dirac or Majorana neutrinos, each case with its own implications. In this section, two-zero textures for Dirac neutrinos are studied on the charged lepton diagonal mass basis and assuming the neutrino mass matrix to be Hermitian.

7.1 Two-zero textures

The number of vanishing elements and their position determines the type of texture. Naturally, not all textures will be allowed by experimental observations. With one vanishing element, the Majorana neutrino case gives one zero equation and is compatible with the oscillation data. For two vanishing elements, only some cases are consistent with the experimental data [118]. Three or more vanishing elements are too restrictive and therefore excluded. In the case of Dirac neutrinos with a Hermitian mass matrix, there are 15 possible textures for two vanishing elements[19]:

$$A_1 : \begin{pmatrix} 0 & 0 & x \\ 0 & x & x \\ x & x & x \end{pmatrix}, \quad A_2 : \begin{pmatrix} 0 & x & 0 \\ x & x & x \\ 0 & x & x \end{pmatrix}; \tag{7.1}$$

$$B_1 : \begin{pmatrix} x & x & 0 \\ x & 0 & x \\ 0 & x & x \end{pmatrix}, \quad B_2 : \begin{pmatrix} x & 0 & x \\ 0 & x & x \\ x & x & 0 \end{pmatrix}, \quad B_3 : \begin{pmatrix} x & 0 & x \\ 0 & 0 & x \\ x & x & x \end{pmatrix}, \quad B_4 : \begin{pmatrix} x & x & 0 \\ x & x & x \\ 0 & x & 0 \end{pmatrix}; \tag{7.2}$$

$$C : \begin{pmatrix} x & x & x \\ x & 0 & x \\ x & x & 0 \end{pmatrix}; \tag{7.3}$$

$$D_1 : \begin{pmatrix} x & x & x \\ x & 0 & 0 \\ x & 0 & x \end{pmatrix}, \quad D_2 : \begin{pmatrix} x & x & x \\ x & x & 0 \\ x & 0 & 0 \end{pmatrix}; \tag{7.4}$$

$$E_1 : \begin{pmatrix} 0 & x & x \\ x & 0 & x \\ x & x & x \end{pmatrix}, \quad E_2 : \begin{pmatrix} 0 & x & x \\ x & x & x \\ x & x & 0 \end{pmatrix}, \quad E_3 : \begin{pmatrix} 0 & x & x \\ x & x & 0 \\ x & 0 & x \end{pmatrix}; \tag{7.5}$$

$$F_1 : \begin{pmatrix} x & 0 & 0 \\ 0 & x & x \\ 0 & x & x \end{pmatrix}, \quad F_2 : \begin{pmatrix} x & 0 & x \\ 0 & x & 0 \\ x & 0 & x \end{pmatrix}, \quad F_3 : \begin{pmatrix} x & x & 0 \\ x & x & 0 \\ 0 & 0 & x \end{pmatrix}. \tag{7.6}$$

---

[19]Note that a vanishing element $(M_\nu)_{ij} = 0$ implies $(M_\nu)_{ji} = 0$ since we are assuming M_ν to be Hermitian.

We follow the notation for Majorana neutrinos given in [118]. In Eqs. (7.1)-(7.6), x represents a non-vanishing entry.

Several studies have examined the texture zeros for Majorana neutrinos [119–124]. The phenomenological implications of texture zeros for the Dirac scenario in the diagonal charged lepton mass matrix basis were also studied previously [125–127]. The purpose of taking this approach is to relate the observables based on the analytical expressions derived from the vanishing elements. This is achieved using a numerical technique based on a scanning in the parameters inside the 3σ region of the Global Fit presented in Table 4.

The following sections provide an overview of the general approach and some implications of the previous textures in normal ordering (NO) and inverted ordering (IO) of the neutrino mass spectrum. Finally, the numerical analysis and the correlations resulting from the numerical analysis for the favored textures are presented.

7.2   General Approach

In the charged lepton diagonal mass basis, the Hermitian Dirac neutrino mass matrix M_ν is diagonalized by the PMNS matrix as[20]

$$U^\dagger_{\text{PMNS}} M_\nu U_{\text{PMNS}} = \hat{m}_\nu \equiv \begin{pmatrix} m_1 & 0 & 0 \\ 0 & m_2 & 0 \\ 0 & 0 & m_3 \end{pmatrix}. \tag{7.7}$$

The parametrization for U_{PMNS} is the same of Eq. (3.30):

$$U = \begin{pmatrix} c_{12}c_{13} & s_{12}c_{13} & s_{13}e^{-i\delta} \\ -s_{12}c_{23} - c_{12}s_{23}s_{13}e^{i\delta} & c_{12}c_{23} - s_{12}s_{23}s_{13}e^{i\delta} & s_{23}c_{13} \\ s_{12}s_{23} - c_{12}c_{23}s_{13}e^{i\delta} & -c_{12}s_{23} - s_{12}c_{23}s_{13}e^{i\delta} & c_{23}c_{13} \end{pmatrix}. \tag{7.8}$$

From Eq. (7.7), we can write the neutrino mass matrix as

$$M_\nu = U_{\text{PMNS}} \, \hat{m}_\nu \, U^\dagger_{\text{PMNS}}. \tag{7.9}$$

The right-hand side of Eq. (7.9) depends only on the neutrino mixing angles, the CP-violating phase, and the neutrino masses. From here, it is clear that in Eq. (7.9), a zero on the left-hand side will imply an equation relating neutrino masses with the CP-phase and the neutrino mixing angles.

The Dirac mass matrices in the SM are arbitrary 3×3 matrices. However, due to the polar theorem of linear algebra, it can be written as the product of a Hermitian matrix times a unitary matrix [128]. Moreover, this unitary matrix can be absorbed in a redefinition of the right-handed fields, since there are no constraints for the form of these fields in the SM. In this way, we can take the neutral mass matrix for Dirac neutrinos to be Hermitian without losing generality.

We have six real numbers and three phases as parameters in a 3×3 Hermitian matrix. Now, using a weak basis transformation, we can reduce the number of phases from three to one, obtaining an Hermitian matrix with six real parameters and just one phase, enough to

---

[20]Note the difference with Eq. (5.34), where the Majorana neutrino mass matrix is diagonalized by $U^T_{\text{PMNS}} M_\nu U_{\text{PMNS}}$.

accommodate the seven physical parameters, namely, the three neutrino masses, the three mixing angles, and the CP-violating phase.

Imposing to zero an element in the neutrino mass matrix reduces the number of free parameters. One texture zero establishes a single relationship between physical parameters, *i.e.*, mixing angles, and neutrinos masses. With two vanishing elements, there are two relations. It is important to note that these relationships may or may not agree with the current experimental oscillation data. The phenomenology of each texture should be studied to see this compatibility.

7.2.1 Numerical Analysis

We obtain a system of two equations (the corresponding to the vanishing entries of M_ν), *i.e.*, $(M_\nu)_{ij} \equiv M_{ij} = 0$ and $(M_\nu)_{kl} \equiv M_{kl} = 0$ with $ij \neq kl$. These equations allow us to write two neutrino masses as functions of the other neutrino mass (we choose the lightest) and the neutrino oscillation parameters. For NO (IO), the equations are of the form:

$$\eta m_1 U_{i1} U_{1j}^* + \kappa m_2 U_{i2} U_{2j}^* + m_3 U_{i3} U_{3j}^* = 0,$$
$$\eta m_1 U_{k1} U_{1l}^* + \kappa m_2 U_{k2} U_{2l}^* + m_3 U_{k3} U_{3l}^* = 0, \tag{7.10}$$

where η and κ are the relative m_1 and m_2 signs respect to m_3. The eigenvalues of a Hermitian matrix are always real. As the masses correspond to the eigenvalues of the neutrino mass matrix, they must take real values. Consequently, the permissible values of δ in Eqs. (7.10) are constrained by the realness of the neutrino masses. The result will indicate whether or not CP is conserved:

- **CP violation:** The neutrino mass matrices with all the zeroes in the diagonal allow CP violation. In such a case, $i = j$ and $k = l$, and the Eqs. (7.10) are both real, no matter the value of the δ CP phase. The textures that allow CP violation are C, E_1, and E_2 in Eqs. (7.3) and (7.5).

- **CP conservation:** All the remaining textures lead to CP conservation. In Eq. (7.10), the realness of the neutrino masses forces δ to take the values 0 or π.

We use the squared mass differences to write two masses in terms of the lightest neutrino mass:

$$\Delta m_{21}^2 = m_2^2 - m_1^2,$$
$$\Delta m_{31}^2 = m_3^2 - m_1^2. \tag{7.11}$$

We then give random values to the square mass differences in the 3σ range from the neutrino oscillations global fit [68]. After this, we assign numerical values to the lightest neutrino masses.

Three textures are found to be compatible with the current neutrino oscillation data. Two textures, A_1 and A_2, are CP conserving (those textures have an off-diagonal vanishing matrix element) and are compatible only for normal ordering. The third one is texture C. This texture is compatible with CP violation for both neutrino mass hierarchies.

In the next section, the results for textures A1, A2, and C are presented.
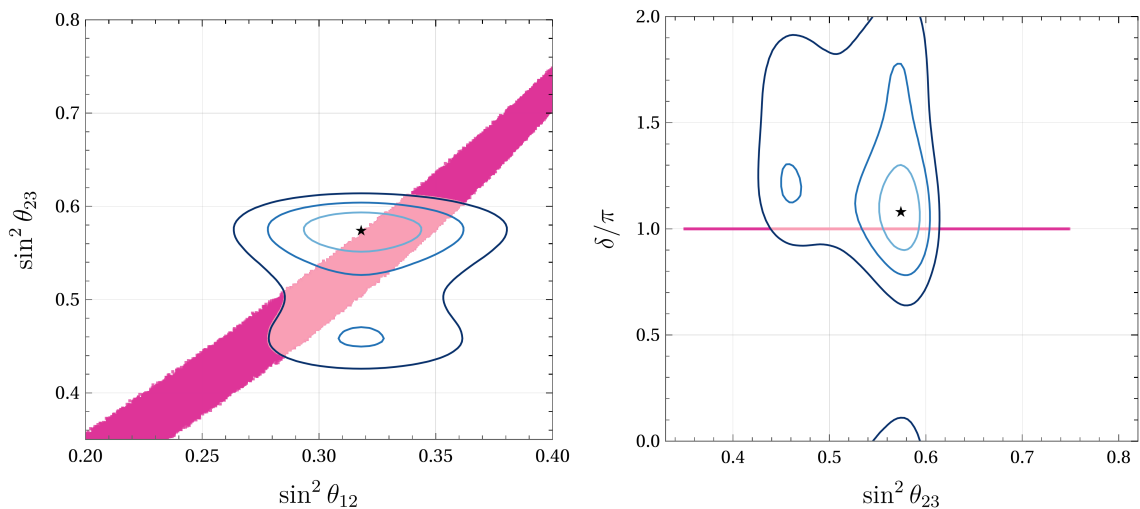
(a) $\sin^2 \theta_{12}$ vs. $\sin^2 \theta_{23}$ for texture A1 in NO.

(b) $\sin^2 \theta_{23}$ vs. δ for texture A1 in NO.
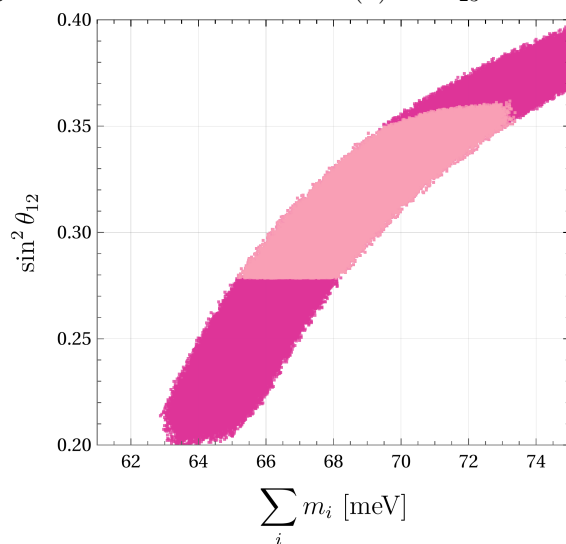
(c) $\sum m_\nu$ vs. $\sin^2 \theta_{12}$ for texture A1 in NO.

Figure 24: Correlations for texture A1 ($M_{ee} = M_{e\mu} = 0$) in NO. Plots 24a and 24b have contours corresponding to the 3σ, 2σ, and 1σ along with the best fit point provided by the Global Fit Collaboration [68]. Points in lighter pink represent solutions inside the contours also consistent with the upper mass limits [35], [12] and [129].

7.3 Allowed Textures

From all the possible Dirac neutrino Hermitian mass matrices with two vanishing elements, only three of these textures are compatible with current experimental data. Textures A1 and A2 are compatible with the normal ordering of the neutrino masses, and texture C is compatible with both hierarchies. These textures show clear correlations between some observables depending on the particular texture. The results of the neutrino phenomenology concerning such correlations are presented in Figs. 24-27. The mass values are compared with the upper limits from KATRIN collaboration [35] ($m_\nu < 1.1$ eV, with m_ν being the absolute mass scale for neutrinos), PLANCK collaboration [12] ($\sum m_\nu < 0.12$ eV) and the most constraining bound up to date from cosmology of $\sum m_\nu < 0.09$ eV [129].
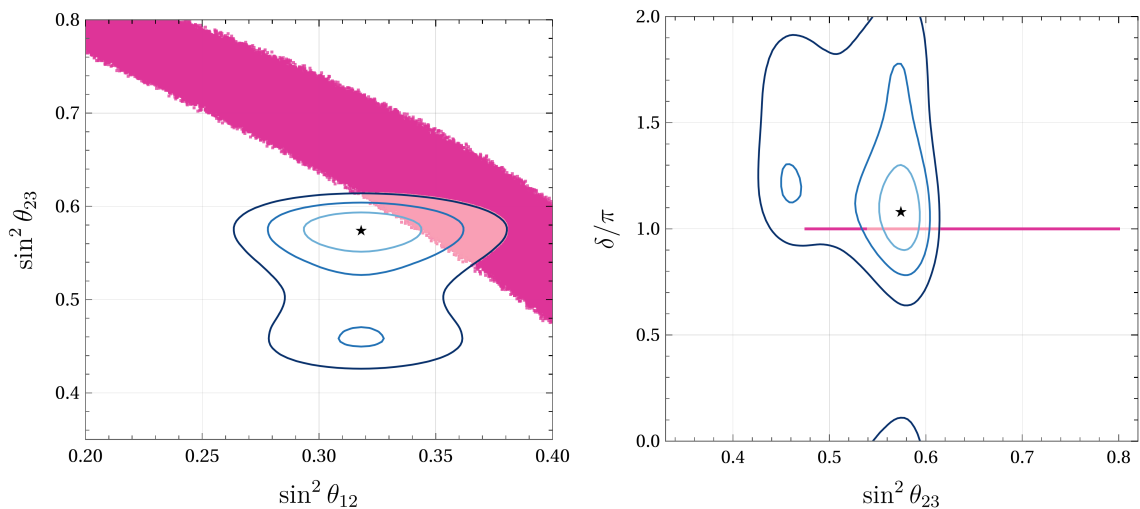
(a) $\sin^2\theta_{12}$ vs. $\sin^2\theta_{23}$ for texture A2 in NO.

(b) $\sin^2\theta_{23}$ vs. δ for texture A2 in NO.
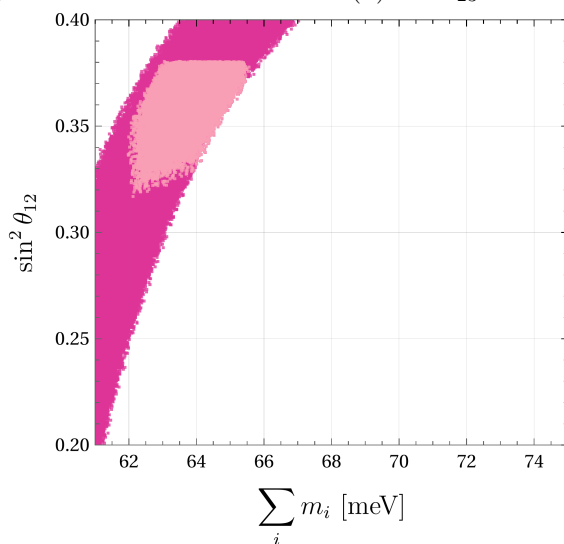
(c) $\sum m_\nu$ vs. $\sin^2\theta_{12}$ for texture A2 in NO.

Figure 25: Correlations for texture A2 ($M_{ee} = M_{e\tau} = 0$) in NO. The 3σ, 2σ, 1σ contours and the best fit point are shown in Figs. 25a and 25b. Points in lighter pink represent solutions inside the contours also consistent with the bounds from [35], [12] and [129].

7.3.1 Texture A1

This texture is only compatible with inverse hierarchy. This restriction arises from the requirement for real masses, which constrains δ to be either π or 0. However, neither of these values falls within the 3σ range for the inverted ordering. The solutions found in the 3σ scan for this texture are presented in Fig 24. Points printed in lighter pink are solutions inside the global fit contour corresponding to 3σ, also consistent with PLANCK, KATRIN and the cosmological upper mass limit. Fig. 24a displays a correlation between the solar and atmospheric mixing angles, showing a wide region of overlap with the Global Fit contours. As the parameter $\sin^2\theta_{12}$ increases, there is a corresponding increase in $\sin^2\theta_{23}$. In Fig. 24b, $\delta = \pi$ indicates CP conservation. Fig. 24c shows the correlation between $\sum m_i$ and the solar mixing angle. For this texture, the mass values are consistent with all the upper limits.

(a) $\sin^2 \theta_{23}$ vs. δ for texture C in IO.

(b) $\sum m_\nu$ vs. $\sin^2 \theta_{12}$ for texture C in IO.
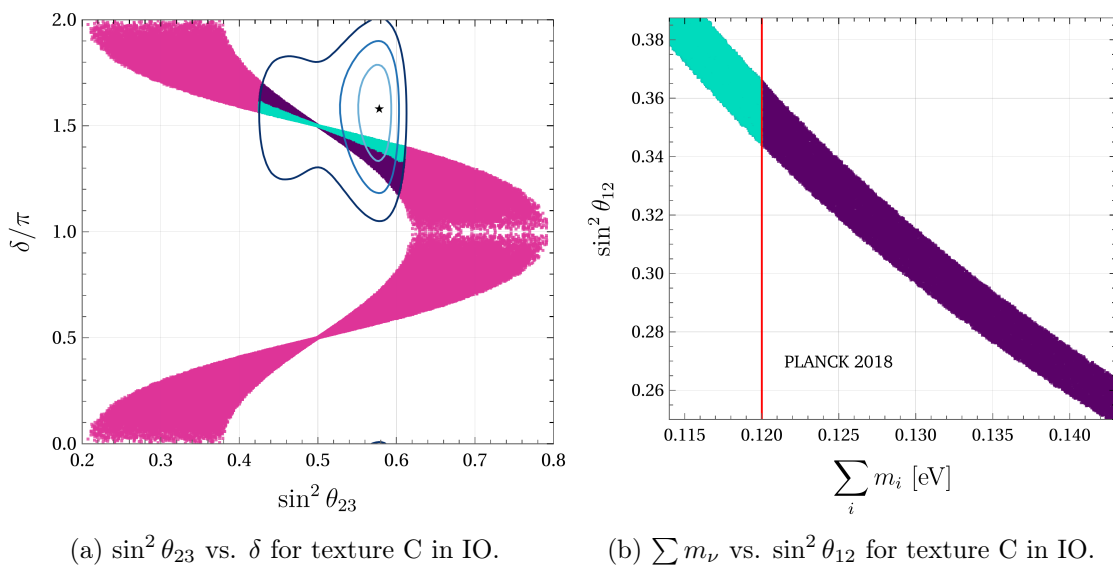
Figure 26: Correlations for texture C ($M_{\mu\mu} = M_{\tau\tau} = 0$) in IO. The 3σ, 2σ, and 1σ contours and the best fit point are shown for Fig. 26a. The red vertical line in Fig. 26b represents the upper constraint given by the PLANCK collaboration [12]. Points inside the contours that fulfill this condition are shown in cyan color for both plots. Points in purple represent solutions inside the contours also consistent with the KATRIN limit, but not with PLANCK.

(a) $\sin^2 \theta_{23}$ vs. δ for texture C in NO.

(b) $\sum m_\nu$ vs. $\sin^2 \theta_{12}$ for texture C in NO.
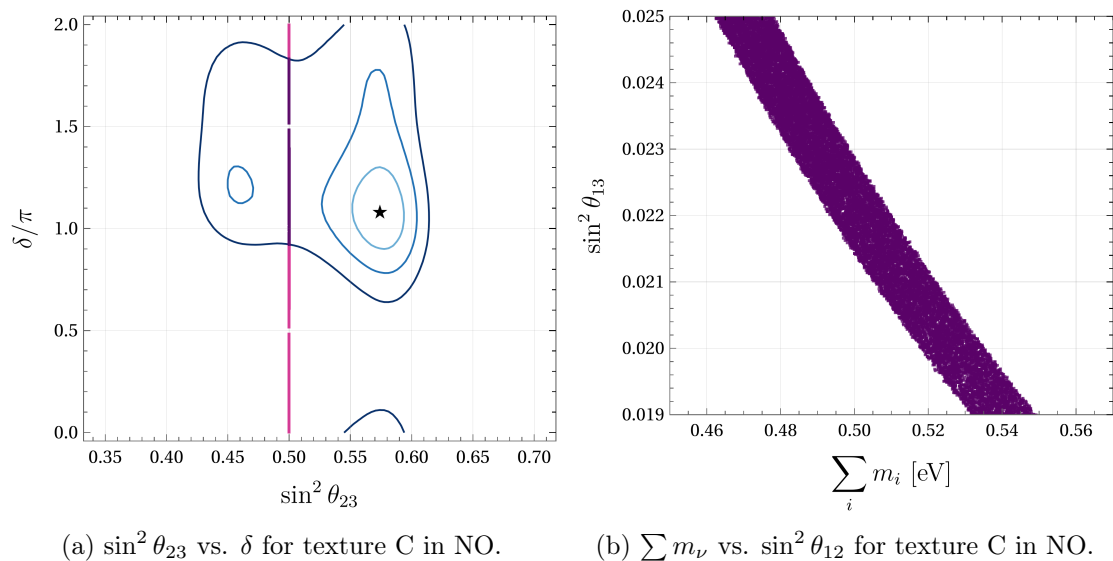
Figure 27: Correlation for texture C ($M_{\mu\mu} = M_{\tau\tau} = 0$) in NO. The 3σ, 2σ, and 1σ contours and the best fit point are shown in Fig. 27a. Points in purple represent solutions inside the contours also consistent with the KATRIN limit, but not with PLANCK.

7.3.2 Texture A2

As in the previous case, this texture is only compatible with normal ordering for the neutrino masses. The solutions for this texture are displayed in Fig 25. The correlation between the solar and atmospheric mixing angles is shown in Fig. 25a. In contrast to texture A1, a decreasing in $\sin^2 \theta_{23}$ implies an increasing in $\sin^2 \theta_{12}$. Fig. 25b indicates CP conservation. The overlap with the contours is also limited to greater values for the angles in this case. In Fig. 25c, the mass correlation is displayed, showing mass values lower than those in texture

74

A1. This is consistent with the upper limits as well.

7.3.3 Texture C in Inverse Ordering

The correlation between the atmospheric angle and the CP phase is displayed in Fig. 26a for the inverse ordering. Solutions inside the contours give a value for the CP phase $\delta \approx 3\pi/2$, leading to CP violation. Fig. 26b shows the negative correlation of the solar mixing angle with $\sum m_i$. Mass values printed in purple are consistent only with the bound from KATRIN, while cyan points are also consistent with the PLANCK bound. However, all points are ruled out by the limit imposed by the Cosmological bound from [129].

7.3.4 Texture C in Normal Ordering

Fig. 27a shows the correlation between the atmospheric angle and the CP phase for normal ordering. Compared to inverse ordering, there is a higher range for CP-phase values inside the contours. Also, the maximal $\theta_{23} \approx \pi/4$ is preferred, implying quasi-degeneration between neutrino masses. The correlation between the reactor mixing angle and $\sum m_i$ is displayed in Fig 27b. The mass values are greater than those in inverse ordering, consistent only with the KATRIN limit.

7.4 Summary

Our results, as those in [126], found that textures A1, A2, and C are compatible with the current experimental neutrino oscillation data. However, the correlation for δ vs. $\sin^2 \theta_{23}$ in texture C with IO are different from those in [126] . The work in [127] considers two-zero textures with Hermitian and non-Hermitian Dirac neutrino mass matrices. In the Hermitian case, they found that textures A1 and C are allowed, while A2 is ruled out.

In summary, the cases compatible with the experimental data are textures A1 and A2 for normal ordering and C for both hierarchies. Textures A1 and A2, with normal ordering, predict CP conservation, while texture C predicts CP violation in both hierarchies. Texture C, with normal ordering, leads to quasi-degenerate neutrino masses.

8   Conclusions

The Standard Model (SM) was originally formulated considering massless neutrinos, since no evidence for their masses were available at that time. Having only upper mass limits as indication, the assumption of massless left-handed neutrinos was enough to describe weak interactions, as discussed in Section 2. However, with the subsequent discovery of neutrino oscillations, it became evident that neutrinos must be massive.

The observation of oscillating neutrinos represents a direct evidence of Beyond the Standard Model (BSM) physics, where the need for a mechanism to generate neutrino masses arises. To consider massive neutrinos in the SM, the addition of a right-handed neutrino or the assumption of neutrinos being Majorana-type particles can be used. However, as pointed out in Section 3, doing so does not explain why the neutrino masses are at least six orders of magnitude smaller than the electron mass, according to current experimental limits.

In this regard, the SM can be extended to explain the smallness of neutrino masses. In Section 4, we learned that neutrino masses can be generated either at tree-level or through radiative mechanisms. The advantage of a radiative mass generation mechanism is an extra suppression factor for each loop, providing a natural explanation for small masses. Moreover, extensions of the SM can also incorporate a dark matter candidate, linking the neutrino mass problem with the unknown nature of the dark sector, whose existence is also evidence for BSM physics.

With these considerations, we have proposed two radiative models for Majorana neutrino masses: one at the one-loop level and the other at the two-loop level, presented in Sections 5 and 6.

In the first one, we extended the SM with a discrete symmetry Z_4, introducing three fermions N_i and a doublet scalar η with charges i under the new symmetry. Being protected by charge conservation of a conserved Z_2, the lightest of these particles represents a dark matter candidate. Through a numerical scan, we found that the parameter spectrum can reproduce neutrino oscillation data, using the inputs from Table 7. This extension is similar to the Scotogenic model, with the difference lying in the addition of a real singlet scalar ϕ. This scalar gives mass to the fermions N_i and also allows for an extra annihilation channel $2N \rightarrow 2\phi$ and $2N \rightarrow 2\,SM$ through ϕ exchange, contributing to the dark matter relic density without the experimental constraints on the Yukawa interaction coming from LFV processes. Additionally, under the kinematic condition $m_N > m_\phi/2$, a cannibal process $3N \rightarrow N + \phi$ is possible. A numerical scan in the parameter spectrum for the relic abundance is presented, where two regions, forbidden and secluded, are briefly discussed.

The second model also considers Majorana neutrino masses, but now the SM is extended with an anomaly free gauged $U(1)_{B-L}$ symmetry, which spontaneously breaks into a Z_3. The dark sector involves a scalar doublet η, a singlet scalar ρ and a vector-like fermion χ. Additionally, three fermions N_k with $B - L$ charges of $(-4, -4, 5)$ are introduced to the theory, ensuring anomaly cancellations. To provide masses for these fermions and prevent accidental symmetries, four extra singlet scalars are included.

In this model, masses are generated at the two-loop level, leading to the possibility of greater values for the Yukawa couplings due to the extra suppression factor of $(16\pi^2)^2$ in the denominator. Its phenomenological implications include the possibility of lepton flavor-violating

processes. We have computed the branching ratio for $\ell_\alpha \to \ell_\beta \gamma$ and $\ell_\alpha \to 3\ell_\beta$, obtaining results consistent with current experimental bounds. The phenomenology of the dark sector, which includes the physics of Z', is still pending for this model.

On the other hand, in Section 7, we explored a different approach to studying neutrino phenomenology. We employed the texture zeros method, where specific entries of the neutrino mass matrix are set to zero, implying correlations between oscillation parameters. We specifically investigated the case of two-zero textures for Dirac neutrinos.

With this study, we have found that textures $(1,1) = (1,2) = 0$ and $(1,1) = (1,3) = 0$ (referred to as A1 and A2 textures) in Normal Ordering, and $(2,2) = (3,3) = 0$ (referred to as the C texture) in Inverse and Normal Ordering, are compatible with recent experimental data and some upper mass limits for Dirac neutrinos. These textures show correlations between several oscillation parameters, consistent with the σ contours of the Global Fit [68]. Textures A in normal hierarchy predict CP conservation, while texture C predicts CP violation in both hierarchies. C texture in NO leads to quasi-degenerate neutrino masses. Incoming experiments should increase the precision for neutrino mixing parameters, enabling to discard or favor some of the previous textures with more certainty.

In summary, we have studied neutrino masses and phenomenology both with SM extensions and with the texture zeros approach. We have proposed two models that reproduce neutrino oscillation data and have dark matter candidates. With the two-zero textures, we have found allowed textures according to current experimental data.

A   Anomalies

In this Appendix, we shortly review some aspects of anomalies in the SM and $U(1)$ extensions of the SM. Rather than provide a rigorous proof and calculation, we mainly describe the general idea and present the anomaly cancellation constraints that we use. For a more comprehensive yet understandable review of quantum anomalies, we refer to, for example, [130], which inspired the discussion in this appendix.

An anomaly occurs when a symmetry is conserved at classical level but not at quantum level, coming from the same Lagrangian. In such cases, that symmetry is said to be *anomalous*. From Noether's theorem, a continuous symmetry implies a conserved current. If a symmetry is anomalous, then it is not actually a symmetry and the associated current will not be conserved. Therefore, in quantum field theory, gauge symmetries must be *anomaly free*, since the non-conservation of currents associated to those symmetries could imply unitarity violation. This restriction is strong and constraints the assigned charges to fermions, implying also a quantized electric charge, as we will see below.

Anomalies of gauge symmetries are called *gauge anomalies*. Global anomalies, coming from global symmetries, do not lead to inconsistencies in quantum theory[21]. Actually, there exist global anomalies in the SM. One example is baryon number, whose associated symmetry is $U(1)_B$. The symmetry $U(1)_B$ being anomalous implies baryon number violation, which is in fact a necessary condition to explain baryon asymmetry in the universe [18].

On the other hand, the need for absence of gauge anomalies in the SM imposes strong restrictions on the fermions. These restrictions arise from the calculation of the anomalies using triangle diagrams as shown in Figure 28. This diagram originally represented the
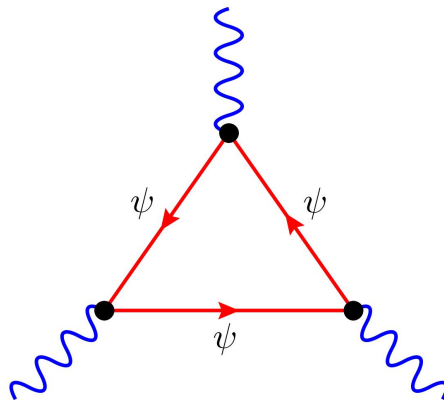
Figure 28: Triangle diagram resulting in chiral anomalies. The internal propagators are fermion particles, whereas the external legs are a combination of gauge boson fields corresponding to the $SU(3)_C, SU(2)_L$ and $U(1)_Y$ interactions.

decay process of $\pi^0 \rightarrow \gamma\gamma$. When the decay rate was successfully computed, it was shown that axial symmetry was broken by quantum corrections, leading to a chiral anomaly [131, 132].

In diagram 28, the propagators are fermions and each corner is a vertex with a coupling to

---

[21]When a symmetry is said to be *anomaly free*, means absence of gauge anomalies only.

an external gauge field. These gauge fields couple to both the vector current $\bar{\psi}\gamma_\mu\psi$ and the axial current $\bar{\psi}\gamma_5\gamma_\mu\psi$. Depending on the gauge fields, different constraints regarding the SM symmetries are obtained. When all the three considered bosons are B_μ, with B_μ the gauge boson associated to $U(1)_Y$, the gauge anomaly reads

$$U(1)_Y^3 : \sum_L Y_l^3 - \sum_R Y_R^3. \tag{A.1}$$

The full amplitude for the diagram considers left- and right-handed particles. The minus sign corresponds to a flip from left- to right-handedness through γ_5. This anomaly is represented as the $U(1)_Y^3$ anomaly, and its vanishing requires

$$0 = \left(2\,Y_L^3 - Y_e^3 - Y_\nu^3\right) + 3\left(2\,Y_Q^3 - Y_u^3 - Y_d^3\right). \tag{A.2}$$

Here, $Y_L, Y_e, Y_\nu, Y_Q, Y_u$ and Y_d are the hypercharges for the left-handed leptons, right-handed charged leptons, right-handed neutrinos, left-handed quarks, right-handed up-type quarks and right-handed down-type quarks. If we check the hypercharges for these particles from Table 1, and recalling that right-handed neutrinos must be singlets under the SM, we can see that the $U(1)_Y^3$ anomaly actually vanishes.

By group theory properties, any anomaly involving exactly one factor of $SU(2)$ or $SU(3)$ vanishes. An $SU(3)_C$ anomaly also vanishes since QCD is non-chiral. The remaining anomalies to be cancelled are $SU(3)_C^2\,U(1)_Y$ and $SU(2)_L^2\,U(1)_Y$. An extra anomaly emerges from gravity interactions, $\text{grav}^2\,U(1)_Y$, where the mediating gauge boson is the graviton. As all anomalies involve the $U(1)_Y$ symmetry, four constraints are derived for the fermion hypercharges, displayed in Table 12.

Anomaly	Constraint
$U(1)_Y^3$	$\left(2Y_L^3 - Y_e^3 - Y_\nu^3\right) + 3\left(2Y_Q^3 - Y_u^3 - Y_d^3\right) = 0$
$SU(3)_C^2\,U(1)_Y$	$2Y_Q - Y_u - Y_d = 0$
$SU(2)_L^2\,U(1)_Y$	$Y_L + 3Y_Q = 0$
$\text{grav}^2\,U(1)_Y$	$\left(2Y_L - Y_e - Y_\nu\right) + 3\left(2Y_Q - Y_u - Y_d\right) = 0$

Table 12: Anomaly constraints on the hypercharges of SM particles.

The constraint $Y_L + 3Y_Q = 0$ means that the electron must have exactly the same electric charge as the proton, implying that the electric charge is quantized. A general solution to the equations of Table 12 is

$$\begin{aligned}
Y_L &= -\frac{a}{2} - b, & Y_e &= -a - b, & Y_\nu &= -b, \\
Y_Q &= \frac{a}{6} + \frac{b}{3}, & Y_u &= \frac{2a}{3} + \frac{b}{3}, & Y_d &= -\frac{a}{3} + \frac{b}{3},
\end{aligned} \tag{A.3}$$

79

for any a and b. In the SM, the solution is $a = 1$ and $b = 0$.

Lets consider now an extension of the SM, with an extra $U'(1)$ symmetry with charges Y_i'. For anomalies to cancel, all conditions in Table 12 must hold with $Y_i \to Y_i'$. In addition, $U(1)_Y^2 U(1)_{Y'}$ and $U(1)_Y U(1)_{Y'}^2$ anomalies must cancel. The only possibility for Y_i' is to satisfy Eq. (A.3) with $Y_i \to Y_i'$. Taking now the orthogonal solution, $a = 0$ and $b = 1$, gives

$$Y_L' = Y_e' = Y_\nu' = -1, \qquad Y_Q' = Y_u' = Y_d' = \frac{1}{3}, \tag{A.4}$$

thus having a charge -1 for leptons and $1/3$ for quarks. This assignment corresponds to the group $U(1)_{B-L}$, introduced in Subsection 2.5. Therefore, the symmetry $U(1)_{B-L}$ is not anomalous and can be promoted to be local.

In Section 6, the charges $(-4, -4, -5)$ under $U(1)_{B-L}$ are assigned to three right-handed neutrinos in the two-loop model. This is done in order to avoid Dirac mass terms at tree-level. It can be shown that this charge assignment is also a valid solution for anomaly cancellation. Let us take the $U(1)_{Y'}^3$ anomaly constraint:

$$U(1)_{Y'}^3 : \sum_L Y_l'^3 - \sum_R Y_R'^3. \tag{A.5}$$

Quarks do not contribute to the anomaly, since the baryon number assignation remains as $1/3$. Then, substituting the corresponding charges for leptons we obtain

$$\begin{aligned} U(1)_{Y'}^3 : \sum Y_L'^3 - \sum Y_e'^3 - \sum Y_\nu'^3 \\ = 6(-1)^3 - 3(-1)^2 - (-4)^3 - (-4)^3 - (5)^3 \\ = 0. \end{aligned} \tag{A.6}$$

A similar check can be made for the $\text{grav}^2 U(1)_Y$ anomaly. Other anomalies do not involve right-handed neutrinos and therefore remain vanished. The anomalies $U(1)_Y^2 U(1)_{Y'}$ and $U(1)_Y U(1)_{Y'}^2$ vanish as in the case (A.4), due to $Y_\nu = 0$. Finally, a vector-like fermion (as χ in the two-loop model) do not contribute to $U'(1)$ anomalies since the left- and right-handed parts cancel each other.

B Two-loop Model: Full Potential Treatment

In this Appendix, we review the full potential of the model described in Section 6. Opening Eq. 6.2, we obtain the full expression:

$$
\begin{aligned}
\mathcal{L}_V =& \mu_H^2\, H^\dagger H + \mu_\eta^2\, \eta^\dagger \eta + \mu_\rho^2\, \rho^* \rho + \mu_{\phi_1}^2\, \phi_1^* \phi_1 + \mu_{\phi_2}^2\, \phi_2^* \phi_2 + \mu_{\phi_6}^2\, \phi_6^* \phi_6 + \mu_{\phi_8}^2\, \phi_8^* \phi_8 \\
&+ \lambda_1 \left(H^\dagger H\right)^2 + \lambda_2 \left(H^\dagger H\right)\left(\eta^\dagger \eta\right) + \lambda_3 \left(H^\dagger \eta\right)\left(\eta^\dagger H\right) + \lambda_4 \left(H^\dagger H\right)\left(\rho^* \rho\right) + \lambda_5 \left(H^\dagger H\right)\left(\phi_1^* \phi_1\right) \\
&+ \lambda_6 \left(H^\dagger H\right)\left(\phi_6^* \phi_6\right) + \lambda_7 \left(H^\dagger H\right)\left(\phi_2^* \phi_2\right) + \lambda_8 \left(H^\dagger H\right)\left(\phi_8^* \phi_8\right) + \lambda_9 \left(\eta^\dagger \eta\right)^2 + \lambda_{10}\left(\eta^\dagger \eta\right)\left(\rho^* \rho\right) \\
&+ \lambda_{11}\left(\eta^\dagger \eta\right)\left(\phi_1^* \phi_1\right) + \lambda_{12}\left(\eta^\dagger \eta\right)\left(\phi_6^* \phi_6\right) + \lambda_{13}\left(\eta^\dagger \eta\right)\left(\phi_2^* \phi_2\right) + \lambda_{14}\left(\eta^\dagger \eta\right)\left(\phi_8^* \phi_8\right) + \lambda_{15}\left(\rho^* \rho\right)^2 \\
&+ \lambda_{16}\left(\rho^* \rho\right)\left(\phi_1^* \phi_1\right) + \lambda_{17}\left(\rho^* \rho\right)\left(\phi_6^* \phi_6\right) + \lambda_{18}\left(\rho^* \rho\right)\left(\phi_2^* \phi_2\right) + \lambda_{19}\left(\rho^* \rho\right)\left(\phi_8^* \phi_8\right) + \lambda_{20}\left(\phi_1^* \phi_1\right)^2 \\
&+ \lambda_{21}\left(\phi_1^* \phi_1\right)\left(\phi_6^* \phi_6\right) + \lambda_{22}\left(\phi_1^* \phi_1\right)\left(\phi_2^* \phi_2\right) + \lambda_{23}\left(\phi_1^* \phi_1\right)\left(\phi_8^* \phi_8\right) + \lambda_{24}\left(\phi_6^* \phi_6\right)^2 \\
&+ \lambda_{25}\left(\phi_6^* \phi_6\right)\left(\phi_2^* \phi_2\right) + \lambda_{26}\left(\phi_1^* \phi_1\right)\left(\phi_8^* \phi_8\right) + \lambda_{27}\left(\phi_2^* \phi_2\right)^2 + \lambda_{28}\left(\phi_2^* \phi_2\right)\left(\phi_8^* \phi_8\right) + \lambda_{29}\left(\phi_8^* \phi_8\right)^2 \\
&+ \left(\xi_1\, \rho^3 \phi_2^* + \xi_2\, \phi_6^* \phi_2^3 + \xi_3\, \phi_8^* \phi_6 \phi_1^2 + \kappa_1\, H^\dagger \eta \rho^* + \kappa_2\, \phi_1^2 \phi_2^* + \kappa_3\, \phi_8 \phi_6^* \phi_2^* + \text{h.c.}\right).
\end{aligned}
$$
(B.1)

Here, the Higgs and the scalar doublet η are

$$
H = \begin{pmatrix} H^+ \\ H^0 \end{pmatrix} \quad \text{and} \quad \eta = \begin{pmatrix} \eta^+ \\ \eta^0 \end{pmatrix}.
$$
(B.2)

The scalar fields in Eq. (B.1) are complex. After SSB, the next substitution is made in the potential:

$$
\begin{aligned}
H^0 &\to \frac{1}{\sqrt{2}}\left(v_H + h_R^0 + i\, h_I^0\right), \\
\eta^0 &\to \frac{1}{\sqrt{2}}\left(v_\eta + \eta_R^0 + i\, \eta_I^0\right), \\
\rho &\to \frac{1}{\sqrt{2}}\left(v_\rho + \rho_R + i\, \rho_I\right), \\
\phi_j &\to \frac{1}{\sqrt{2}}\left(v_{\phi_j} + \phi_{jR} + i\, \phi_{jI}\right),
\end{aligned}
$$
(B.3)

with $j = 1, 2, 6, 8$. Then, we find the tadpole equations given by

$$
\left.\frac{\partial V}{\partial v_\Psi}\right|_{\Psi=0} = 0.
$$
(B.4)

where Ψ is one each of the fields and v_Ψ is its VEV. Eq. (B.4) will give us a tadpole equation for each field. For η we obtain

$$
\eta: \quad \frac{1}{2}\Big[v_\eta\left(v_\rho^2\lambda_{10} + v_{\phi_1}^2\lambda_{11} + v_{\phi_6}^2\lambda_{12} + v_{\phi_2}^2\lambda_{13} + v_{\phi_8}^2\lambda_{14} + 2v_\eta^2\lambda_9 + 2\mu_\eta^2 + 2v_\eta^2\lambda_9 + 2\mu_\eta^2\right)
$$
$$
+ v_H^2 v_\eta\left(\lambda_2 + \lambda_3\right) + \sqrt{2}v_H v_\rho \kappa_2\Big] = 0.
$$
(B.5)

For ρ, we have

$$
\rho: \quad \frac{1}{2}\Big[v_\rho\left(3v_\rho v_{\phi_2}\xi_1 + v_\eta^2\lambda_{10} + 2v_\rho^2\lambda_{15} + v_{\phi_1}^2\lambda_{16} + v_{\phi_6}^2\lambda_{17} + v_{\phi_2}^2\lambda_{18} + v_{\phi_8}^2\lambda_{19} + v_H^2\lambda_4 + 2\mu_\rho^2 + 2\mu_\rho^2\right)
$$
$$
+ \sqrt{2}v_H v_\eta \kappa_2\Big] = 0.
$$
(B.6)

One possible solution to both equations is setting $v_\eta = v_\rho = 0$ simultaneously. With this election, the other tadpole equations lead to

$$\mu_H^2 = -\frac{2v_H^3\lambda_1 + v_H v_{\phi_1}^2\lambda_5 + v_H v_{\phi_6}^2\lambda_6 + v_H v_{\phi_2}^2\lambda_7 + v_H v_{\phi_8}^2\lambda_8}{2v_H}, \tag{B.7}$$

$$\mu_{\phi_1}^2 =$$
$$-\frac{2v_{\phi_1}v_{\phi_6}v_{\phi_8}\zeta_3 + 2\sqrt{2}v_{\phi_1}v_{\phi_2}\kappa_1 + 2v_{\phi_1}^3\lambda_{20} + v_{\phi_1}v_{\phi_6}^2\lambda_{21} + v_{\phi_1}v_{\phi_2}^2\lambda_{22} + v_{\phi_1}v_{\phi_8}^2\lambda_{23} + v_H^2 v_{\phi_1}\lambda_5}{2v_{\phi_1}}, \tag{B.8}$$

$$\mu_{\phi_2}^2 =$$
$$-\frac{3v_{\phi_2}^2 v_{\phi_6}\zeta_2 + \sqrt{2}v_{\phi_1}^2\kappa_1 + \sqrt{2}v_{\phi_6}v_{\phi_8}\kappa_3 + v_{\phi_1}^2 v_{\phi_2}\lambda_{22} + v_{\phi_2}v_{\phi_6}^2\lambda_{25} + 2v_{\phi_2}^3\lambda_{27} + v_{\phi_2}v_{\phi_8}^2\lambda_{28} + v_H^2 v_{\phi_2}\lambda_7}{2v_{\phi_2}}, \tag{B.9}$$

$$\mu_{\phi_6}^2 =$$
$$-\frac{v_{\phi_2}^3\zeta_2 + v_{\phi_1}^2 v_{\phi_8}\zeta_3 + \sqrt{2}v_{\phi_2}v_{\phi_8}\kappa_3 + v_{\phi_1}^2 v_{\phi_6}\lambda_{21} + 2v_{\phi_6}^3\lambda_{24} + v_{\phi_2}^2 v_{\phi_6}\lambda_{25} + v_{\phi_6}v_{\phi_8}^2\lambda_{26} + v_H^2 v_{\phi_6}\lambda_6}{2v_{\phi_6}}, \tag{B.10}$$

$$\mu_{\phi_8}^2 =$$
$$-\frac{v_{\phi_1}^2 v_{\phi_6}\zeta_3 + \sqrt{2}v_{\phi_2}v_{\phi_6}\kappa_3 + v_{\phi_1}^2 v_{\phi_8}\lambda_{23} + v_{\phi_6}^2 v_{\phi_8}\lambda_{26} + v_{\phi_2}^2 v_{\phi_8}\lambda_{28} + 2v_{\phi_8}^3\lambda_{29} + v_H^2 v_{\phi_8}\lambda_8}{2v_{\phi_8}}. \tag{B.11}$$

The couplings μ_η^2 and μ_ρ^2 remain as free parameters in the model.

The mass matrices are obtained with

$$\mathcal{M}_{ij} = \left.\frac{\partial^2 V}{\partial\Psi_i\partial\Psi_j}\right|_{\Psi=0}. \tag{B.12}$$

We obtain the same mass matrix for the scalar and pseudoscalar fields of the dark sector and two mass matrices for the scalar and pseudoscalar visible fields. The resulting mass matrices are displayed in next page.

$$\mathcal{M}^R_{DM} = \mathcal{M}^I_{DM} = \mathcal{M}_{DM} = \begin{pmatrix} \frac{1}{2}\left(v_{\phi_1}^2\lambda_{11} + v_{\phi_6}^2\lambda_{12} + v_{\phi_2}^2\lambda_{13} + v_H^2(\lambda_2 + \lambda_3)\right) + \mu_\eta^2 & \dfrac{v_H\kappa_2}{\sqrt{2}} \\[2ex] \dfrac{v_H\kappa_2}{\sqrt{2}} & \frac{1}{2}\left(v_{\phi_1}^2\lambda_{16} + v_{\phi_6}^2\lambda_{17} + v_{\phi_2}^2\lambda_{18} + v_{\phi_8}^2\lambda_{19} + v_H^2\lambda_4\right) + \mu_\rho^2 \end{pmatrix}$$

$$\mathcal{M}^R_{\text{Visible}} = \begin{pmatrix}
2v_H^2\lambda_1 & v_H v_{\phi_1}\lambda_5 & v_H v_{\phi_6}\lambda_6 & v_H v_{\phi_2}\lambda_7 & v_H v_{\phi_8}\lambda_8 \\[1.5ex]
v_H v_{\phi_1}\lambda_5 & 2v_{\phi_1}^2\lambda_{20} & v_{\phi_1}(v_{\phi_8}\zeta_3 + v_{\phi_6}\lambda_{21}) & v_{\phi_1}(\sqrt{2}\kappa_1 + v_{\phi_2}\lambda_{22}) & v_{\phi_1}(v_{\phi_6}\zeta_3 + v_{\phi_8}\lambda_{23}) \\[1.5ex]
v_H v_{\phi_6}\lambda_6 & v_{\phi_1}(v_{\phi_8}\zeta_3 + v_{\phi_6}\lambda_{21}) & -\dfrac{v_{\phi_2}^3\zeta_2 + v_{\phi_1}^2 v_{\phi_8}\zeta_3 + \sqrt{2}v_{\phi_2}v_{\phi_8}\kappa_3 - 4v_{\phi_6}^3\lambda_{24}}{2v_{\phi_6}} & \dfrac{3v_{\phi_2}v_{\phi_6}\zeta_2}{2} + \dfrac{v_{\phi_8}\kappa_3}{\sqrt{2}} + v_{\phi_2}v_{\phi_6}\lambda_{25} & \dfrac{v_{\phi_1}^2\zeta_3}{2} + \dfrac{v_{\phi_2}\kappa_3}{\sqrt{2}} + v_{\phi_6}v_{\phi_8}\lambda_{26} \\[2.5ex]
v_H v_{\phi_2}\lambda_7 & v_{\phi_1}(\sqrt{2}\kappa_1 + v_{\phi_2}\lambda_{22}) & \dfrac{3v_{\phi_2}v_{\phi_6}\zeta_2}{2} + \dfrac{v_{\phi_8}\kappa_3}{\sqrt{2}} + v_{\phi_2}v_{\phi_6}\lambda_{25} & \dfrac{3v_{\phi_2}^2\zeta_2}{2} - \dfrac{v_{\phi_1}^2\kappa_1 + v_{\phi_6}v_{\phi_8}\kappa_3}{\sqrt{2}v_{\phi_2}} + 2v_{\phi_2}^2\lambda_{27} & \dfrac{v_{\phi_6}\kappa_3}{\sqrt{2}} + v_{\phi_2}v_{\phi_8}\lambda_{28} \\[2.5ex]
v_H v_{\phi_8}\lambda_8 & v_{\phi_1}(v_{\phi_6}\zeta_3 + v_{\phi_8}\lambda_{23}) & \dfrac{v_{\phi_1}^2\zeta_3}{2} + \dfrac{v_{\phi_2}\kappa_3}{\sqrt{2}} + v_{\phi_6}v_{\phi_8}\lambda_{26} & \dfrac{v_{\phi_6}\kappa_3}{\sqrt{2}} + v_{\phi_2}v_{\phi_8}\lambda_{28} & -\dfrac{v_{\phi_1}^2 v_{\phi_6}\kappa_3 - 4v_{\phi_8}^3\lambda_{29}}{2v_{\phi_8}}
\end{pmatrix}$$

$$\mathcal{M}^I_{\text{Visible}} = \begin{pmatrix}
0 & 0 & 0 & 0 & 0 \\[1.5ex]
0 & -2(v_{\phi_6}v_{\phi_8}\zeta_3 + \sqrt{2}v_{\phi_2}\kappa_1) & -v_{\phi_1}v_{\phi_8}\zeta_3 & \sqrt{2}v_{\phi_1}\kappa_1 & v_{\phi_1}v_{\phi_6}\zeta_3 \\[1.5ex]
0 & -v_{\phi_1}v_{\phi_8}\zeta_3 & -\dfrac{v_{\phi_2}^3\zeta_2 + v_{\phi_1}^2 v_{\phi_8}\zeta_3 + \sqrt{2}v_{\phi_2}v_{\phi_8}\kappa_3}{2v_{\phi_6}} & \dfrac{3v_{\phi_2}^2\zeta_2}{2} - \dfrac{v_{\phi_8}\kappa_3}{\sqrt{2}} & \dfrac{v_{\phi_1}^2\zeta_3}{2} + \dfrac{v_{\phi_2}\kappa_3}{\sqrt{2}} \\[2.5ex]
0 & \sqrt{2}v_{\phi_1}\kappa_1 & \dfrac{3v_{\phi_2}^2\zeta_2}{2} - \dfrac{v_{\phi_8}\kappa_3}{\sqrt{2}} & -\dfrac{9}{2}v_{\phi_2}v_{\phi_6}\zeta_2 - \dfrac{v_{\phi_1}^2\kappa_1 + v_{\phi_6}v_{\phi_8}\kappa_3}{\sqrt{2}v_{\phi_2}} & \dfrac{v_{\phi_6}\kappa_3}{\sqrt{2}} \\[2.5ex]
0 & v_{\phi_1}v_{\phi_6}\zeta_3 & \dfrac{v_{\phi_1}^2\zeta_3}{2} + \dfrac{v_{\phi_2}\kappa_3}{\sqrt{2}} & \dfrac{v_{\phi_6}\kappa_3}{\sqrt{2}} & -\dfrac{v_{\phi_6}(v_{\phi_1}^2\zeta_3 + \sqrt{2}v_{\phi_2}\kappa_3)}{2v_{\phi_8}}
\end{pmatrix}$$

C   Master Integrals for CLBZ Two-loop Diagrams

The strategy when solving two-loop diagrams is to rewrite the amplitude in terms of master integrals. According to the classification of genuine two-loop diagrams given in [133], our model corresponds to a CLBZ (Cheng-Lee-Babu-Zee [82, 83, 134]) type, presented in Fig. 29. The label "genuine two-loop diagram" refers to those where no one-loop nor tree-level neutrino masses exist. In CLBZ genuine two-loop diagrams, there are two types of
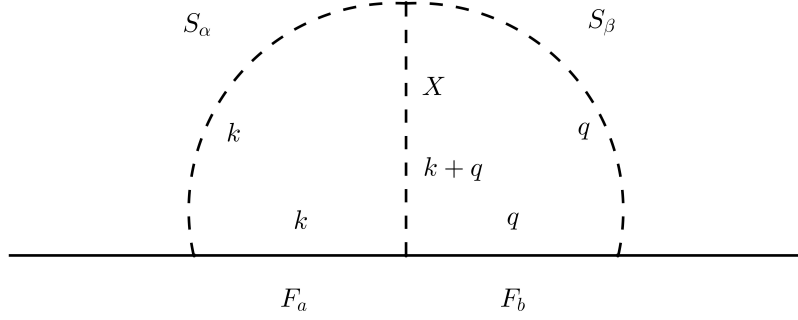
Figure 29: Genuine two-loop diagram corresponding to a CLBZ type, according to the classification in [133].

integrals:

$$\mathcal{I}_{ab,\alpha\beta,X} = \frac{1}{(2\pi)^8} \int d^4k \int d^4q \frac{1}{(k^2 - m_a^2)(k^2 - m_\alpha^2)(q^2 - m_b^2)(q^2 - m_\beta^2)[(q+k)^2 - m_X^2]}, \tag{C.1}$$

$$\mathcal{I}_{ab,\alpha\beta,X}^{\{k^2,q^2,(k+q)^2\}} = \frac{1}{(2\pi)^8} \int d^4k \int d^4q \frac{\{k^2, q^2, (k+q)^2\}}{(k^2 - m_a^2)(k^2 - m_\alpha^2)(q^2 - m_b^2)(q^2 - m_\beta^2)[(q+k)^2 - m_X^2]}. \tag{C.2}$$

The term $\{k^2, q^2, (k+q)^2\}$ implies that the numerator can be any of k^2, q^2 or $(k+q)^2$. The fermion masses are labeled as a, b and the scalar masses as α, β. Here, X is the inner scalar particle. Integrals C.1 and C.2 are rewritten in terms of master integrals as follows. First, we rescale the integral with respect to m_X^2 with

$$k, q \to \frac{k}{m_X}, \frac{q}{m_X}, \qquad d^4k, d^4q \to \frac{d^4k}{(m_X)^4}, \frac{d^4q}{(m_X)^4}. \tag{C.3}$$

Hence, we have

$$\mathcal{I}_{ab,\alpha\beta,X} = \frac{1}{(2\pi)^8} \frac{1}{m_x^2} \hat{\mathcal{I}}_{ab,\alpha\beta},$$

$$\mathcal{I}_{ab,\alpha\beta,X}^{\{k^2,q^2,(k+q)^2\}} = \frac{1}{(2\pi)^8} \hat{\mathcal{I}}_{ab,\alpha\beta}^{\{k^2,q^2,(k+q)^2\}} \tag{C.4}$$

with

$$\hat{\mathcal{I}}_{ab,\alpha\beta} = \int d^4k \int d^4q \frac{1}{(k^2 - r_a)(k^2 - t_\alpha)(q^2 - r_b)(q^2 - t_\beta)[(q+k)^2 - 1]} \tag{C.5}$$

$$\hat{\mathcal{I}}_{ab,\alpha\beta}^{\{k^2,q^2,(k+q)^2\}} = \int d^4k \int d^4q \frac{\{k^2, q^2, (k+q)^2\}}{(k^2 - r_a)(k^2 - t_\alpha)(q^2 - r_b)(q^2 - t_\beta)[(q+k)^2 - 1]} \tag{C.6}$$

Here, $r_{a,b} = (m_{F_{a,b}}/m_X)^2$ and $t_{\alpha,\beta} = (m_{S_{\alpha,\beta}}/m_X)^2$. Using the properties

$$\frac{1}{(k^2 - x_1)(k^2 - x_2)} = \frac{1}{x_1 - x_2}\left(\frac{1}{k^2 - x_1} - \frac{1}{k^2 - x_2}\right) \qquad \text{and}$$

$$\frac{q^2}{(k^2 - x_1)(q^2 - x_2)} = \frac{1}{k^2 - x_1} + \frac{x_2}{(k^2 - x_1)(q^2 - x_2)}, \tag{C.7}$$

integrals C.5 and C.6 can be reduced to "master integrals" of the form:

$$I(s,t) = \mu^\epsilon \int d^n k \int d^n q \frac{1}{(k^2 - s)(q^2 - t)[(k + q)^2 - 1]} \tag{C.8}$$

and

$$B_0(0, s, t) = \int \frac{d^4 k}{(2\pi)^4} \frac{1}{(k^2 - s)(k^2 - t)}. \tag{C.9}$$

Integral C.8 has been solved in [135]. The finite part of the solution yields

$$\hat{g}(s,t) = \frac{s}{2}\ln s \ln t + \sum_\pm \pm \frac{s(1 - s) + 3st + 2(1 - t)x_\pm}{2\omega}$$

$$\times \left[\text{Li}_2\left(\frac{x_\pm}{x_\pm - s}\right) - \text{Li}_2\left(\frac{x_\pm - s}{x_\pm}\right) + \text{Li}_2\left(\frac{t - 1}{x_\pm}\right) - \text{Li}_2\left(\frac{t - 1}{x_\pm - s}\right)\right], \tag{C.10}$$

with the standard di-logarithm

$$\text{Li}_2(x) = -\int_0^x \frac{\ln(1 - y)}{y}dy, \tag{C.11}$$

and

$$x_\pm = \frac{1}{2}(-1 + s + t \pm \omega), \qquad \omega = \sqrt{1 + s^2 + t^2 - 2(s + t + st)}. \tag{C.12}$$

Integral C.9 is the well-known one-loop scalar Passarino-Veltman function B_0 [93] in the vanishing external momentum limit ($p \to 0$). Defining

$$B_0(0, s, t) = \frac{1}{(2\pi)^4}\hat{B}_0(0, s, t), \tag{C.13}$$

the finite part of the solution is given by

$$\hat{B}_0(0, s, t) = -\pi^2 i\left(\frac{s\ln s - t\ln t}{s - t}\right) = \pi^2 \hat{B}_0'(0, s, t). \tag{C.14}$$

Thus, integrals C.5 and C.6 give [133]:

$$\pi^{-4}\hat{\mathcal{I}}_{ab,\alpha\beta} = \frac{1}{(t_\alpha - r_a)(t_\beta - r_b)}\left\{-\hat{g}(t_\alpha, t_\beta) + \hat{g}(r_a, t_\beta) + \hat{g}(t_\alpha, r_b) - \hat{g}(r_a, r_b)\right\}, \tag{C.15}$$

$$\pi^{-4}\hat{\mathcal{I}}_{ab,\alpha\beta}^{(k^2)} = \left\{\frac{1}{t_\beta - r_b}[-\hat{g}(r_a, t_\beta) + \hat{g}(r_a, r_b)]\right.$$

$$\left. + \frac{t_\alpha}{(t_\alpha - r_a)(t_\beta - r_b)}[-\hat{g}(t_\alpha, t_\beta) + \hat{g}(t_\alpha, r_b) + \hat{g}(r_a, t_\beta) - \hat{g}(r_a, r_b)]\right\}, \tag{C.16}$$

85

$$\pi^{-4}\hat{\mathcal{I}}_{ab,\alpha\beta}^{(q^2)} = \left\{ \frac{1}{t_\alpha - r_a}[-\hat{g}(t_\alpha, r_b) + \hat{g}(r_a, r_b)] \right.$$
$$\left. + \frac{t_\beta}{(t_\alpha - r_a)(t_\beta - r_b)}[-\hat{g}(t_\alpha, t_\beta) + \hat{g}(t_\alpha, r_b) + \hat{g}(r_a, t_\beta) - \hat{g}(r_a, r_b)] \right\},$$

(C.17)

$$\pi^{-4}\hat{\mathcal{I}}_{ab,\alpha\beta}^{[(k+q)^2]} = \left\{ \hat{B}_0'(0, r_a, t_\alpha)\,\hat{B}_0'(0, r_b, t_\beta) + \frac{-\hat{g}(t_\alpha, t_\beta) + \hat{g}(t_\alpha, r_b) + \hat{g}(r_a, t_\beta) - \hat{g}(r_a, r_b)}{(t_\alpha - r_a)(t_\beta - r_b)} \right\}.$$

(C.18)

The last expressions correspond only to the finite piece of the integrals. For CLBZ types, the divergent piece always cancels [133], giving finite results.

D   Loop Functions in LFV

In this appendix, the loop functions used for LFV processes are presented:

$$F_2(x) = \frac{1 - 6x + 3x^2 + 2x^3 - 6x^2 \log x}{6(1-x)^4}, \tag{D.1}$$

$$G_2(x) = \frac{2 - 9x + 18x^2 - 11x^3 + 6x^3 \log x}{6(1-x)^4}, \tag{D.2}$$

$$D_1(x,y) = -\frac{1}{(1-x)(1-y)} - \frac{x^2 \log x}{(1-x)^2(x-y)} - \frac{y^2 \log y}{(1-y)^2(y-x)}, \tag{D.3}$$

$$D_2(x,y) = -\frac{1}{(1-x)(1-y)} - \frac{x \log x}{(1-x)^2(x-y)} - \frac{y \log y}{(1-y)^2(y-x)}. \tag{D.4}$$

The case with degenerate masses for χ_i corresponds to the limit $x \to y$. Then, functions D become

$$D_1(x) = \frac{-1 + x^2 - 2x \log x}{(1-x)^3}, \tag{D.5}$$

$$D_2(x) = \frac{-2 + 2x - (1+x) \log x}{(1-x)^3}. \tag{D.6}$$

References

[1] S. L. Glashow. "Partial Symmetries of Weak Interactions". In: *Nucl. Phys.* 22 (1961), pp. 579–588. DOI: 10.1016/0029-5582(61)90469-2.

[2] Steven Weinberg. "A Model of Leptons". In: *Phys. Rev. Lett.* 19 (1967), pp. 1264–1266. DOI: 10.1103/PhysRevLett.19.1264.

[3] Abdus Salam. "Weak and Electromagnetic Interactions". In: *Conf. Proc. C* 680519 (1968), pp. 367–377. DOI: 10.1142/9789812795915_0034.

[4] Murray Gell-Mann. "A Schematic Model of Baryons and Mesons". In: *Phys. Lett.* 8 (1964), pp. 214–215. DOI: 10.1016/S0031-9163(64)92001-3.

[5] Richard P. Feynman. "Very high-energy collisions of hadrons". In: *Phys. Rev. Lett.* 23 (1969). Ed. by L. M. Brown, pp. 1415–1417. DOI: 10.1103/PhysRevLett.23.1415.

[6] J. D. Bjorken and Emmanuel A. Paschos. "Inelastic Electron Proton and gamma Proton Scattering, and the Structure of the Nucleon". In: *Phys. Rev.* 185 (1969), pp. 1975–1982. DOI: 10.1103/PhysRev.185.1975.

[7] David J. Gross and Frank Wilczek. "Ultraviolet Behavior of Nonabelian Gauge Theories". In: *Phys. Rev. Lett.* 30 (1973). Ed. by J. C. Taylor, pp. 1343–1346. DOI: 10.1103/PhysRevLett.30.1343.

[8] H. David Politzer. "Reliable Perturbative Results for Strong Interactions?" In: *Phys. Rev. Lett.* 30 (1973). Ed. by J. C. Taylor, pp. 1346–1349. DOI: 10.1103/PhysRevLett.30.1346.

[9] R. L. Workman and Others. "Review of Particle Physics". In: *PTEP* 2022 (2022), p. 083C01. DOI: 10.1093/ptep/ptac097.

[10] F. Zwicky. "Republication of: The redshift of extragalactic nebulae". In: *General Relativity and Gravitation* 41.1 (Jan. 2009), pp. 207–224. DOI: 10.1007/s10714-008-0707-4.

[11] Vera C. Rubin and Jr. Ford W. Kent. "Rotation of the Andromeda Nebula from a Spectroscopic Survey of Emission Regions". In: 159 (Feb. 1970), p. 379. DOI: 10.1086/150317.

[12] N. Aghanim et al. "Planck 2018 results. VI. Cosmological parameters". In: *Astron. Astrophys.* 641 (2020). [Erratum: Astron.Astrophys. 652, C4 (2021)], A6. DOI: 10.1051/0004-6361/201833910. arXiv: 1807.06209 [astro-ph.CO].

[13] Gianfranco Bertone, Dan Hooper, and Joseph Silk. "Particle dark matter: Evidence, candidates and constraints". In: *Phys. Rept.* 405 (2005), pp. 279–390. DOI: 10.1016/j.physrep.2004.08.031. arXiv: hep-ph/0404175.

[14] D. S. Akerib et al. "Results from a search for dark matter in the complete LUX exposure". In: *Phys. Rev. Lett.* 118.2 (2017), p. 021303. DOI: 10.1103/PhysRevLett.118.021303. arXiv: 1608.07648 [astro-ph.CO].

[15] E. Aprile et al. "Dark Matter Search Results from a One Ton-Year Exposure of XENON1T". In: *Phys. Rev. Lett.* 121.11 (2018), p. 111302. DOI: 10.1103/PhysRevLett.121.111302. arXiv: 1805.12562 [astro-ph.CO].

[16] C. Amole et al. "Dark Matter Search Results from the Complete Exposure of the PICO-60 C_3F_8 Bubble Chamber". In: *Phys. Rev. D* 100.2 (2019), p. 022001. DOI: 10.1103/PhysRevD.100.022001. arXiv: 1902.04031 [astro-ph.CO].

[17] Xiangyi Cui et al. "Dark Matter Results From 54-Ton-Day Exposure of PandaX-II Experiment". In: *Phys. Rev. Lett.* 119.18 (2017), p. 181302. DOI: 10.1103/PhysRevLett.119.181302. arXiv: 1708.06917 [astro-ph.CO].

[18] A. D. Sakharov. "Violation of CP Invariance, C asymmetry, and baryon asymmetry of the universe". In: *Pisma Zh. Eksp. Teor. Fiz.* 5 (1967), pp. 32–35. DOI: 10.1070/PU1991v034n05ABEH002497.

[19] G. Steigman. "Observational tests of antimatter cosmologies". In: *Ann. Rev. Astron. Astrophys.* 14 (1976), pp. 339–372. DOI: 10.1146/annurev.aa.14.090176.002011.

[20] Andrew G. Cohen, A. De Rujula, and S. L. Glashow. "A Matter - antimatter universe?" In: *Astrophys. J.* 495 (1998), pp. 539–549. DOI: 10.1086/305328. arXiv: astro-ph/9707087.

[21] Michael Dine and Alexander Kusenko. "The Origin of the matter - antimatter asymmetry". In: *Rev. Mod. Phys.* 76 (2003), p. 1. DOI: 10.1103/RevModPhys.76.1. arXiv: hep-ph/0303065.

[22] Antonio Riotto and Mark Trodden. "Recent progress in baryogenesis". In: *Ann. Rev. Nucl. Part. Sci.* 49 (1999), pp. 35–75. DOI: 10.1146/annurev.nucl.49.1.35. arXiv: hep-ph/9901362.

[23] Raymond Davis, Don S. Harmer, and Kenneth C. Hoffman. "Search for Neutrinos from the Sun". In: *Phys. Rev. Lett.* 20 (21 1968), pp. 1205–1209. DOI: 10.1103/PhysRevLett.20.1205. URL: https://link.aps.org/doi/10.1103/PhysRevLett.20.1205.

[24] Y. Fukuda et al. "Evidence for oscillation of atmospheric neutrinos". In: *Phys. Rev. Lett.* 81 (1998), pp. 1562–1567. DOI: 10.1103/PhysRevLett.81.1562. arXiv: hep-ex/9807003.

[25] Q. R. Ahmad et al. "Direct evidence for neutrino flavor transformation from neutral current interactions in the Sudbury Neutrino Observatory". In: *Phys. Rev. Lett.* 89 (2002), p. 011301. DOI: 10.1103/PhysRevLett.89.011301. arXiv: nucl-ex/0204008.

[26] K. Eguchi et al. "First results from KamLAND: Evidence for reactor anti-neutrino disappearance". In: *Phys. Rev. Lett.* 90 (2003), p. 021802. DOI: 10.1103/PhysRevLett.90.021802. arXiv: hep-ex/0212021.

[27] M. H. Ahn et al. "Measurement of Neutrino Oscillation by the K2K Experiment". In: *Phys. Rev. D* 74 (2006), p. 072003. DOI: 10.1103/PhysRevD.74.072003. arXiv: hep-ex/0606032.

[28] D. G. Michael et al. "Observation of muon neutrino disappearance with the MINOS detectors and the NuMI neutrino beam". In: *Phys. Rev. Lett.* 97 (2006), p. 191801. DOI: 10.1103/PhysRevLett.97.191801. arXiv: hep-ex/0607088.

[29] S. Abe et al. "Precision Measurement of Neutrino Oscillation Parameters with KamLAND". In: *Phys. Rev. Lett.* 100 (2008), p. 221803. DOI: 10.1103/PhysRevLett.100.221803. arXiv: 0801.4589 [hep-ex].

[30] Y. Abe et al. "Indication of Reactor $\bar{\nu}_e$ Disappearance in the Double Chooz Experiment". In: *Phys. Rev. Lett.* 108 (2012), p. 131801. DOI: 10.1103/PhysRevLett.108.131801. arXiv: 1112.6353 [hep-ex].

[31] F. P. An et al. "Observation of electron-antineutrino disappearance at Daya Bay". In: *Phys. Rev. Lett.* 108 (2012), p. 171803. DOI: 10.1103/PhysRevLett.108.171803. arXiv: 1203.1669 [hep-ex].

[32] J. K. Ahn et al. "Observation of Reactor Electron Antineutrino Disappearance in the RENO Experiment". In: *Phys. Rev. Lett.* 108 (2012), p. 191802. DOI: 10.1103/PhysRevLett.108.191802. arXiv: 1204.0626 [hep-ex].

[33] K. Abe et al. "Indication of Electron Neutrino Appearance from an Accelerator-produced Off-axis Muon Neutrino Beam". In: *Phys. Rev. Lett.* 107 (2011), p. 041801. DOI: 10.1103/PhysRevLett.107.041801. arXiv: 1106.2822 [hep-ex].

[34] K. Abe et al. "Precise Measurement of the Neutrino Mixing Parameter θ_{23} from Muon Neutrino Disappearance in an Off-Axis Beam". In: *Phys. Rev. Lett.* 112.18 (2014), p. 181801. DOI: 10.1103/PhysRevLett.112.181801. arXiv: 1403.1532 [hep-ex].

[35] M. Aker et al. "Improved Upper Limit on the Neutrino Mass from a Direct Kinematic Method by KATRIN". In: *Phys. Rev. Lett.* 123.22 (2019), p. 221802. DOI: 10.1103/PhysRevLett.123.221802. arXiv: 1909.06048 [hep-ex].

[36] M. Aker et al. "Direct neutrino-mass measurement with sub-electronvolt sensitivity". In: *Nature Phys.* 18.2 (2022), pp. 160–166. DOI: 10.1038/s41567-021-01463-1. arXiv: 2105.08533 [hep-ex].

[37] J. Schechter and J. W. F. Valle. "Neutrinoless Double beta Decay in SU(2) x U(1) Theories". In: *Phys. Rev. D* 25 (1982), p. 2951. DOI: 10.1103/PhysRevD.25.2951.

[38] S. Abe et al. "Search for the Majorana Nature of Neutrinos in the Inverted Mass Ordering Region with KamLAND-Zen". In: *Phys. Rev. Lett.* 130.5 (2023), p. 051801. DOI: 10.1103/PhysRevLett.130.051801. arXiv: 2203.02139 [hep-ex].

[39] M. Agostini et al. "Final Results of GERDA on the Search for Neutrinoless Double-β Decay". In: *Phys. Rev. Lett.* 125.25 (2020), p. 252502. DOI: 10.1103/PhysRevLett.125.252502. arXiv: 2009.06079 [nucl-ex].

[40] G. Anton et al. "Search for Neutrinoless Double-β Decay with the Complete EXO-200 Dataset". In: *Phys. Rev. Lett.* 123.16 (2019), p. 161802. DOI: 10.1103/PhysRevLett.123.161802. arXiv: 1906.02723 [hep-ex].

[41] D. Q. Adams et al. "Search for Majorana neutrinos exploiting millikelvin cryogenics with CUORE". In: *Nature* 604.7904 (2022), pp. 53–58. DOI: 10.1038/s41586-022-04497-4. arXiv: 2104.06906 [nucl-ex].

[42] R. V. Harlander, S. Y. Klein, and M. Lipp. "FeynGame". In: *Comput. Phys. Commun.* 256 (2020), p. 107465. DOI: 10.1016/j.cpc.2020.107465. arXiv: 2003.00896 [physics.ed-ph].

[43] Robert Harlander, Sven Yannick Klein, and Magnus Schaaf. "FeynGame-2.1 – Feynman diagrams made easy". In: Jan. 2024. arXiv: 2401.12778 [hep-ph].

[44] Carlo Giunti and Chung W Kim. *Fundamentals of neutrino physics and astrophysics*. Oxford university press, 2007.

[45] Francis Halzen and Alan D Martin. *Quark & Leptons: An introductory course in modern particle physics*. John Wiley & Sons, 2008.

[46] Matthew D Schwartz. *Quantum field theory and the standard model*. Cambridge university press, 2014.

[47] T. Nakano and K. Nishijima. "Charge Independence for V-particles". In: *Prog. Theor. Phys.* 10 (1953), pp. 581–582. DOI: 10.1143/PTP.10.581.

[48] M. Gell-Mann. "The interpretation of the new particles as displaced charge multiplets". In: *Nuovo Cim.* 4.S2 (1956), pp. 848–866. DOI: 10.1007/BF02748000.

[49] Peter W. Higgs. "Broken Symmetries and the Masses of Gauge Bosons". In: *Phys. Rev. Lett.* 13 (1964). Ed. by J. C. Taylor, pp. 508–509. DOI: 10.1103/PhysRevLett.13.508.

[50] F. Englert and R. Brout. "Broken Symmetry and the Mass of Gauge Vector Mesons". In: *Phys. Rev. Lett.* 13 (1964). Ed. by J. C. Taylor, pp. 321–323. DOI: 10.1103/PhysRevLett.13.321.

[51] G. S. Guralnik, C. R. Hagen, and T. W. B. Kibble. "Global Conservation Laws and Massless Particles". In: *Phys. Rev. Lett.* 13 (1964). Ed. by J. C. Taylor, pp. 585–587. DOI: 10.1103/PhysRevLett.13.585.

[52] Serguei Chatrchyan et al. "Observation of a New Boson at a Mass of 125 GeV with the CMS Experiment at the LHC". In: *Phys. Lett. B* 716 (2012), pp. 30–61. DOI: 10.1016/j.physletb.2012.08.021. arXiv: 1207.7235 [hep-ex].

[53] Georges Aad et al. "Observation of a new particle in the search for the Standard Model Higgs boson with the ATLAS detector at the LHC". In: *Phys. Lett. B* 716 (2012), pp. 1–29. DOI: 10.1016/j.physletb.2012.08.020. arXiv: 1207.7214 [hep-ex].

[54] S. Schael et al. "Precision electroweak measurements on the Z resonance". In: *Phys. Rept.* 427 (2006), pp. 257–454. DOI: 10.1016/j.physrep.2005.12.006. arXiv: hep-ex/0509008.

[55] S. Schael et al. "Electroweak Measurements in Electron-Positron Collisions at W-Boson-Pair Energies at LEP". In: *Phys. Rept.* 532 (2013), pp. 119–244. DOI: 10.1016/j.physrep.2013.07.004. arXiv: 1302.3415 [hep-ex].

[56] Nicola Cabibbo. "Unitary Symmetry and Leptonic Decays". In: *Phys. Rev. Lett.* 10 (1963), pp. 531–533. DOI: 10.1103/PhysRevLett.10.531.

[57] Makoto Kobayashi and Toshihide Maskawa. "CP Violation in the Renormalizable Theory of Weak Interaction". In: *Prog. Theor. Phys.* 49 (1973), pp. 652–657. DOI: 10.1143/PTP.49.652.

[58] Samoil Bilenky. *Introduction to the physics of massive and mixed neutrinos*. Vol. 817. 2010. DOI: 10.1007/978-3-642-14043-3.

[59] Steven Weinberg. *The Quantum theory of fields. Vol. 1: Foundations*. Cambridge University Press, June 2005. ISBN: 978-0-521-67053-1, 978-0-511-25204-4. DOI: 10.1017/CBO9781139644167.

[60] Raymond Frederick Streater and Arthur Strong Wightman. *PCT, spin and statistics, and all that*. Vol. 52. Princeton University Press, 2000.

[61] B. Pontecorvo. "Mesonium and anti-mesonium". In: *Sov. Phys. JETP* 6 (1957), p. 429.

[62] B. Pontecorvo. "Inverse beta processes and nonconservation of lepton charge". In: *Zh. Eksp. Teor. Fiz.* 34 (1957), p. 247.

[63] Ziro Maki, Masami Nakagawa, and Shoichi Sakata. "Remarks on the unified model of elementary particles". In: *Prog. Theor. Phys.* 28 (1962), pp. 870–880. DOI: 10.1143/PTP.28.870.

[64] B. Pontecorvo. "Neutrino Experiments and the Problem of Conservation of Leptonic Charge". In: *Zh. Eksp. Teor. Fiz.* 53 (1967), pp. 1717–1725.

[65] Raymond Davis Jr., Don S. Harmer, and Kenneth C. Hoffman. "Search for neutrinos from the sun". In: *Phys. Rev. Lett.* 20 (1968), pp. 1205–1209. DOI: 10.1103/PhysRevLett.20.1205.

[66] K. S. Hirata et al. "Observation of B-8 Solar Neutrinos in the Kamiokande-II Detector". In: *Phys. Rev. Lett.* 63 (1989), p. 16. DOI: 10.1103/PhysRevLett.63.16.

[67] JUNO Collaboration / Johannes Gutenberg University-Mainz. *All things neutrino*. https://neutrinos.fnal.gov/mysteries/mass-ordering/mass-hierarchy-jgu-mainz-web/. Accessed: 2023-11-20.

[68] P. F. de Salas et al. "2020 global reassessment of the neutrino oscillation picture". In: *JHEP* 02 (2021), p. 071. DOI: 10.1007/JHEP02(2021)071. arXiv: 2006.11237 [hep-ph].

[69]   Ivan Esteban et al. "The fate of hints: updated global analysis of three-flavor neutrino oscillations". In: *JHEP* 09 (2020), p. 178. DOI: 10.1007/JHEP09(2020)178. arXiv: 2007.14792 [hep-ph].

[70]   L. Wolfenstein. "Neutrino Oscillations in Matter". In: *Phys. Rev. D* 17 (1978), pp. 2369–2374. DOI: 10.1103/PhysRevD.17.2369.

[71]   R. N. Mohapatra and P. B. Pal. *Massive neutrinos in physics and astrophysics*. Vol. 41. 1991.

[72]   Kai Zuber. *Neutrino Physics*. Boca Raton: Taylor & Francis, 2020. ISBN: 978-1-351-76458-2, 978-1-315-19561-2, 978-1-03-224220-0, 978-1-138-71889-0. DOI: 10.1201/9781315195612.

[73]   Steven Weinberg. "Baryon and Lepton Nonconserving Processes". In: *Phys. Rev. Lett.* 43 (1979), pp. 1566–1570. DOI: 10.1103/PhysRevLett.43.1566.

[74]   Tsutomu Yanagida. "Horizontal gauge symmetry and masses of neutrinos". In: *Conf. Proc. C* 7902131 (1979). Ed. by Osamu Sawada and Akio Sugamoto, pp. 95–99.

[75]   Murray Gell-Mann, Pierre Ramond, and Richard Slansky. "Complex Spinors and Unified Theories". In: *Conf. Proc. C* 790927 (1979), pp. 315–321. arXiv: 1306.4669 [hep-th].

[76]   Rabindra N. Mohapatra and Goran Senjanovic. "Neutrino Mass and Spontaneous Parity Nonconservation". In: *Phys. Rev. Lett.* 44 (1980), p. 912. DOI: 10.1103/PhysRevLett.44.912.

[77]   J. Schechter and J. W. F. Valle. "Neutrino Masses in SU(2) x U(1) Theories". In: *Phys. Rev. D* 22 (1980), p. 2227. DOI: 10.1103/PhysRevD.22.2227.

[78]   George Lazarides, Q. Shafi, and C. Wetterich. "Proton Lifetime and Fermion Masses in an SO(10) Model". In: *Nucl. Phys. B* 181 (1981), pp. 287–300. DOI: 10.1016/0550-3213(81)90354-0.

[79]   J. Schechter and J. W. F. Valle. "Neutrino Decay and Spontaneous Violation of Lepton Number". In: *Phys. Rev. D* 25 (1982), p. 774. DOI: 10.1103/PhysRevD.25.774.

[80]   Robert Foot et al. "Seesaw Neutrino Masses Induced by a Triplet of Leptons". In: *Z. Phys. C* 44 (1989), p. 441. DOI: 10.1007/BF01415558.

[81]   A. Zee. "A Theory of Lepton Number Violation, Neutrino Majorana Mass, and Oscillation". In: *Phys. Lett. B* 93 (1980). [Erratum: Phys.Lett.B 95, 461 (1980)], p. 389. DOI: 10.1016/0370-2693(80)90349-4.

[82]   A. Zee. "Quantum Numbers of Majorana Neutrino Masses". In: *Nucl. Phys. B* 264 (1986), pp. 99–110. DOI: 10.1016/0550-3213(86)90475-X.

[83]   K. S. Babu. "Model of 'Calculable' Majorana Neutrino Masses". In: *Phys. Lett. B* 203 (1988), pp. 132–136. DOI: 10.1016/0370-2693(88)91584-5.

[84]   Ernest Ma. "Verifiable radiative seesaw mechanism of neutrino mass and dark matter". In: *Phys. Rev. D* 73 (2006), p. 077301. DOI: 10.1103/PhysRevD.73.077301. arXiv: hep-ph/0601225.

[85]   Alexander Merle and Moritz Platscher. "Parity Problem of the Scotogenic Neutrino Model". In: *Phys. Rev. D* 92.9 (2015), p. 095002. DOI: 10.1103/PhysRevD.92.095002. arXiv: 1502.03098 [hep-ph].

[86]   Gerard 't Hooft. "Naturalness, chiral symmetry, and spontaneous chiral symmetry breaking". In: *NATO Sci. Ser. B* 59 (1980). Ed. by Gerard 't Hooft et al., pp. 135–157. DOI: 10.1007/978-1-4684-7571-5_9.

[87] Salvador Centelles Chuliá et al. "Scotogenic dark symmetry as a residual subgroup of Standard Model symmetries". In: *Chin. Phys. C* 44.8 (2020), p. 083110. DOI: 10.1088/1674-1137/44/8/083110. arXiv: 1901.06402 [hep-ph].

[88] Ernest Ma. "Z(3) Dark Matter and Two-Loop Neutrino Mass". In: *Phys. Lett. B* 662 (2008), pp. 49–52. DOI: 10.1016/j.physletb.2008.02.053. arXiv: 0708.3371 [hep-ph].

[89] Jisuke Kubo and Daijiro Suematsu. "Neutrino masses and CDM in a non-supersymmetric model". In: *Phys. Lett. B* 643 (2006), pp. 336–341. DOI: 10.1016/j.physletb.2006.11.005. arXiv: hep-ph/0610006.

[90] Cesar Bonilla et al. "Dark matter stability and Dirac neutrinos using only Standard Model symmetries". In: *Phys. Rev. D* 101.3 (2020), p. 033011. DOI: 10.1103/PhysRevD.101.033011. arXiv: 1812.01599 [hep-ph].

[91] Rahul Srivastava, Cesar Bonilla, and Eduardo Peinado. "The role of residual symmetries in dark matter stability and the neutrino nature". In: *LHEP* 2.1 (2019), p. 124. DOI: 10.31526/lhep.1.2019.124. arXiv: 1903.01477 [hep-ph].

[92] Y. Chikashige, Rabindra N. Mohapatra, and R. D. Peccei. "Are There Real Goldstone Bosons Associated with Broken Lepton Number?" In: *Phys. Lett. B* 98 (1981), pp. 265–268. DOI: 10.1016/0370-2693(81)90011-3.

[93] G. Passarino and M. J. G. Veltman. "One Loop Corrections for e+ e- Annihilation Into mu+ mu- in the Weinberg Model". In: *Nucl. Phys. B* 160 (1979), pp. 151–207. DOI: 10.1016/0550-3213(79)90234-7.

[94] J. A. Casas and A. Ibarra. "Oscillating neutrinos and $\mu \rightarrow e, \gamma$". In: *Nucl. Phys. B* 618 (2001), pp. 171–204. DOI: 10.1016/S0550-3213(01)00475-8. arXiv: hep-ph/0103065.

[95] Manfred Lindner et al. "Fermionic WIMPs and vacuum stability in the scotogenic model". In: *Phys. Rev. D* 94.11 (2016), p. 115027. DOI: 10.1103/PhysRevD.94.115027. arXiv: 1608.00577 [hep-ph].

[96] G. C. Branco et al. "Theory and phenomenology of two-Higgs-doublet models". In: *Phys. Rept.* 516 (2012), pp. 1–102. DOI: 10.1016/j.physrep.2012.02.002. arXiv: 1106.0034 [hep-ph].

[97] Cesar Bonilla et al. "Fermion Dark Matter and Radiative Neutrino Masses from Spontaneous Lepton Number Breaking". In: *New J. Phys.* 22.3 (2020), p. 033009. DOI: 10.1088/1367-2630/ab7254. arXiv: 1908.04276 [hep-ph].

[98] Takashi Toma and Avelino Vicente. "Lepton Flavor Violation in the Scotogenic Model". In: *JHEP* 01 (2014), p. 160. DOI: 10.1007/JHEP01(2014)160. arXiv: 1312.2840 [hep-ph].

[99] Avelino Vicente and Carlos E. Yaguna. "Probing the scotogenic model with lepton flavor violating processes". In: *JHEP* 02 (2015), p. 144. DOI: 10.1007/JHEP02(2015)144. arXiv: 1412.2545 [hep-ph].

[100] Valentina De Romeri et al. "Dark matter in the scotogenic model with spontaneous lepton number violation". In: *Phys. Rev. D* 107.9 (2023), p. 095019. DOI: 10.1103/PhysRevD.107.095019. arXiv: 2210.07706 [hep-ph].

[101] Eric D. Carlson, Marie E. Machacek, and Lawrence J. Hall. "Self-interacting dark matter". In: *Astrophys. J.* 398 (1992), pp. 43–52. DOI: 10.1086/171833.

[102] Patrick J. Fitzpatrick et al. "New pathways to the relic abundance of vector-portal dark matter". In: *Phys. Rev. D* 106.8 (2022), p. 083517. DOI: 10.1103/PhysRevD.106.083517. arXiv: 2011.01240 [hep-ph].

[103]   Michael E. Peskin and Tatsu Takeuchi. "A New constraint on a strongly interacting Higgs sector". In: *Phys. Rev. Lett.* 65 (1990), pp. 964–967. DOI: 10.1103/PhysRevLett.65.964.

[104]   Michael E. Peskin and Tatsu Takeuchi. "Estimation of oblique electroweak corrections". In: *Phys. Rev. D* 46 (1992), pp. 381–409. DOI: 10.1103/PhysRevD.46.381.

[105]   Avelino Vicente. "Computer tools in particle physics". In: (July 2015). arXiv: 1507.06349 [hep-ph].

[106]   Florian Staub. "SARAH 4 : A tool for (not only SUSY) model builders". In: *Comput. Phys. Commun.* 185 (2014), pp. 1773–1790. DOI: 10.1016/j.cpc.2014.02.018. arXiv: 1309.7223 [hep-ph].

[107]   Werner Porod. "SPheno, a program for calculating supersymmetric spectra, SUSY particle decays and SUSY particle production at e+ e- colliders". In: *Comput. Phys. Commun.* 153 (2003), pp. 275–315. DOI: 10.1016/S0010-4655(03)00222-4. arXiv: hep-ph/0301101.

[108]   Werner Porod, Florian Staub, and Avelino Vicente. "A Flavor Kit for BSM models". In: *Eur. Phys. J. C* 74.8 (2014), p. 2992. DOI: 10.1140/epjc/s10052-014-2992-2. arXiv: 1405.1434 [hep-ph].

[109]   Geneviève Bélanger et al. "micrOMEGAs5.0 : Freeze-in". In: *Comput. Phys. Commun.* 231 (2018), pp. 173–186. DOI: 10.1016/j.cpc.2018.04.027. arXiv: 1801.03509 [hep-ph].

[110]   Leon M. G. de la Vega et al. "Closing the dark photon window to thermal dark matter". In: (Nov. 2023). arXiv: 2311.17987 [hep-ph].

[111]   Savas Dimopoulos and Howard Georgi. "Softly Broken Supersymmetry and SU(5)". In: *Nucl. Phys. B* 193 (1981), pp. 150–162. DOI: 10.1016/0550-3213(81)90522-8.

[112]   A. M. Baldini et al. "Search for the lepton flavour violating decay $\mu^+ \to e^+\gamma$ with the full dataset of the MEG experiment". In: *Eur. Phys. J. C* 76.8 (2016), p. 434. DOI: 10.1140/epjc/s10052-016-4271-x. arXiv: 1605.05081 [hep-ex].

[113]   Bernard Aubert et al. "Searches for Lepton Flavor Violation in the Decays tau+- —> e+- gamma and tau+- —> mu+- gamma". In: *Phys. Rev. Lett.* 104 (2010), p. 021802. DOI: 10.1103/PhysRevLett.104.021802. arXiv: 0908.2381 [hep-ex].

[114]   U. Bellgardt et al. "Search for the Decay $\mu^+ \to e^+e^+e^-$". In: *Nucl. Phys. B* 299 (1988), pp. 1–6. DOI: 10.1016/0550-3213(88)90462-2.

[115]   K. Hayasaka et al. "Search for Lepton Flavor Violating Tau Decays into Three Leptons with 719 Million Produced Tau+Tau- Pairs". In: *Phys. Lett. B* 687 (2010), pp. 139–143. DOI: 10.1016/j.physletb.2010.03.037. arXiv: 1001.3221 [hep-ex].

[116]   J. Hisano et al. "Lepton flavor violation via right-handed neutrino Yukawa couplings in supersymmetric standard model". In: *Phys. Rev. D* 53 (1996), pp. 2442–2459. DOI: 10.1103/PhysRevD.53.2442. arXiv: hep-ph/9510309.

[117]   Ernesto Arganda and Maria J. Herrero. "Testing supersymmetry with lepton flavor violating tau and mu decays". In: *Phys. Rev. D* 73 (2006), p. 055003. DOI: 10.1103/PhysRevD.73.055003. arXiv: hep-ph/0510405.

[118]   Paul H. Frampton, Sheldon L. Glashow, and Danny Marfatia. "Zeroes of the neutrino mass matrix". In: *Phys. Lett. B* 536 (2002), pp. 79–82. DOI: 10.1016/S0370-2693(02)01817-8. arXiv: hep-ph/0201008.

[119]   D. Meloni, A. Meroni, and E. Peinado. "Two-zero Majorana textures in the light of the Planck results". In: *Phys. Rev. D* 89.5 (2014), p. 053009. DOI: 10.1103/PhysRevD.89.053009. arXiv: 1401.3207 [hep-ph].

[120]   Julien Alcaide, Jordi Salvado, and Arcadi Santamaria. "Fitting flavour symmetries: the case of two-zero neutrino mass textures". In: *JHEP* 07 (2018), p. 164. DOI: 10.1007/JHEP07(2018)164. arXiv: 1806.06785 [hep-ph].

[121]   Harald Fritzsch, Zhi-zhong Xing, and Shun Zhou. "Two-zero Textures of the Majorana Neutrino Mass Matrix and Current Experimental Tests". In: *JHEP* 09 (2011), p. 083. DOI: 10.1007/JHEP09(2011)083. arXiv: 1108.4534 [hep-ph].

[122]   Shun Zhou. "Update on two-zero textures of the Majorana neutrino mass matrix in light of recent T2K, Super-Kamiokande and NOνA results". In: *Chinese Physics C* 40.3, 033102 (Mar. 2016), p. 033102. DOI: 10.1088/1674-1137/40/3/033102. arXiv: 1509.05300 [hep-ph].

[123]   Zhi-zhong Xing. "Texture zeros and Majorana phases of the neutrino mass matrix". In: *Phys. Lett. B* 530 (2002), pp. 159–166. DOI: 10.1016/S0370-2693(02)01354-0. arXiv: hep-ph/0201151.

[124]   Madan Singh. "Testing texture two-zero neutrino mass matrices under current experimental scenario". In: *EPL* 129.1 (2020), p. 1. DOI: 10.1209/0295-5075/129/11002. arXiv: 1909.01552 [hep-ph].

[125]   Claudia Hagedorn and Werner Rodejohann. "Minimal mass matrices for dirac neutrinos". In: *JHEP* 07 (2005), p. 034. DOI: 10.1088/1126-6708/2005/07/034. arXiv: hep-ph/0503143.

[126]   Xue-wen Liu and Shun Zhou. "Texture Zeros for Dirac Neutrinos and Current Experimental Tests". In: *Int. J. Mod. Phys. A* 28 (2013), p. 1350040. DOI: 10.1142/S0217751X13500401. arXiv: 1211.0472 [hep-ph].

[127]   Happy Borgohain and Debasish Borah. "Survey of Texture Zeros with Light Dirac Neutrinos". In: *J. Phys. G* 48.7 (2021), p. 075005. DOI: 10.1088/1361-6471/abde9b. arXiv: 2007.06249 [hep-ph].

[128]   G. C. Branco et al. "Weak Basis Transformations and Texture Zeros in the Leptonic Sector". In: *Phys. Lett. B* 670 (2009), pp. 340–349. DOI: 10.1016/j.physletb.2008.10.059. arXiv: 0711.1613 [hep-ph].

[129]   Eleonora Di Valentino, Stefano Gariazzo, and Olga Mena. "Most constraining cosmological neutrino mass bounds". In: *Phys. Rev. D* 104.8 (2021), p. 083504. DOI: 10.1103/PhysRevD.104.083504. arXiv: 2106.15267 [astro-ph.CO].

[130]   Matthew D. Schwartz. *Quantum Field Theory and the Standard Model*. Cambridge University Press, Mar. 2014. ISBN: 978-1-107-03473-0, 978-1-107-03473-0.

[131]   Stephen L. Adler. "Axial vector vertex in spinor electrodynamics". In: *Phys. Rev.* 177 (1969), pp. 2426–2438. DOI: 10.1103/PhysRev.177.2426.

[132]   J. S. Bell and R. Jackiw. "A PCAC puzzle: $\pi^0 \to \gamma\gamma$ in the σ model". In: *Nuovo Cim. A* 60 (1969), pp. 47–61. DOI: 10.1007/BF02823296.

[133]   D. Aristizabal Sierra et al. "Systematic classification of two-loop realizations of the Weinberg operator". In: *JHEP* 03 (2015), p. 040. DOI: 10.1007/JHEP03(2015)040. arXiv: 1411.7038 [hep-ph].

[134]   T. P. Cheng and Ling-Fong Li. "Neutrino Masses, Mixings and Oscillations in SU(2) x U(1) Models of Electroweak Interactions". In: *Phys. Rev. D* 22 (1980), p. 2860. DOI: 10.1103/PhysRevD.22.2860.

[135]   Paul W. Angel et al. "Testable two-loop radiative neutrino mass model based on an LLd^cQd^c effective operator". In: *JHEP* 10 (2013). [Erratum: JHEP 11, 092 (2014)], p. 118. DOI: 10.1007/JHEP10(2013)118. arXiv: 1308.0463 [hep-ph].